To the Graduate Council:

I am submitting herewith a thesis written by SHANMUGHAM SUBRAMANIAM entitled "SYNTHESIS, AND THERMAL AND MECHANICAL PROPERTIES OF $Ba_{1+x}Zr_4P_{6-2x}Si_{2x}O_{24}$." I have examined the final copy of this thesis for form and content and recommend that it be accepted in partial fulfillment of the requirements for the degree of Master of Science, with a major in Metallurgical Engineering .

Carl J. McHargue, Major Professor

We have read this thesis
and recommend its acceptance:

Accepted for the Council:

Associate Vice Chancellor
and Dean of The Graduate School

STATEMENT OF PERMISSION TO USE

In presenting this thesis in partial fulfillment of the requirements for a Master's degree at The University of Tennessee, Knoxville, I agree that the Library shall make it available to borrowers under rules of the Library. Brief quotations from this thesis are allowable without special permission, provided that accurate acknowledgment of the source is made.

Permission for extensive quotation from or reproduction of this thesis may be granted by my major professor, or in his absence, by the Head of Interlibrary Services when, in the opinion of either, the proposed use of the material is for scholarly purposes. Any copying or use of the material in this thesis for financial gain shall not be allowed without my written permission.

Signature 

Date 07/13/93

SYNTHESIS, AND THERMAL AND MECHANICAL PROPERTIES OF $Ba_{1+x}Zr_4P_{6-2x}Si_{2x}O_{24}$

A Thesis

Presented for the

Master of Science

Degree

The University of Tennessee, Knoxville

SHANMUGHAM SUBRAMANIAM

August 1993

DEDICATION

This thesis is dedicated to

all those who have contributed and devoted their life

to the improvement of mankind.

ACKNOWLEDGMENTS

I would like to thank my advisor, Dr. Carl J. McHargue, for his guidance. I would like to express my sincere gratitude to Mr. David P. Stinton, Oak Ridge National Laboratory (ORNL), Mr. Santosh Y. Limaye, LoTEC., Inc., Drs. Theodore M. Besmann, ORNL, and Antonio J. Pedraza for their support, interest and encouragement throughout this work. I am thankful to Dr. Victor J. Tennery, Director, High Temperature Materials Laboratory (HTML), ORNL, for allowing access to his research facilities. Thanks are also due to Drs. Paul F. Becher, Camden R. Hubbard, Matthew K. Ferber, Karren L. More, and Thomas R. Watkins, Ms. Millicent C. Clark, Ms. Shirley B. Waters and others at the HTML, ORNL.

I would also like to thank the sponsor of the project, the U.S. Department of Energy, Assistant Secretary for Conservation and Renewable Energy, Office of Transportation Technologies, as part of the Ceramic Tech. Project of the Materials Development Program, under contract DE-AC05-84OR21400 with Martin Marietta Energy Systems, Inc.

Special thanks to Drs. Sreeram Srinivasan and Woo Y. Lee, ORNL for their suggestions, advice and putting up with me through my hours of painstaking effort and struggle. I would also like to thank my friends Nithya, Alka, and Jyotsna for their support. Finally, I would like to thank my parents, S. Shanmugham and S. Lalitha, sister, S. Sumathi, relatives, and friends who have encouraged me in all my endeavors.

ABSTRACT

$Ba_{1+x}Zr_4P_{6-2x}Si_{2x}O_{24}$ or BaZPS belongs to the family of ultra-low expansion materials popularly known as NZP, after the prototype composition, $NaZr_2P_3O_{12}$. BaZPS compositions with x=0.000, 0.175, 0.250, 0.375, and 0.500 were synthesized by a solid-state reaction method, and the mechanical and thermal properties were investigated as a function of silicon content. In addition, the grain size effect on the mechanical and thermal properties was studied for BaZPS with x=0.000, 0175, and 0.500, and the critical grain sizes were determined. The bulk linear thermal expansion values were found to decrease with increasing silicon content, and was negative for BaZPS with x=0.500. BaZPS with x=0.175 had very low thermal expansion anisotropy and exhibited good mechanical behavior as well. BaZPS with x=0.375 had the highest strength, and hardness values, and is likely suitable for high temperature applications. All the BaZPS compositions showed an increase in flexural strength with increasing temperature, and this behavior was ascribed to the healing of microcracks at higher temperatures. The critical grain size transitions were found to be proportional to the inverse square of the maximum thermal expansion difference. For example, BaZPS with x=0.500 had the highest thermal expansion anisotropy, and showed the smallest critical grain size transition.

TABLE OF CONTENTS

LIST OF TABLES

LIST OF FIGURES

Chapter 1

Introduction

The use of advanced ceramics for high temperature applications has been on the increase since World War II. In the early 1980's, the need for very low thermal expansion materials for applications such as mirror substrates for space satellites generated considerable scientific interest, and led to the discovery of a family of ultra low-thermal expansion materials popularly known as NZP, after the prototype composition $NaZr_2P_3O_{12}$ (Alamo and Roy 1984, Roy et al. 1984, Lenain et al. 1984). Since then, several compositions, and crystalline systems in the NZP family with near-zero thermal expansion have been developed and $Ba_{1+x}Zr_4P_{6-2x}Si_{2x}O_{24}$ or BaZPS is one such system (Limaye 1989).

Ultra-low thermal expansion materials are expected to have high thermal shock resistance. The motivation for developing materials with high temperature shock resistance has come from applications such as diesel engines (exhaust port liners, manifold insulation), gas turbine engines (thermal barrier coatings, combustor liners), and metallurgical applications (brazing and carburizing fixtures). It has been recognized that materials with low thermal expansion, low thermal expansion anisotropy, high flexural strength, and high Young's modulus are suitable for such applications.

Over the past 10 years, studies on NZP materials have focused on

determining their thermal properties (Roy et al. 1984, Lenain et al. 1984, Oota and Yamai 1986, Limaye et al. 1987, Huang 1990, Limaye et al. 1991), although very few researchers have reported their mechanical properties (Balagopal 1989). Also, grain size-microcracking relationships have been studied for few NZP materials (Yamai and Ota 1993). Thermal properties (axial and bulk linear thermal expansion) of a few BaZPS compositions have been reported (Limaye 1989, Huang 1990), and mechanical properties have not been investigated thoroughly. Hence, if these materials are to see significant application, it is of paramount importance that a comprehensive study of the thermal, and mechanical properties of BaZPS is carried out to expand the property database. The present effort is designed to address this problem.

The objective of the present study was to systematically investigate the effect of composition on the mechanical and thermal properties of BaZPS compositions. For this purpose, BaZPS with x=0.000, 0.175, 0.250, 0.375, and 0.500 were synthesized by a solid-state reaction method. In addition, the effect of grain size on the thermal and mechanical behavior was investigated for BaZPS with x=0.000, 0.175, and 0.500 by varying the time at the sintering temperature, and three different grain-sized materials were produced for each of the above three compositions.

Huang (1990) investigated the axial thermal expansion behavior of BaZPS with x=0.000, 0.125, 0.250, 0.375, and 0.500, and indicated that compositions between 0.125-0.250 would exhibit very low thermal expansion anisotropy. One

of the objectives of the present study was to test Huang's hypothesis by determining the axial thermal expansions of BaZPS with x=0.175.

Materials for high temperature applications must demonstrate dimensional integrity and should not develop microcracks during thermal excursions. It has been recognized that a crystalline ceramic body made from a non-cubic material possessing near-zero thermal expansion coefficient may still exhibit microcracking due to high degrees of anisotropy in the lattice thermal expansion coefficient (Bush and Hummel 1959, Tvergaard and Hutchinson 1988). The degree of microcracking considerably affects the thermal and mechanical behavior of a material, and investigators have reported that in a single-phase polycrystalline material there exists a critical grain size below which microcracking does not occur (Kuszyk and Bradt 1973, Cleveland and Bradt 1978). Another objective of the present investigation was to determine the critical grain size of the BaZPS compositions with x=0.000, 0.175, and 0.500.

In the next chapter, a literature review pertaining to NZP materials synthesis, crystal structure, phase transformations, thermal expansion, and their other significant properties will be presented. Also, the effect of thermal expansion anisotropy on microcracking, and mechanical properties will be elaborated. Chapter 3 provides a summary of the experimental procedure adopted. In chapter 4, the experimental results will be presented and chapter 5 will discuss the results in detail. Chapter 6 contains the conclusions and suggestions for future work.

Chapter 2

Literature Review

NZP materials first gained importance as a good ionic conductor in the 1970's. Boilot et al. (1979), while investigating the ionic conduction in $Na_{1+x}Si_xZr_2P_{3-x}O_{12}$ ($1 \leq x \leq 3$) observed that the bulk linear thermal expansion varied from positive to negative with composition. This tailorable thermal expansion property of NZP materials generated considerable scientific and technological interest, and since then they have been studied extensively. In addition, NZP materials have been found to be useful for radioactive waste immobilization, ferroelectric and pigment applications. In this chapter, an elaborate literature review pertaining to NZP materials synthesis, crystal structure, phase transformations, thermal expansion, and other significant properties is presented. Also, the thermal expansion anisotropy and its influence on microcracking and mechanical properties are discussed.

2.1 Synthesis of NZP materials

Several methods are available to synthesize NZP materials. Recently, Agrawal (1992) summarized the techniques available as follows:

1. Solid state reaction method
2. Wet chemical methods (sol gel, co-precipitation, etc.)

3. Ion exchange method
4. Hydrothermal method
5. Combustion method or self propagating synthesis
6. Evaporative decomposition of solutions

Limaye et al. (1991) reported the synthesis of $Ca_{1-x}Sr_xZr_4P_6O_{24}$ by a solid state reaction method. They used $CaCO_3$, $SrCO_3$, ZrO_2, and $NH_4H_2PO_4$ as the starting materials. Stoichiometric amounts of the precursor powders of the desired composition were mixed, ground in acetone to homogenize the mixture, and air dried at room temperature. Calcination was then performed in three stages to produce a single phase composition: at 200°C for 16 hours to drive off H_2O and NH_3, at 600°C for 4 hours to remove crystalline water, and at 900°C for 16 hours to remove CO_2 from carbonates. The calcined powder was then crushed in a mortar with a pestle and mixed with 15% polyvinyl alcohol, cold pressed at 140 MPa, and sintered at 1300°C for 48 hrs to produce a densified ceramic. Several researchers have also reported the synthesis of other NZP materials using similar techniques (Hong 1976, Miller et al. 1979, Takahasi et al. 1980, Delmas et al. 1981, Alamo and Roy 1984, Lenain et al. 1984, 1985, Agrawal and Stubican 1985, Agrawal et al. 1986, Oota et al. 1986, Limaye et al. 1987, Huang 1990, Hirschfeld et al. 1991). Advantages of this method include simplicity, and low cost. However, the method has its limitations since it requires several heating steps, a high calcination temperature, long time periods, and results in poor sinterability and difficulty in producing single phase compositions.

Boilot et al. (1979) synthesized $Na_{1+x}Zr_2P_{3-x}Si_xO_{12}$ (Nasicons) using Na_2SiO_4, $(NH_4)_2HPO_4$, and $ZrO(NO_3)_2$ solutions at 1000°C by a sol-gel method. Gordon et al. (1981) synthesized Nasicons by a similar technique using inorganic precursors at temperatures between 1175°C to 1300°C. However, both research groups reported the presence of unreacted ZrO_2 in their preparations. Recently, Agrawal and Adair (1990) synthesized one of the Nasicon compositions ($NaZr_2P_3O_{12}$) using a solution sol-gel technique at temperatures as low as 120°C and obtained a phase pure material at 500°C.

Figure 2.1 depicts the process flow chart of Agrawal and Adair (1990). Stoichiometric amounts of the precursor solutions of 2M $NaNO_3.H_2O$, and colloidal 2.4M ZrO_2 (nitrate stabilized) were first mixed and then an appropriate amount of 8.55M H_3PO_4 was added slowly with continuous stirring to result in a solution with a pH of 1.3. The mixture was then heated at 80°C for 24 hrs for gelation, followed by drying at 120°C for 24 hrs. Calcination was then done between 300°C and 500°C. The calcined powder was then ground, and heat treated between 600°C and 1000°C for 24 hrs to produce a densified Nasicon. Previously, Lenain et al. (1984) and Limaye et al. (1987) synthesized alkali zirconium phosphates and alkaline zirconium phosphates respectively, using comparable techniques. Several investigators have also reported the synthesis of other NZP compositions using similar methods (Roy et al. 1982, Perthius and Columban 1984, Roy et al. 1984, Alamo and Roy 1984, Boilot et al. 1986, Agrawal and Roy 1986, Ramashesa and Jacob 1988, Hirschfeld et al. 1991). This method possesses several attractive

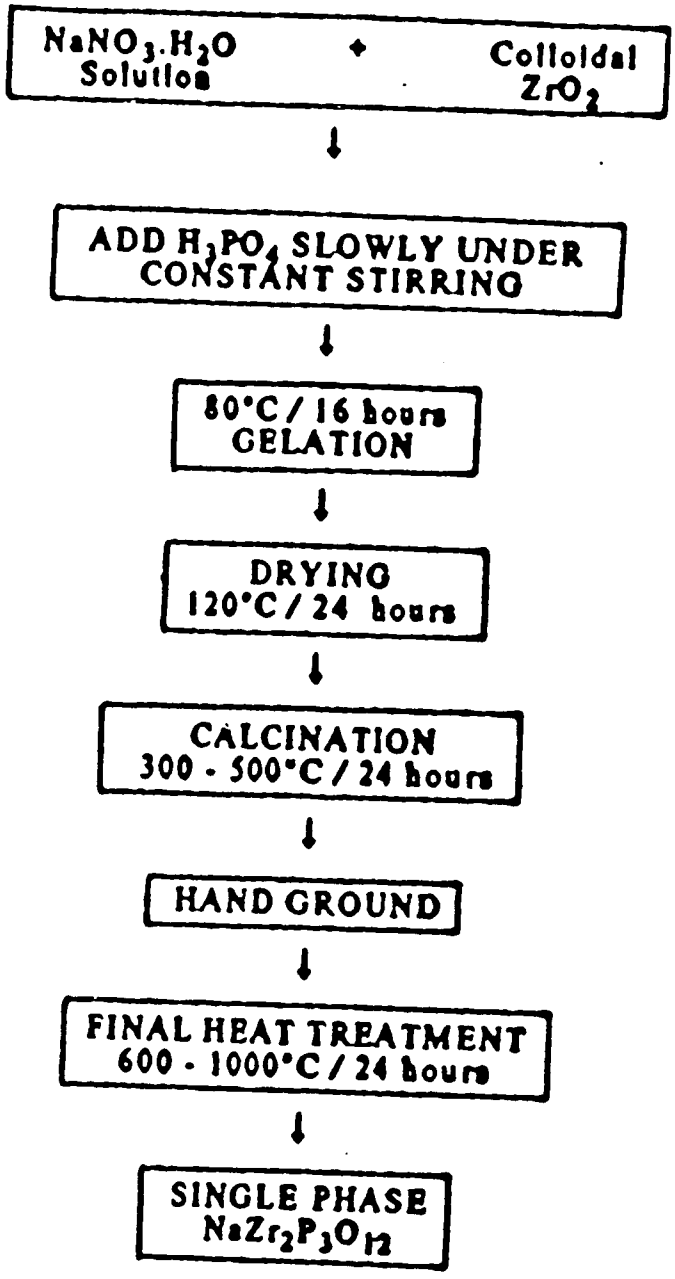

Figure 2.1 Procedure for synthesis of $NaZr_2P_3O_{12}$ (Agrawal and Adair 1990)

SOURCE Agrawal, D. K. and J.H. Adair (1990) "Low-Temperature Sol-Gel Synthesis of $NaZr_2P_3O_{12}$," J. Am. Ceram. Soc. **73**, 2153-55

features: better homogeneity, higher crystallinity, higher density, lower firing temperatures, and higher reactivity. However, costly precursors, and the care required for handling complex compositions, are the major drawbacks for this technique.

Hong (1976) reported that the Na^+ ions in $NaZr_2P_3O_{12}$ and $Na_3Zr_2Si_2PO_{12}$ could be reversibly ion exchanged in molten salts with Li^+, Ag^+, and K^+, with the chemical concentration gradient being the driving force. Powders of $NaZr_2P_3O_{12}$ and $Na_3Zr_2Si_2PO_{12}$ were held for 4 hrs in molten $LiNO_3$, $AgNO_3$, and KNO_3, respectively, with the powder to salt weight ratio being 1:20. The products were then washed with water to remove the nitrates, and air dried. Similarly, La Ginestra et al. (1979) obtained silver-zirconium phosphate system by ion exchange of zirconium phosphate with different Ag^+ loadings (13% to 96%).

Clearfield et al. (1981) synthesized sodium zirconium silicophosphates using a hydrothermal method in a parr bomb fitted with a teflon liner. Sodium silicate was weighed and dissolved in deionized water in the bomb. A preweighed sample of α-zirconium phosphate and excess NaOH was then added, and the bomb was sealed. The bomb was then held at 300°C under a pressure of 12000 KPa for varying time periods. The recovered solid was then washed free of the base and air dried to obtain a single phase composition. Recently, Dongare et al. (1992) reported the synthesis of crystalline sodium zirconium phosphate using a similar method and single crystals of alkali zirconium/hafnium phosphates have also been grown by a comparable technique (Sljukic et al. 1967). Other NZP

compositions have also been produced by many research groups using analogous methods (Clearfield et al. 1980, 1984, Komarneni et al. 1986, Byrappa et al. 1986, Komarneni 1988). All the above studies suggest that the hydrothermal method may be a low temperature route for the synthesis of very fine powders of NZP compounds.

The combustion method involves an exothermic chemical reaction between oxidizer(s) and fuel with a large amount of energy release causing high temperature conditions which result in the formation of the desired product. Recently, Agrawal (1992) reported the synthesis of several NZP compositions using a suitable combination of precursor(s) (H_3PO_4, $NH_4H_2PO_4$), oxidizer(s) ($NaNO_3$, $ZrO(NO_3)_2.xH_2O$, etc.), and fuel (urea) with ratios of 1:1:3 to 1:2:6 at temperatures less than 800°C. This method is safe, simple, one step, relatively low temperature process, consumes little energy, and rapidly produces single-phase fine powders with high surface area.

2.2 Crystal structure of NZP materials

The prototype composition, $NaZr_2P_3O_{12}$, crystal structure was first reported by Hagman and Kierkegarrd (1968), and later corroborated by Hong (1976), and Hazen et al. (1987). It has rhombohedral symmetry with a R-3c, #167 space group, and hexagonal unit cell dimensions of a = 0.88043 ± 0.2 nm and c = 2.27585 ± 0.9 nm. The crystal structure details are summarized in Table 2.1, and the basic crystal structure is illustrated in Figure 2.2.

Table 2.1 The crystal structure information of $NaZr_2P_3O_{12}$ (Hagman and Kierkegaard 1968)

Space group: R-3c

Unit cell dimensions: a = 8.803 ± 2 Å
c = 22.7585 ± 9 Å
V = 1527.7 Å ^{3}

Cell content: 6 $NaZr_2P_3O_{12}$

6 Na in 6(b) : (0,0,0; 0,0,1/2)
12 Zr in 12(c) : ±(0,0,z; 0,0,1/2+z)
18 P in 18(e) : ±(x,0,1/4; 0,x,1/4; -x,-x,1/4)
36 O_1 and 36 O_2 in 2 x 36 (f) : ±(x,y,z; -y,x-y,z; y-x,-x,z; -y,-x, z+1/2; x,x-y,z+1/2; y-x,y,z+1/2)

Atomic parameters with estimated standard deviations (±σ)

Atom	x	y	z
Na_1	0	0	0
Zr	0	0	0.1456±1
P	0.2909±6	0	0.25
O_1	0.1860±15	-0.0144±15	0.1949±5
O_2	0.1913±15	0.1683±15	0.0866±5

SOURCE Hagman, L.O. and P. Kierkegaard (1968) "The crystal structure of $NaMe_2^{IV}(PO_4)_3$; Me^{IV}=Ge, Ti, Zr, " Acta Chem. Scand. **22**, 1822-32

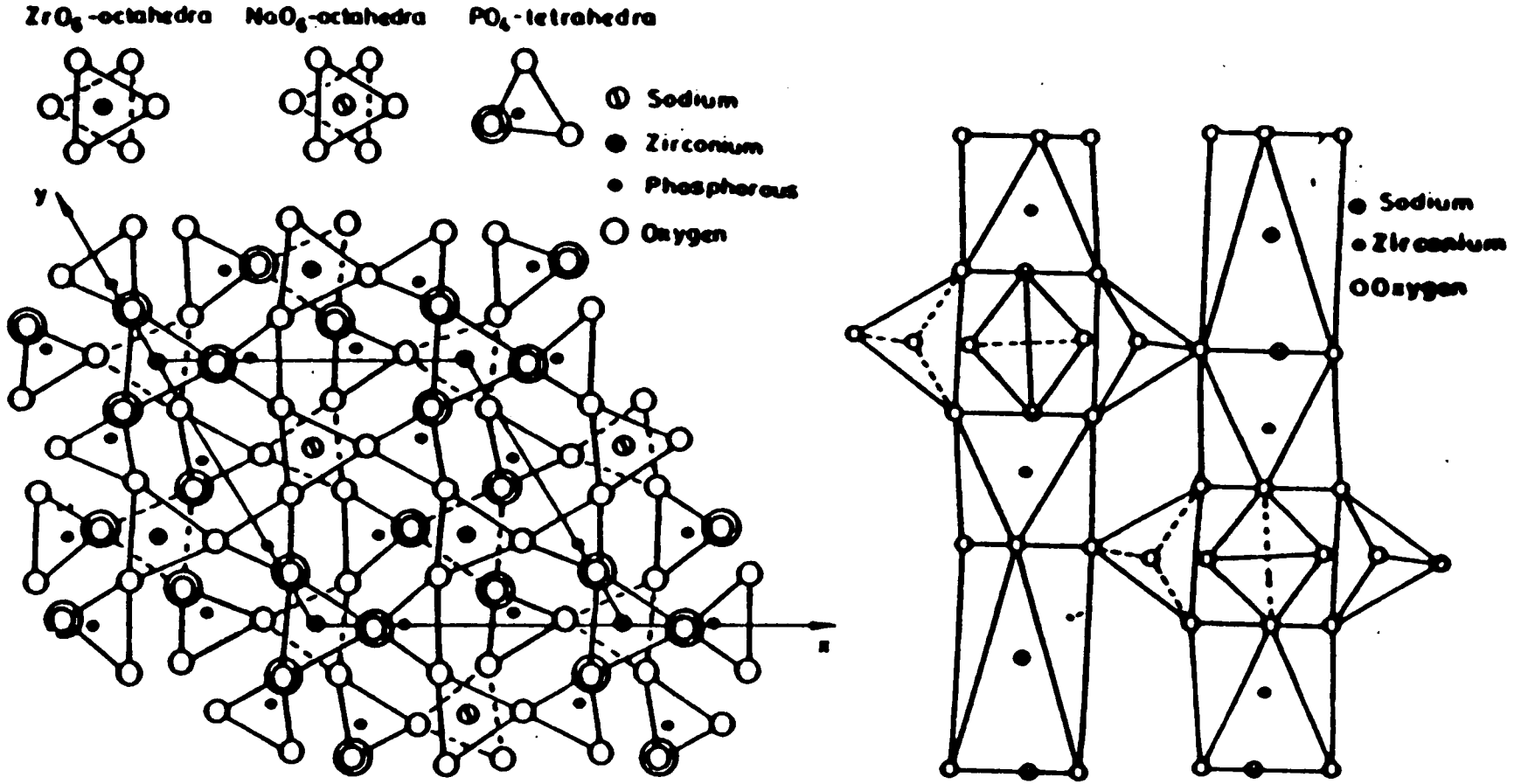

Figure 2.2 NZP basic structure viewed along (left) and (right) perpendicular to the c axis (Roy et al. 1989)

SOURCE Roy, R., D.K. Agrawal, and H.A. McKinstry (1989) "Very low thermal expansion coefficient materials," Annu. Rev. Mater. Sci. **19**, 59-81

The structure of $NaZr_2P_3O_{12}$ consists of a three dimensional skeletal network of PO_4 tetrahedra sharing corners with ZrO_6 octahedra. Each PO_4 tetrahedra is on a two-fold rotation axis and connected to four ZrO_6 octahedra, and each ZrO_6 octahedra is on a 3-fold rotation axis and linked to six PO_4 tetrahedra. The basic unit of the network is comprised of 2 octahedra connected by 3 tetrahedra corresponding to $[Zr_2P_3O_{12}]^-$. These units are linked to form ribbons along the c axis. The ribbons are connected together by PO_4 tetrahedra perpendicular to the c axis to develop a three dimensional network. The articulation of these ribbons create structural holes in which the sodium atoms reside (Na1 position).

The crystal structure details of other NZP materials have also been reported (Sljukic et al. 1969, Masse et al. 1972, Sizova et al. 1973, Hong 1976, Effremov and Kalinin 1978, Hong 1979, Delmas et al. 1981, Rudolf et al. 1985, Petit et al. 1986, Boilot et al. 1988, Rodrigo et al. 1989). Apart from x-ray diffraction methods, other techniques such as perturbed angular correlation spectroscopy (Baudry et al. 1985), Raman and infrared spectroscopy (Tarte et al. 1986), and neutron diffraction (Rudolf et al. 1985) have also been utilized to characterize the structural information of several NZP materials.

2.3 Phase transformations in NZP materials

Hong (1976) reported that the room temperature crystal structure of $Na_{1+x}Zr_2Si_xP_{3-x}O_{12}$ ($0 \leq x \leq 3$) changed from rhombohedral symmetry (space group R-3c) to monoclinic symmetry (space group C2/c) in the composition range

$x \leq 2.2$. This was later confirmed by Boilot et al. (1979). Additionally, they found that the compositions in the interval $1.6 < x < 2.2$ also had monoclinic symmetry at room temperature which transforms to rhombohedral symmetry at around 150°C. von Alpen et al. (1979) also reported the phase transition in the above system with $x = 2$. They found a second order phase transformation at around 150°C by three techniques: ac-impedance, specific heat measurements, and high temperature x-ray diffraction.

Delmas et al. (1981) studied the crystal chemistry of three solid solutions of $Na_{1+x}Zr_{2-x}L_xP_3O_{12}$ (L=Cr, In, Yb). X-ray diffraction was used to characterize the single phase at room temperature of compositions $0 \leq x \leq x_L^{max}$ with $x_{Cr}^{max} = 2.0$, $x_{In}^{max} = 1.85$, and $x_{Yb}^{max} = 1.90$. They reported that except for $Na_3Cr_2P_3O_{12}$ (monoclinic: space group C2/c), all other compositions have rhombohedral symmetry (space group R-3c). Further, the differential thermal analyzer (DTA) studies of $Na_3Cr_2P_3O_{12}$ detected two transitions, one each at 135°C and 165°C, and confirmed the appearance of an intermediate phase between monoclinic and rhombohedral phases.

Pintard-Screpel and co-workers (Agrawal and Roy 1986), while studying the superionic conductivity of $Na_3Fe_2P_3O_{12}$, reported two polymorphic phase transitions: $\alpha \rightleftharpoons \beta$ at 95°C and $\beta \rightleftharpoons \gamma$ at 145°C. The γ form being rhombohedral and iso-structural with NZP, the β form a super structure of the γ form, and the α form a distorted monoclinic form of γ. Recently, Agrawal and Roy (1986) corroborated

this by performing DTA studies and found two exothermic peaks at 90°C and 140°C during heating and cooling cycles. Further, they observed from the dilatometric curve that the composition $Na_2Ca_{0.5}Fe_2P_3O_{12}$ undergoes a phase transition at 95°C.

In 1989, Ohasi and Matsuhiro reported phase transitions in $BaZr_4P_6O_{24}$ (BaZP) and $SrZr_4P_6O_{24}$ (SrZP). They observed that BaZP and SrZP did not contract nor expand above 900°C and 1200°C, respectively. Further, several x-ray diffraction peaks were also missing for the compositions above those temperatures. From their high temperature x-ray data analysis, they reported an order-disorder transformation for both the compositions. They explained that Sr ions in SrZP and Ba ions in BaZP show an ordered arrangement at half of the 6b sites below the transition temperature, and a random arrangement of Sr and Ba ions at all 6b sites above the transformation temperature.

Recently, Rodrigo and Alamo (1991) reported that $NaSn_2P_3O_{12}$ undergoes a fast and reversible phase transition at 575°C, with the phase being rhombohedral above and below the transition point.

2.4 Thermal expansion of NZP compounds

Boilot et al. (1979) reported that the bulk thermal expansion values varied from positive to negative in the $Na_{1+x}Si_xZr_2P_{3-x}O_{12}$ ($1 \leq x \leq 3$) system. They found that the $Na_2SiZr_2P_2O_{12}$ composition exhibited negative thermal expansion. This caught the attention of Roy and co-workers who performed a systematic

investigation in their laboratory. Alamo and Roy (1984) investigated the above system with $0 \leq x \leq 1$ and $Na_{1+4z}Zr_{2-z}P_3O_{12}$ ($0 \leq z \leq 0.5$), and found that the thermal expansion can be varied continuously from moderately positive to moderately negative values with variation in x and z. Further, they observed that these ceramics permit a wide range of cationic substitutions.

Roy et al. (1984) reported the discovery of a new structural family for use in ultra-low thermal expansion ceramics. They named the family of materials CTP, after the prototype composition $Ca_{0.5}Ti_2P_3O_{12}$. Dilatometric measurements were carried out on 10 different compositions between room temperature and 500°C, which revealed that the extreme values of thermal expansion were ($Ca_{0.25}Na_{0.5}Zr_2P_3O_{12}$) +6.3 and ($NaTi_2P_3O_{12}$) -5.5 x 10^{-6} $°C^{-1}$. In addition, they found that the prototype composition, $NaZr_2P_3O_{12}$, exhibited strong anisotropy in unit cell parameters (α_a = - 6.42, and α_c = + 25.5 x 10^{-6} $°C^{-1}$) and ascribed the low thermal expansion behavior of the other members of the family to this characteristic.

Sljukic et al. (1967) synthesized the whole alkali series of NZP compounds and reported that the lattice parameters varied in opposite directions with increase in the size of the alkali ion (c-parameter increased and the a-parameter decreased). This was later confirmed by Lenain et al. (1984). They also reported that except for rubidium (α = - 7.6 x 10^{-7} $°C^{-1}$), all other members of the alkali family exhibited positive thermal expansion, with the cesium compound showing the smallest overall expansion (α = 0.21 x 10^{-6} $°C^{-1}$).

Agrawal and Roy (1985) determined the thermal expansion of 21 diphasic

composites. They adopted a strategy in which they mixed two thermodynamically compatible ceramic phases (one with negative [NZP type material] and the other with positive thermal expansion).

Oota and Yamai (1986) have studied the thermal expansion behavior of $Na_{1+x}Zr_2Si_xP_{3-x}O_{12}$ ($0 \leq x \leq 3$). They reported that the a-axis thermal expansion coefficients changed from negative to zero with increasing x, while the c-axis coefficients had high positive values with a minimum at x = 2.0. They also found that the bulk thermal expansion values changed from negative to positive with increasing x, with the compositions $0 \leq x \leq 1$ exhibiting extremely low thermal expansion. In addition, it was determined that lattice parameters and thermal expansion coefficients varied with content and ionic radii of interstitial ions. They observed that the c-axis thermal expansion coefficients as well as the c parameters increased significantly with the increase in alkali content at the M_I site in $M_I(M_{II})_3Zr_2P_3O_{12}$. Also, the a-axis thermal expansion coefficients as well as the a-parameters increased with increasing M_{II} content. Their results are summarized in Table 2.2.

In 1987, Limaye et al. reported the synthesis and thermal expansion behavior of $MZr_4P_6O_{24}$ (M = Mg, Ca, Sr, and Ba). They performed thermal expansion measurements on the sintered samples using dilatometry, high temperature x-ray diffraction, and laser speckle interferometry. They noted that $CaZr_4P_6O_{24}$ showed negative thermal expansion ($\alpha = -2.11 \times 10^{-6}\ °C^{-1}$), while the other members of the series exhibited positive values between 25 - 500°C. They

Table 2.2 Variation of lattice parameters and thermal expansion coefficients with content and ionic radii of interstitial ions (Oota and Yamai 1986)

Parameter	Change with increasing Na content		Change with increasing ionic radius at M_I site
	M_I site	M_{II} site	
a	unaltered	increase	slight decrease
c	increase	unaltered	increase
α_a	slight decrease	increase	slight increase
α_c	increase	unaltered	decrease

SOURCE Oota, T. and I. Yamai (1986) "Thermal Expansion Behavior of $NaZr_2(PO_4)_3$-Type Compounds," J. Am. Ceram. Soc. **69**, 1-6

discovered that the Sr and Ba series exhibited positive expansion in the a-axis and negative expansion in the c-axis, while the Ca series displayed opposite behavior. Also, they indicated the possibility of utilizing the opposite, anisotropic behavior in the Ca and Sr series to form crystalline solutions with near-zero thermal expansion and very low thermal expansion anisotropy. In a subsequent study, Limaye et al. (1991) discussed the synthesis and thermal expansion behavior of $Ca_{1-x}Sr_xZr_4P_6O_{24}$ ($0 \leq x \leq 1$). They reported that the composition with $x = 0.5$ showed almost zero axial thermal expansion anisotropy.

Limaye (1989) reported the thermal expansion behavior of $Ba_{1+x}Zr_4P_{6-2x}Si_{2x}O_{24}$ ($x = 0$, 0.25, and 0.50). He found that the bulk thermal expansion decreased with increasing x (from positive to negative). Also, the a-axis thermal expansion coefficients changed from positive to negative with increasing x, while the c-axis thermal expansion coefficients showed a reverse trend. Recently, Huang (1990) also reported the same behavior.

In 1990, Huang performed a systematic investigation of the thermal expansion behavior of 17 NZP materials, which included 9 alkali/alkaline earth zirconium phosphates and 8 alkali/alkaline earth titanium phosphates. He observed that the axial thermal expansion in the c direction is larger than that in the a direction for alkali zirconium/titanium phosphates, and the pattern reversed for alkaline earth compounds with larger alkaline earth ions.

2.5 Other significant properties of NZP materials

2.5.1 Ionic Conductivity

Hong (1976) first reported fast ion conduction in solid solutions between sodium zirconium phosphate and sodium zirconium silicate, $Na_{1+x}Zr_2Si_xP_{3-x}O_{12}$. Subsequently, Goodenough et al. (1976) demonstrated fast Na^+ ion transport in several structures and found that $Na_{1+x}Zr_2Si_xP_{3-x}O_{12}$ with x = 2 had a Na^+ ion resistivity of $\varrho_{300} \leq 5\Omega$-cm at 300°C, comparable to that of the best β" alumina. Since then, several similar sodium-ion conducting ceramics have been synthesized, including $Na_5YSi_4O_{12}$ (Hong et al. 1987), and a family of Nasicon materials possessing isostructural characteristics, $Na_{1+x}Zr_{2-x}M_xP_3O_{12}$, and $Na_3Sc_2P_3O_{12}$ (Hong 1979).

Kafalas and Cava (1979) studied the effect of hydrostatic pressure and composition on ionic conductivity of $Na_{1+x}Zr_2Si_xP_{3-x}O_{12}$ ($0 \leq x \leq 3$). They found that the maximum ionic conductivity occurred at x = 2.3 (30% higher than the conductivity at x = 2.0) and argued that the incorporation of additional Si in place of P could result in enhanced chemical stability under battery operating conditions. Boilot et al. (1988) observed in $Na_{1+x}Zr_2Si_xP_{3-x}O_{12}$ ($2 < x < 2.4$), a partial occupation of a mid-Na interstitial site within the conduction path, and observed a maximum at x=2. They concluded, based on the structural results, that the enhanced conductivity at x=2 arises from Na interactions instead of geometry changes of the framework.

2.5.2 Ferroelectric properties

Keester and Jacobs (Okonenko et al. 1978) found that $NaU_2P_3O_{12}$, and $NaTh_2P_3O_{12}$ exhibited ferroelectric properties. This, they attributed to the presence of large voids in the structure of these compounds, and that the voids contained relatively small Na atoms which could be easily displaced from the centrosymmetric positions by electrostatic forces . Kalinin (Okonenko et al. 1978) observed that $Na_3Sc_2P_3O_{12}$ had similar voids to the above compounds, although much larger than the sodium atoms could contain. Later, Okonenko et al. (1978) reported in $Na_3Sc_2P_3O_{12}$, the existence of a second order phase transition from the polar to non-polar phase (accompanied by observable changes in the permittivity and dielectric losses), the existence of a domain structure in the polar phase, and the fact that the symmetry of the low temperature phase can be derived from the symmetry of the high temperature phase by superimposing the polar vector symmetry. They concluded, based on the above observations, that $Na_3Sc_2P_3O_{12}$ was a ferroelectric material.

2.5.3 Radioactive waste immobilization

Roy et al. (1982) has suggested that the NZP structure is an ideal candidate for Cs and Sr immobilization due to the leaching and refractory attributes of NZP's. Also, NZP materials offer the promise of accommodating a wider range of radwaste ions, could be formed by dry-firing methods at relatively low temperature, and could be easily processed. In addition, their compatibility with monazite allows

the further advantage of maximizing actinide insolubility, depending on the partition of actinides between the two phosphates. Yang (1984) reported that Zr-P-O gels are amenable to batch adsorption as well as column adsorption of nuclear wastes and could be directly fired after adsorption to obtain NZP waste forms. The leach resistance of such waste forms made below 1000°C is comparable to other potential candidate ceramic waste forms.

2.5.4 Pigments

Cuadrado and Alamo (1988) reported that Cr-doped zirconium phosphates could be used as pigments at high temperatures. They synthesized $Na_{1+x}Cr_xZr_{2-x}P_3O_{12}$, and $Ca_{0.5+x/2}Cr_xZr_{2-x}P_3O_{12}$ with $0.06 \leq x \leq 1.00$ and found that the color ranged from pink to grayish green as Cr was substituted for a larger size cation. Also, they observed that the pigments applied in several glazes develop different effects, opacifying or devitrifying, and display from beige to greenish colors.

2.5.5 Ionic Substitution

Alamo and Roy (1986) showed that the NZP structure is remarkably stable towards ionic substitutions, supporting a wide range of homovalent, as well as heterovalent substitutions because of the flexibility of its skeleton, the strength of its bonds, and the existence of a variety of holes that can be empty or occupied. The standard formula for the NZP structure is $M'_1{}^{x}M''_3{}^{VI}A_2{}^{VI}B_3{}^{IV}O_{12}$. The ionic

substitutions are achieved on the M' and M" sites, which are the holes or vacancies formed by the rather strong skeleton and which can be left empty without any effect on the crystal structure. The different classes of substitution that are possible is summarized in Table 2.3. A c vs a plot for the phosphates in the first substitutional group is shown in Figure 2.3. They observed that for the same M', the larger the A atom, the larger were the a and c values. Also, for the same A atom, the larger the M', the larger is c, but a becomes smaller. Selected NZP materials which have been reported in the literature are given in Table 2.4.

2.6 Microcracking and thermal expansion anisotropy

Localized residual stresses typically arise in non-cubic polycrystalline materials due to thermal expansion anisotropy. These stresses, when high enough, may cause microcracking in brittle ceramics and plastic deformation in metals. Sosman (1927) observed that ceramics consisting of grains with thermal expansion anisotropy exhibit thermal expansion hysterisis. Boas and Honeycombe (1944) proposed that plastic deformation in non-cubic metals like Zn, Sn, and Cd is due to thermal expansion anisotropy.

Buessem et al. (1952) offered a good explanation for the thermal hysterisis of aluminum titanate. They argued that aluminum titanate, being highly anisotropic, internal microcracks forms due to localized stresses, which exceed internal strength, during cooling from the sintering temperature. Further, they attributed the thermal hysterisis to these microcracks, since they heal and develop

Table 2.3 Ionic substitution schemes in the NZP structure (Alamo and Roy 1986)

Structure formula: $M'_1{}^{X}M''_3{}^{VI}A_2{}^{VI}B_3{}^{IV}O_{12}$

Substitution scheme	M'_1	M''_3	$A_2{}^{VI}$	$B_3{}^{IV}$	O_{12}
Isovalent substitution in M' site	Li, Na, K,Rb, Cs, Mg, Ca, Sr, Ba	-	-	-	-
Isovalent substitution in VI fold	-	-	Sn, Ti,Zr, Hf,Th	-	-
Balanced substitution VI and IV	-	-	$Ta^{5+}Zr^{4+}$	$Si^{4}P_2{}^{5+}$	-
Balanced substitution IV and M'	-	Na^{+}	-	$Si^{4}P_2{}^{5+}$	-
Heterovalent substitution at M ' site	$[Ca]_{0.5}[]_{0.5}$	-	-	-	-
Balanced substitution M' and other sites	$[]_1$ $[]_1$	- -	$Ta^{5+}Zr^{4+}$ -	- $S^{6+}P_2{}^{5+}$	- -

SOURCE Alamo, J. and R. Roy (1986) "Crystal Chemistry of the $NaZr_2(PO_4)_3$, NZP or CTP, Structure Family," J. Mater. Sci. **21**, 444-450

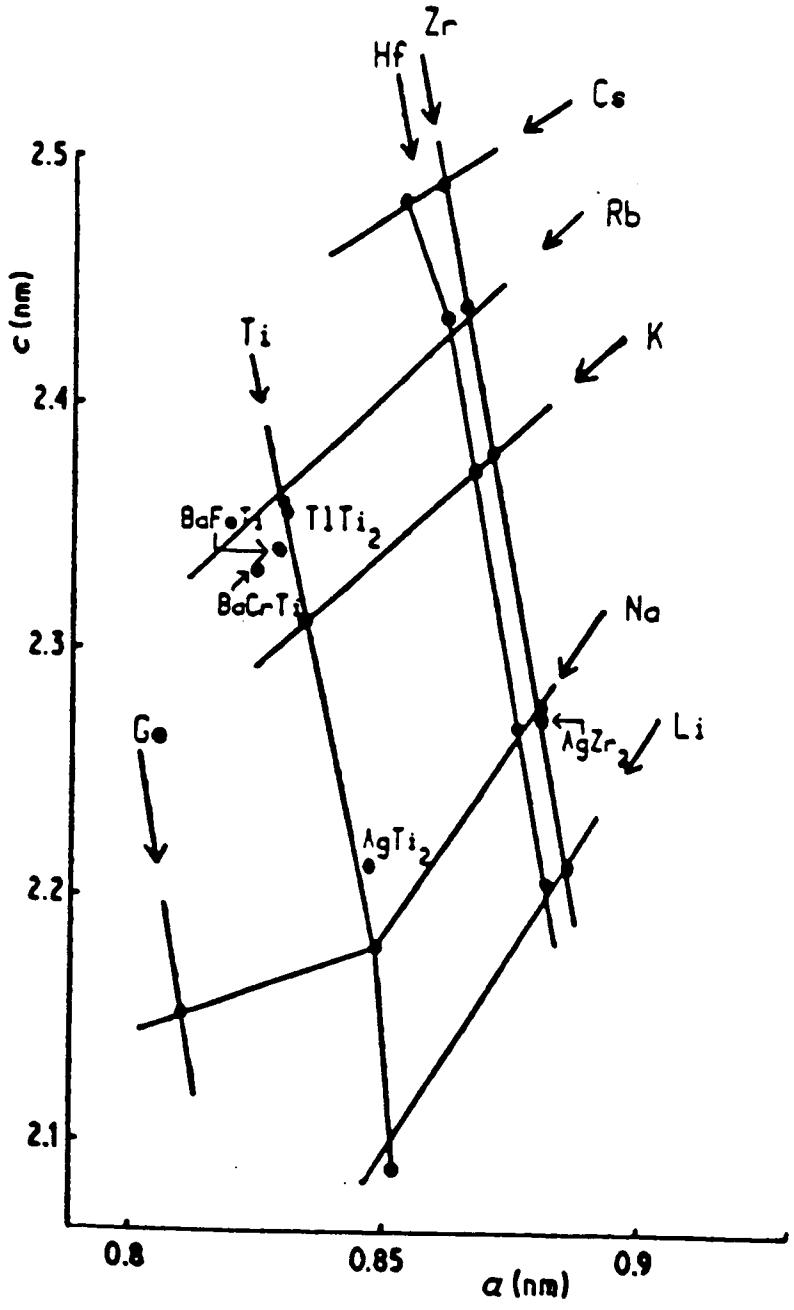

Figure 2.3 c vs a plots for $M'A_2(PO_4)_3$ where A=(Ge, Ti, Hf, Zr), and M'=(Li, Na, K, Rb, Cs, Tl, Ag (Alamo and Roy 1986)

SOURCE Alamo, J. and R. Roy (1986) "Crystal Chemistry of the $NaZr_2(PO_4)_3$,NZP or CTP, Structure Family," J. Mater. Sci. **21**, 444-450

Table 2.4 Selected NZP materials from the literature

Composition	Reference
$LiZr_2P_3O_{12}$	Lenain et al. 1984
$Na_5Zr_{1.5}Si_2PO_{12}$	Boilot et al. 1979
$NaZr_2P_3O_{12}$	Huang 1990
$CaZr_4P_6O_{24}$ + 10%MgO	Agrawal and Roy 1985
$BaZr_4P_6O_{24}$	Limaye et al. 1987
$NaTi_2P_3O_{12}$	Rodrigo and Alamo 1991
$NbZrP_3O_{12}$	Oota and Yamai 1986
$NH_4Zr_2P_3O_{12}$	Komarneni 1986
$NaZnCrS_3O_{12}$	Perret et al. 1975
$AgTi_2P_3O_{12}$	Masse 1970
$Li_{1+x}Ti_{2-x}In_xP_3O_{12}$	Tran Qui and Hamdoune 1988
$KZr_2P_3O_{12}$	Sljukic et al. 1967
$H_3OZr_2P_3O_{12}$	Subramaniam 1984
$NaNi_2ZrP_3O_{12}$	Byrappa 1986b
$Na_{1+x}Zr_{2-x}Yb_xP_3O_{12}$	Delmas et al. 1981
$Li_{1-x}Zr_{2-x}Ta_xP_3O_{12}$	Taylor et al. 1977
$Ag_3Zr_2Si_2PO_{12}$	Hong 1976
$KGe_2P_3O_{12}$	Tarte et al. 1986
$Na_{1+x}Zr_{2-x}Y_xP_3O_{12}$	Nagai et al. 1980

during a thermal cycle. Wright (1972) established a relationship between thermal expansion hysterisis and microcracking temperature using acoustic emission measurements. Recently, Ohya et al. (1987) proved that grain boundary microcracking was accompanied by both acoustic emission and expansion of the specimen.

Internal microcrack formation in a polycrystalline material exerts considerable influence on its thermal and mechanical properties (Buessem et al. 1961). It was also reported that the ceramic materials exhibiting thermal expansion anisotropy, hence microcracking, had some unusual properties:

1. Strength, Young's modulus and thermal expansion coefficient were very low at room temperature, and increased markedly with increase in temperature.
2. Hysterisis between heating and cooling in property vs temperature curves and
3. Large, delayed, irreversible strain under constant load at room temperature.

Several researchers have studied the influence of grain size on the phenomena of microcracking (Kuszyk and Bradt 1973, Ohya et al. 1987, Yamai and Ota 1987). All the research groups reported that large grain-sized materials were more susceptible to microcracking than fine-grained materials. Evans (1978) showed that in a single-phase polycrystal, the critical facet size for the onset of microfracture, l_{co}, is

$$l_{co} = \frac{5.2\ (1+\nu)^2\ \gamma_{gb}}{E\ (\Delta\alpha\ \Delta T)^2} \qquad (2.1)$$

where v is poisson's ratio, γ_{gb}, the grain boundary fracture energy, E, the Young's

modulus, $\Delta\alpha$, half the maximum thermal expansion anisotropy, and ΔT, the temperature differential at which rapid stress relaxation occurs.

Kuszyk and Bradt (1973) studied the influence of grain size on thermal expansion anisotropy in $MgTi_2O_5$. They observed that specimens with grain size smaller than 3 μm did not show microcracking. Further, specimens with fine grain sizes exhibited high modulus and low damping, and large grain sized specimens had low modulus and high damping. Also, the flexural strength and work of fracture results were similar to the modulus and damping curve behavior, exhibiting the same grain size transitions. Most of the studies in the above area deal with effect of grain size independent of porosity. Some studies have proved that the Young's modulus and flexural strength increase with decreasing porosity. However, the combined effect of grain size and porosity is not well understood. Likachev (1961) has offered a theoretical treatment of residual stresses using matrix algebra and variational principles. Theoretical explanations of microcracking due to thermal expansion anisotropy have been discussed by Clarke (1964), Buessem and Lange (1966), Kirchner and Gruver (1970), Evans (1978), Rice and Pohanka (1979), Rice et al. (1981), Krstic (1984), and Tvergaard and Hutchinson (1988).

2.7 Thermal expansion anisotropy and mechanical properties

The crystalline anisotropy influence on the mechanical properties have been investigated by several researchers. Howe (1952) observed an increase in

strength, and elastic modulus of graphite with increasing temperature and attributed it to thermal expansion anisotropy. Bush and Hummel (1958) studied the modulus of rupture and modulus of elasticity of sintered magnesium titanate as a function of temperature and thermal history. They observed that the strength and Young's modulus increased with increasing temperature up to 1000°C. They found that the flexural strength almost doubled with increasing the temperature from 600 to 1000°C and explained this in terms of extensive healing of internal ruptures.

Bush and Hummel (1959) studied the effect of internal ruptures on mechanical properties of β-eucryptite. They discovered the flexural strength at room temperature to be abnormally low, and ascribed it to the occurrence of internal fractures during cooling from the firing temperature. However, with increasing temperature the flexural strength increased due to healing of the fractures, and attained a maximum at 800°C. The strength dropped with further increase in temperature to 1000°C. They attributed this decrease to plasticity or formation of additional internal disruptions. Also, the grains that heal during heating to 800°C, refracture during cooling, but at a lower temperature than the healing temperature resulting in a small hysterisis in strength (being higher during cooling than heating). The same trend was also observed in modulus of elasticity. The results of Manning and Hunter (1973) were similar with regard to the modulus of elasticity of Nb_2O_5. They also proved that sintered specimens exhibit more susceptibility to microcracking than hot-pressed bodies. This, they maintained,

directly contributed to the hot-pressed specimens exhibiting higher modulus values than the sintered samples.

Many theories have been advanced to illuminate the existence of a high temperature strength maximum. Bush and Hummel (1958) associated the increase in strength with the healing of microcracks at higher temperatures. Crouch and Joliffe (1970) suggested that at higher temperatures particle to particle contact increases due to thermal expansion differences causing a crack to follow a more tortuous path, resulting in increased strength. However, Padgett and Clemens (1970) ascribed the strength maximum to the relief of inherent stresses in the body which are created during pressing.

Gupta (1976) demonstrated that crack healing and strengthening in thermally shocked alumina are related to pore evolution in the microstructure during healing. The strengthening process has also been attributed to crack blunting. Inglis (1913) suggested that the blunting process may either decrease the flaw size or increase the radius of curvature at the crack tip, thus, causing an increase in the applied stress necessary for crack propagation as the critical fracture stress is attained at the crack tip. Several researchers have also proposed that the elimination of surface flaws could result in strength increase (Lange 1970). Recently, Adams (1980) suggested the concept of viscous flow and maintained that the viscous flow closes the cracks, thus reducing the critical flaw size, and contributed to the strength increase.

Chapter 3

Experimental Procedure

3.1 Introduction

In the present work, five BaZPS compositions (x=0.000, 0.175, 0.250, 0.375, 0.500) were synthesized by a solid state reaction method and the thermal and mechanical properties were studied. The phase(s) present in the synthesized compositions were identified from room temperature x-ray diffraction patterns, and the unit cell parameters were determined from the profile fit x-ray data. The densities were determined using specific gravity and geometrical methods. The amount of porosity and secondary phase particles of BaZPS compositions were determined from the obtained secondary electron micrographs and the grain size information was obtained from optical micrographs. The mode of fracture was identified from the micrographs of the fracture surfaces. The bulk linear thermal expansion of the BaZPS compositions were determined using a computer-controlled dilatometer. The mechanical properties investigated included room temperature Young's modulus, and room and high temperature flexural strengths and hardness. The Young's modulus of the compositions was measured by impulse excitation technique. The room temperature flexural strength of the compositions were determined using a standard method, and the high temperature flexural strengths were determined using a specially designed flexure test system.

The Knoop hardness of the compositions was determined employing a hardness tester. High temperature x-ray diffractomety was carried out on BaZPS with x = 0.175 to determine the axial thermal expansions and the extent of thermal expansion anisotropy.

3.2 Synthesis by solid state reaction method

Five compositions of BaZPS ceramics with x=0, 0.175, 0.250, 0.375 and 0.500 were synthesized using a solid state reaction method, also referred as powder mixing method, at LoTEC, Inc.

3.2.1 Starting materials

$BaZrO_3$ (Ferro Corporation), ZrP_2O_7 (Magnesium Elektron), and SiO_2 (U.S. Silica) were used as the starting materials (~99% pure and grain size 1-2μm) and the BET surface area of the particles were ~ 5 m^2/gm.

3.2.2 Synthesis procedure

The proper stoichiometric amounts of the precursor powders of the constituents of the desired composition were mixed and ball milled to result in a homogenized powder. The mixture was then dried in air at room temperature and calcined at 1300°C. The calcined powder was then mixed with appropriate amounts of binder and water to form a slurry. The resulting slurry was poured into square molds of 60 x 60 x 6 mm and allowed to solidify. The ceramic slabs

obtained were then bisqued at a suitable temperature to drive off the binder. The binder-free slabs were then sintered at 1600°C for 3000 minutes. To determine the significance of grain size, additionally three BaZPS compositions (x = 0.000, 0.175, and 0.500), were synthesized at 1600°C for 30 minutes and 300 minutes as well.

The procedure used for calculating the atom and weight percent of the constituents in the synthesized compositions is illustrated (Figure 3.1). The elemental atom and weight percent corresponding to the compositions synthesized is summarized (Table 3.1, and 3.2, respectively). The process flow chart is depicted (Figure 3.2). The sintered compositions, and their abbreviations are listed in Table 3.3.

3.3. Characterization

3.3.1 Room temperature x-ray diffraction

The phase(s) present in each of the five compositions of BaZPS were identified using standard x-ray powder diffraction (XRD) techniques. Each of the five sintered BaZPS compositions were crushed in a steel mortar to a very fine powder. About 50 mg of the crushed powder was then mixed with 30 mg of Si powder (NBS) and a few drops of methanol was then added to form a slurry. The slurry was deposited on a Si substrate to form a thin paste and placed in the sample fixture of the x-ray unit. After a few minutes, methanol evaporated leaving behind a thin film of the sample.

BaZPS Formula: $Ba_{1+x}Zr_4P_{6-2x}Si_{2x}O_{24}$

Procedure for calculating the atom percent (at (%)) of the BaZPS constituents

Total number of atoms in BaZPS = 35+x

Atom percent of the constituent= $\frac{\text{No of atoms of the constituent}}{\text{Total no of atoms in BaZPS}}$

at(%) computation formulas				
Ba	Zr	P	Si	O
(1+x)/(35+x)	4/(35+x)	(6-2x)/(35+x)	2x/(35+x)	24/(35+x)

Procedure for computing the weight percent (wt (%)) of the BaZPS constituents

Atomic weight is denoted by AW

Molecular weight (MW) of BaZPS is given by:

(1+x) x Ba AW + 4 x Zr AW + (6-2x) x P AW + (2x) x Si AW + 24 x O AW

wt(%) of the constituent= $\frac{\text{No of atoms of the constituent x AW of the constituent}}{\text{Molecular weight of BaZPS}}$

wt(%) computation formulas				
Ba	Zr	P	Si	O
$\frac{(1+x) \times 136.34}{\text{BaZPS MW}}$	$\frac{4 \times 91.22}{\text{BaZPS MW}}$	$\frac{(6-2x) \times 30.974}{\text{BaZPS MW}}$	$\frac{(2x) \times 28.09}{\text{BaZPS MW}}$	$\frac{24 \times 15.999}{\text{BaZPS MW}}$

Figure 3.1 Procedure for calculating the at(%) and wt(%) of the constituents in BaZPS

Table 3.1 Atom percent of the constituents in the synthesized $Ba_{1+x}Zr_4P_{6-2x}Si_{2x}O_{24}$ compositions

x value in $Ba_{1+x}Zr_4P_{6-2x}Si_{2x}O_{24}$	at(%) of				
	Ba	Zr	P	Si	O
0.000	2.857	11.428	17.143	0.000	68.572
0.175	3.340	11.372	16.063	0.995	68.230
0.250	3.546	11.348	15.602	1.418	68.086
0.375	3.886	11.307	14.841	2.121	67.845
0.500	4.225	11.268	14.084	2.817	67.606

Table 3.2 Weight percent of the constituents in the synthesized $Ba_{1+x}Zr_4P_{6-2x}Si_{2x}O_{24}$ compositions

x value in $Ba_{1+x}Zr_4P_{6-2x}Si_{2x}O_{24}$	wt(%)				
	Ba	Zr	P	Si	O
0.000	12.810	34.036	17.336	0.000	35.818
0.175	14.736	33.320	15.981	0.898	35.065
0.250	15.537	33.022	15.418	1.271	34.752
0.375	16.840	32.538	14.501	1.879	34.242
0.500	18.105	32.068	13.611	2.469	33.747

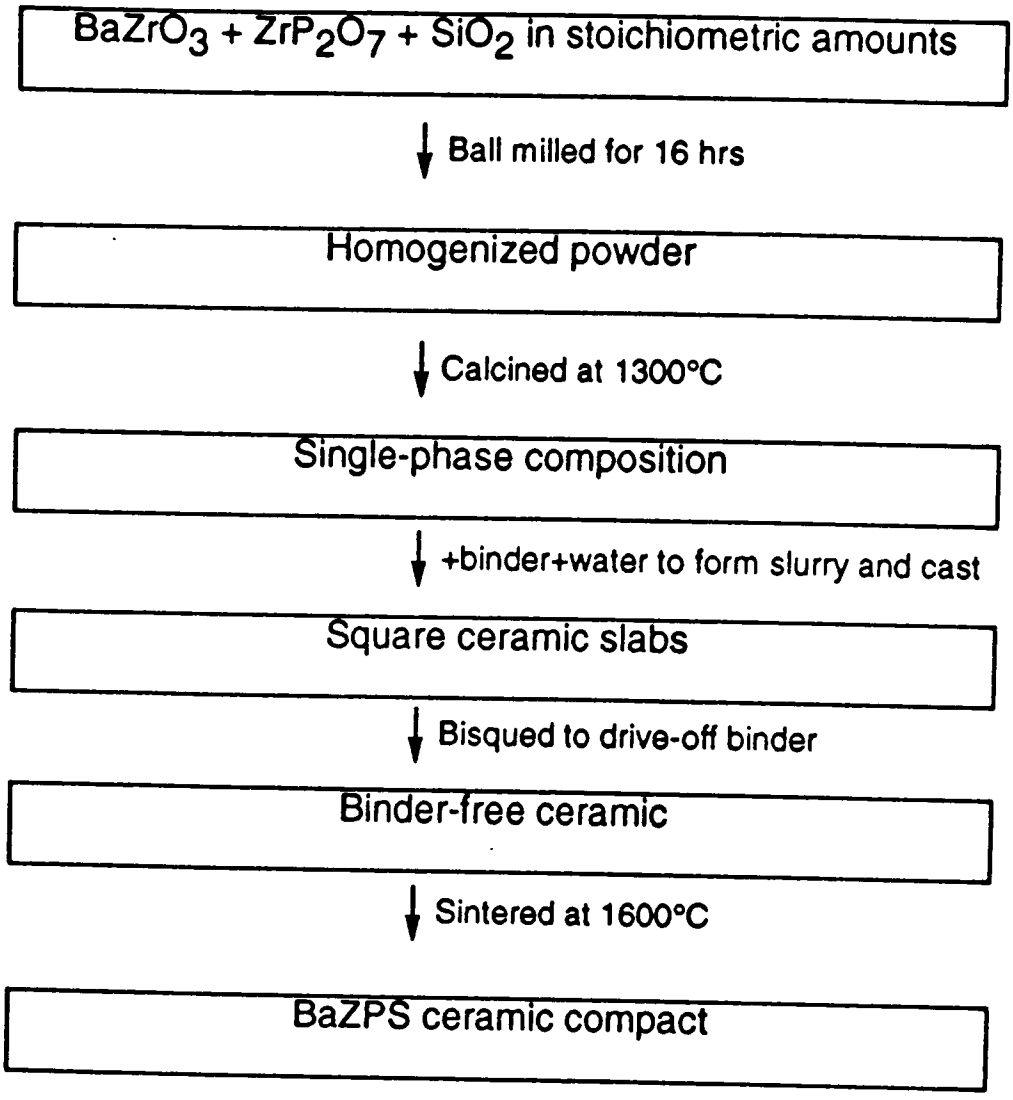

Figure 3.2 Flow chart of the general procedure for synthesis of $Ba_{1+x}Zr_4P_{6-2x}Si_{2x}O_{24}$

Table 3.3 Summary of the synthesized BaZPS compositions and their abbreviations

x value in $Ba_{1+x}Zr_4P_{6-2x}Si_{2x}O_{24}$	General abbreviation of the composition	Abbreviations of the synthesized compositions		
		Sintered for 30 minutes	sintered for 300 minutes	sintered for 3000 minutes
0.000	BS0	BS01	BS02	BS03
0.175	BS17	BS171	BS172	BS173
0.250	BS25			BS253
0.375	BS37			BS373
0.500	BS50	BS501	BS502	BS503

X-ray powder diffraction data from each of the five compositions were obtained on a Scintag 2θ/θ goniometer (Scintag, Inc.) equipped with a germanium single-crystal solid-state detector and a Cu x-ray tube. The patterns were collected over a scan range of 5 to 98° 2θ at the rate of 0.1 °/min. The obtained patterns were identified by comparison with the Joint Committee on Powder Diffraction Standards (JCPDS) pattern of barium zirconium phosphate (File # 34-95). The background correction and $K\alpha_2$ peak stripping was then done and the peak positions and intensities were determined using a profile fitting program (Scintag 1989).

For computing unit cell parameters accurately, the following procedure was adopted. To account for possible instrumental and sample mounting aberrations, the observed peaks were calibrated by the CALIBR93 program (Hubbard and Sokol 1990), using the certified peak positions for the Si internal standard. The crystal system and approximate unit-cell parameters were entered using the EDPK93 program (Hubbard and Sokol 1990), and the cell parameters were refined by the LSQ93 program (Hubbard and Sokol 1990), a local version of the lattice parameter refinement program.

3.3.2 Density measurement

Densities of the sintered BaZPS compositions were determined by two techniques: the geometrical and specific gravity methods. The densities obtained were then compared with the corresponding theoretical density.

In the geometrical method, the density was obtained by dividing the mass of the sintered sample by its geometrical volume. In the specific gravity method, the samples were first weighed in air and then weighed in water. The saturated sample was then weighed in air. Density of the sintered sample, ρ_a, was then computed using the formulae:

$$\rho_a\,(gm/cm^3) = \frac{W1}{W3-W2} \times \rho_w \qquad (3.1)$$

where W1, W2, and W3, represent the weights of the sintered sample in air, water and in saturated condition, respectively, and ρ_w is the density of water. The theoretical density, ρ_t, was calculated using the formula:

$$\rho_t\,(gm/cm^3) = \frac{Z \times M_a}{N_A \times V} \qquad (3.2)$$

where Z is the number of formula units per unit cell, M_a, the formula weight, N_A, Avogadro's number, and V, the unit cell volume.

3.3.3 Microstructural characterization

Polished cross-sections of each of the five compositions were prepared as described below. The sample was mounted with the 4 x 3 mm side facing the die and epoxy was poured over it and allowed to set for 16 hours. The specimen was then removed from the die and an identification mark was engraved. The sample was ground parallel using a 200 grit, resinoid bonded diamond wheel followed by another round of grinding on a 600 grit, resinoid bonded grinding wheel on a

surface grinder. The sample was then rough polished using a 6 μm diamond paste (DP) on a wire mesh cloth followed by rough polishing using a 6 μm DP on a perforated cloth. Final polishing was carried out in two steps. First, the sample was polished using a 3 μm DP on a texmet cloth. Then, the sample was polished using a 0.5 μm DP on a nylon cloth to obtain an optical surface finish. The polished samples were coated with a thin layer of gold to reduce the tendency for electrical charge build-up. The polished samples thus prepared were viewed in a Hitachi S-800 field emission gun scanning electron microscope (SEM), operated at 25 keV. The amount of porosity, and secondary phase particles of the compositions were determined using a point sampling method and the results reported are an average obtained from 7 micrographs. The sample compositions of the end members (BaZPS with $x = 0.000$, and 0.500) were also determined from the polished samples using energy dispersive x-ray analysis (EDS).

The polished samples were etched with a 10% HF solution for around 25 minutes. The large grain-sized samples required etching for an additional 5 minutes. The etched samples were viewed using an optical microscope and the grain sizes were determined using the linear intercept method (average of 5 micrographs).

The room temperature fracture cross-sections of the sintered samples were studied using the SEM at 5keV, with a thin layer of gold to reduce the tendency for electrical charge build-up. The mode of fracture was then identified from the recorded micrographs.

3.3.4 Bulk linear thermal expansion measurement

The bulk linear thermal expansion of BaZPS compositions were determined using a computer-controlled dual push rod dilatometer made by Theta Industries, Inc. The thermal expansion measurement was carried out between 25 and 900°C. A 25.4 mm long single-crystal alumina rod was used as the reference material and the sintered samples used were 25.4 x 4 x 3 mm. The furnace was heated at the rate of 10°C/min, maintained at the maximum temperature for a period of 10 min, and then cooled at the rate of 10°C/min to 300°C. Below 300°C, natural cooling was employed by switching off the furnace.

3.3.5 High temperature x-ray diffractometry

High temperature x-ray diffractometry was carried out to determine the axial thermal expansion of BS173 using a Scintag PAD X θ/θ diffractometer (Scintag, Inc.) equipped with a constant potential x-ray generator operating at 45KV/40mA with a Cu target, an Edmund Buehler high temperature XRD furnace with a beryllium window and Pt/Rh heating strip, and a liquid nitrogen cooled germanium single-crystal solid-state detector. The major advantage of this set up is that the specimen remains horizontal and is unperturbed by the goniometer movements. Further, the high temperature furnace remains stationary and the diffraction patterns are collected on the same area of the sample throughout the experiment.

A type-s thermocouple spot welded to the bottom surface of the heating strip enables temperature measurement of the sample. The sintered BS173

sample was crushed in a steel mortar to a very fine powder. About 50 mg of the crushed powder was then mixed with 30 mg of Si powder (NBS). This mixture was then used in the high temperature diffractometer. About 50 mg of the prepared mixture was mixed with a few drops of methanol to form a slurry. The slurry was then spread evenly on the Pt/Rh heating strip. Methanol evaporated after a few minutes leaving behind a thin film of the sample on the strip. A calibrated Micristar temperature controller ensured that the selected heating/cooling rates are maintained and the strip temperature is kept within ±1°C.

X-ray diffraction patterns were obtained in an argon atmosphere over the scan range of 17.5 to 67.5°2θ at the rate of 0.1°/min, at 27°C, 200°C, 400°C, 600°C, 800°C, and 900°C during heating, and at 850°C, and 27°C during cooling. Heating and cooling rates were 10°C/min. Data collection was started after a 1 min hold at all the temperatures. The procedure followed for computing unit cell parameters is described in detail in section 3.3.1.

The axial thermal expansion coefficients at different temperatures can be calculated from the measured lattice parameters. α_a, and α_c, represent the thermal expansions in the a and c directions, respectively, and are calculated using the following formulae:

$$\alpha_a = \frac{a2-a1}{(T2-T1)\ x\ a1} \qquad (3.3)$$

and,

$$\alpha_c = \frac{c2-c1}{(T2-T1)\ x\ c1} \qquad (3.4)$$

where a1, and c1, are the lattice parameters at temperature T1; and a2, and c2, are the lattice parameters at temperature T2, with T2>T1.

3.3.6 Young's modulus measurement

The room temperature Young's modulus of each of the five BaZPS compositions was determined using an impulse excitation technique (IET). In this method, the transient vibration of a test object is analyzed after excitation by means of a mechanical impulse. A Grindo-sonic instrument (J. W. Lemmens, Inc.) was used which utilizes an electronic circuit to isolate the harmonics and the fundamental resonant frequency from the noise spectrum. It, then determines the period corresponding to the fundamental frequency by using a crystal reference oscillator and displayed in digital form. A block diagram of the IET method is illustrated in Figure 3.3.

The test object is positioned preferably at the nodes of the desired vibrational mode. The vibrational mode may be longitudinal, flexural or torsional. The size of the samples used were about 50 x 4 x 3 mm. For the present work, the longitudinal mode of vibration was studied because the flexural and torsional modes of vibration would be difficult to induce in samples having very small thickness and width, and could lead to erroneous measurements. When the excitation impulse is positioned correctly, to induce a longitudinal mode of vibration, it produces a fundamental resonant frequency value which is repeatable. The excitation impulse was produced by tapping on the sample using a hard

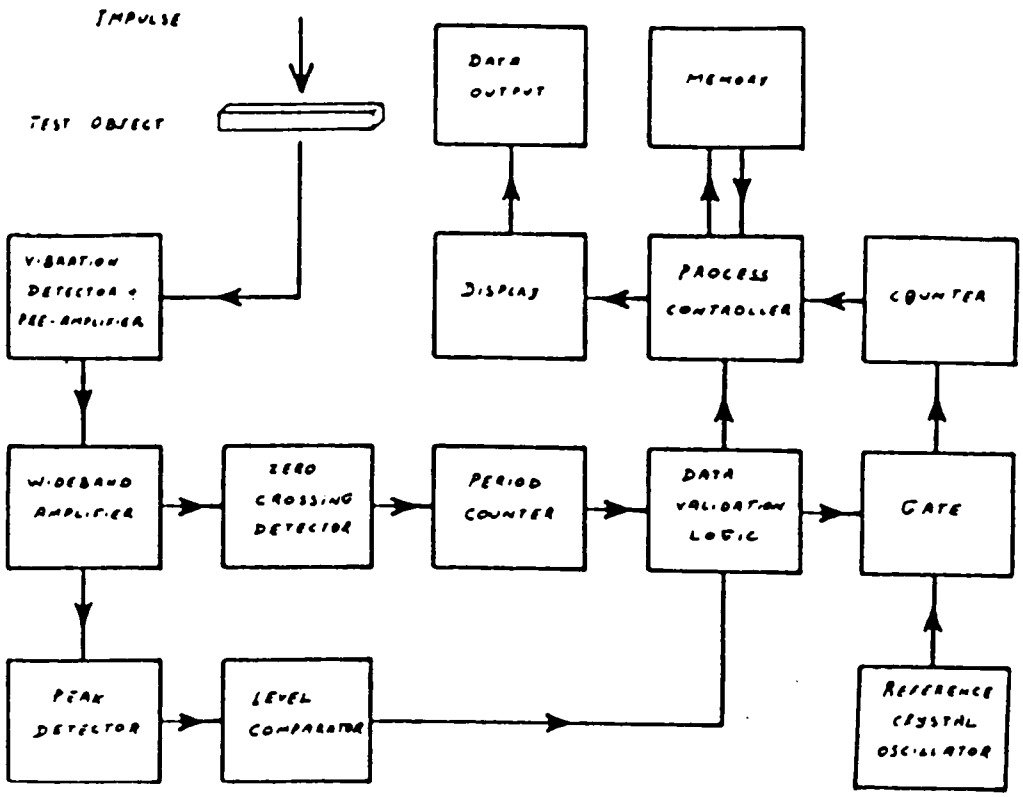

Figure 3.3 Block diagram of the impulse excitation technique

SOURCE Wolfenden et al. (1989) "Dynamic Young's Modulus Measurements in Metallic Materials: Results of an Interlaboratory Testing Program," JTEVA **17**, 2-13

rubber ball ~6.17 mm in diameter at the end of a thin steel wire ~122 mm long. The vibrational motion was detected by means of a hand held piezo-electric probe. The resulting relaxation takes the form of a damped vibration. The vibration produced depends on the nature of the material as well as the geometry and mass of the test piece. The damped vibration is then amplified and electronically analyzed to obtain the fundamental resonant frequency. After that, the Young's modulus, E, is calculated using the prism equation for the longitudinal mode provided by Spinner and Tefft (1961):

$$E = \left(\frac{\varrho}{S}\right)\left(2\frac{lf}{n}\right)^2 \qquad (3.5)$$

where S is given by,

$$S = 1 - \left(\frac{\pi n^2 \mu^2 d^2}{8l^2}\right) \qquad (3.6)$$

d is given by

$$d = \sqrt{\frac{2(a^2+b^2)}{3}} \qquad (3.7)$$

and, where f is the harmonic frequency of order n, l is the length of the specimen, ϱ is the density, a and b are the length and width of the sample, respectively, μ is the poisson's ratio, d is the equivalent diameter, and t is the thickness.

3.3.7 Room temperature flexural strength measurement

The room temperature flexural strength of the BaZPS compositions was determined using a testing machine (Model 1122) manufactured by Instron Corporation. The flexural strength, often termed the modulus-of-rupture (MOR), was determined using a four-point bend test fixture (with 40 mm and 20 mm as outer and inner spans, respectively) on an Instron equipped with a 500 Kg compression load cell.

The flexural test specimens were 50 x 4 x 3 mm with all surfaces ground to 0.0004 mm finish (MIL-STD-1942A 1990). To minimize edge failures, the long edges of the tensile surface were beveled. The specimen was placed in the fixture and loaded during the downward motion of the crosshead. The crosshead speed utilized was 5.08 mm/min. Three specimens of each of the compositions were tested at room temperature.

The flexural strength, σ_f, was computed using the formula:

$$\sigma_f = \frac{3P(L-a)}{2bh^2} \qquad (3.8)$$

where P is the failure load, L and a are the outer and inner span lengths of the fixture, respectively, and b and h are the width and height of the sample, respectively.

3.3.8 High temperature flexural strength measurement

High temperature fast fracture tests were performed in a specially designed flexure test system (FTS) capable of separately testing up to three flexure samples concurrently in series or parallel. The MOR bars used were 50 x 4 x 3 mm and machined according to specifications described in section 3.3.7.

The MOR bars were subjected to a four-point loading using a fixture having an outer and inner span of 40 and 20 mm, respectively. The testing of the bars were carried out at 200°C, 600°C, and 1000°C. At each temperature, three specimens of each of the BaZPS compositions were tested. The furnace was ramped to the desired test temperature and the samples soaked for 5 minutes, and tested using the series option.

3.3.9 Hardness measurement

The hardness testing was conducted on a TUKON SERIES 200 hardness tester manufactured by Wilson Instruments, Inc. The BaZPS sample used was 12 x 4 x 3 mm. The samples were mounted with the 12 x 4 mm side facing the die and epoxy was poured over it and allowed to set for 16 hours. The specimens were then removed from the die and an identification mark was engraved. The samples were ground parallel using a 200 grit, resinoid bonded diamond wheel followed by another round of grinding on a 600 grit, resinoid bonded grinding wheel on a surface grinder. The samples were rough polished using a 6 μm DP on a wire mesh cloth followed by rough polishing utilizing a 6 μm DP on a perforated

cloth. Final polishing was carried out in two steps. First, the samples were polished using a 3 μm DP on a texmet cloth. Then, the sample was polished using a 0.5 μm DP on a nylon cloth to obtain an optical surface finish.

The hardness indentations were made using a Knoop indenter with loads of 50-300 gms at a constant loading time of 10 sec. The diagonal of the indentations were measured using a VIA-110 Video Hardness Measurement system, which is attached to the hardness tester. The VIA-110 was calibrated first using the recommended calibration procedure before the measurements were made. The Knoop hardness was then calculated using the relation:

$$H_k = 139.6 \left(\frac{P}{d^2}\right) \qquad (3.9)$$

where H_k is the Knoop hardness in GPa, P is the load in grams, and d is the diagonal of the indentation in μm.

3.3.10 Differential scanning calorimetry

A differential scanning calorimeter (DSC) manufactured by Stanton Redcroft Instruments was used to study whether any phase transitions were occuring in the BS17 compositions. BS172 was used as the sample and was placed in the Pt crucible with sapphire as the reference material, and the DSC furnace was ramped at 50°C/min between 20°C and 1000°C.

Chapter 4

Results

In this chapter, the mechanical and thermal property results of the BaZPS compositions are reported. The densities of the BaZPS ceramics sintered for 3000 minutes were more than 84.44% of the theoretical density. Room temperature x-ray diffraction results indicate that all the BaZPS ceramics were essentially single phase. However, few unindentified peaks existed in BS173 and BS503. The amount of porosity and secondary phase particles were determined from the SEM micrographs of the polished cross-sections, and were found to be less than 25.2%, and 4.7%, respectively. The mode of fracture of the BaZPS ceramics were identified from the SEM images of the fracture surfaces and changed from predominantly transgranular fracture to intergranular fracture (BS50 compositions) with increasing silicon content. EDS studies confirmed the stoichiometry of the matrix phase in BS03, BS173 and BS503. BaZPS ceramics were found to exhibit very low thermal expansion ($< 2.14 \times 10^{-6}\ ^{\circ}C^{-1}$) and BS173 shows very low thermal expansion anisotropy. BaZPS compositions possess good flexural strength, and BS373 showed the highest flexural strength. The room temperature hardness, and the Young's modulus results indicate that the BS373 composition has the highest hardness and stiffness. DSC results indicate that the BS17 compositions undergo a phase transition between 560°C and 780°C.

4.1 Synthesis

The BaZPS compositions were synthesized using the procedure described in section 3.2. The synthesized BaZPS compositions prior to sintering were 60-65% of the theoretical density. After sintering, their density varied from 77.5% to 98% of the theoretical density. This increase could be attributed to the densification that occurred during the sintering process.

4.2 Room temperature x-ray diffraction

4.2.1 Phase(s) identification

Room temperature x-ray diffraction patterns were obtained for BS03, BS173, BS253, BS373, and BS503 and are shown in Figures 4.1-4.5. The BS03 pattern well matched the JCPDS pattern for $BaZr_4P_6O_{24}$ (File # 34-95), thus identifying the matrix phase. Standard JCPDS patterns are not available for compositions, BS173, BS253, BS373, and BS503, and hence comparison was made with the $BaZr_4P_6O_{24}$ JCPDS pattern. It was observed that the obtained patterns did match well with the JCPDS pattern. The BS03 pattern compared with the JCPDS pattern of $BaZr_4P_6O_{24}$ is shown in Figure 4.6.

4.2.2 Unit-cell parameter results

The obtained x-ray patterns of BS03, BS173, BS253, BS373, and BS503 were profile fit, and then calibrated using the certified peak positions for the Si

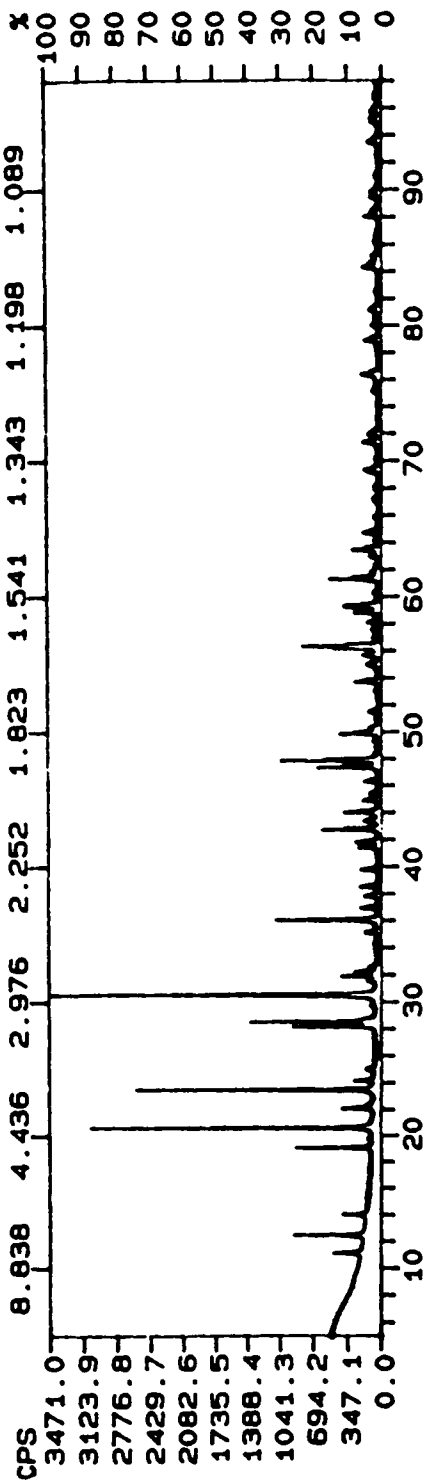

Figure 4.1 Room temperature x-ray diffraction pattern of BS03

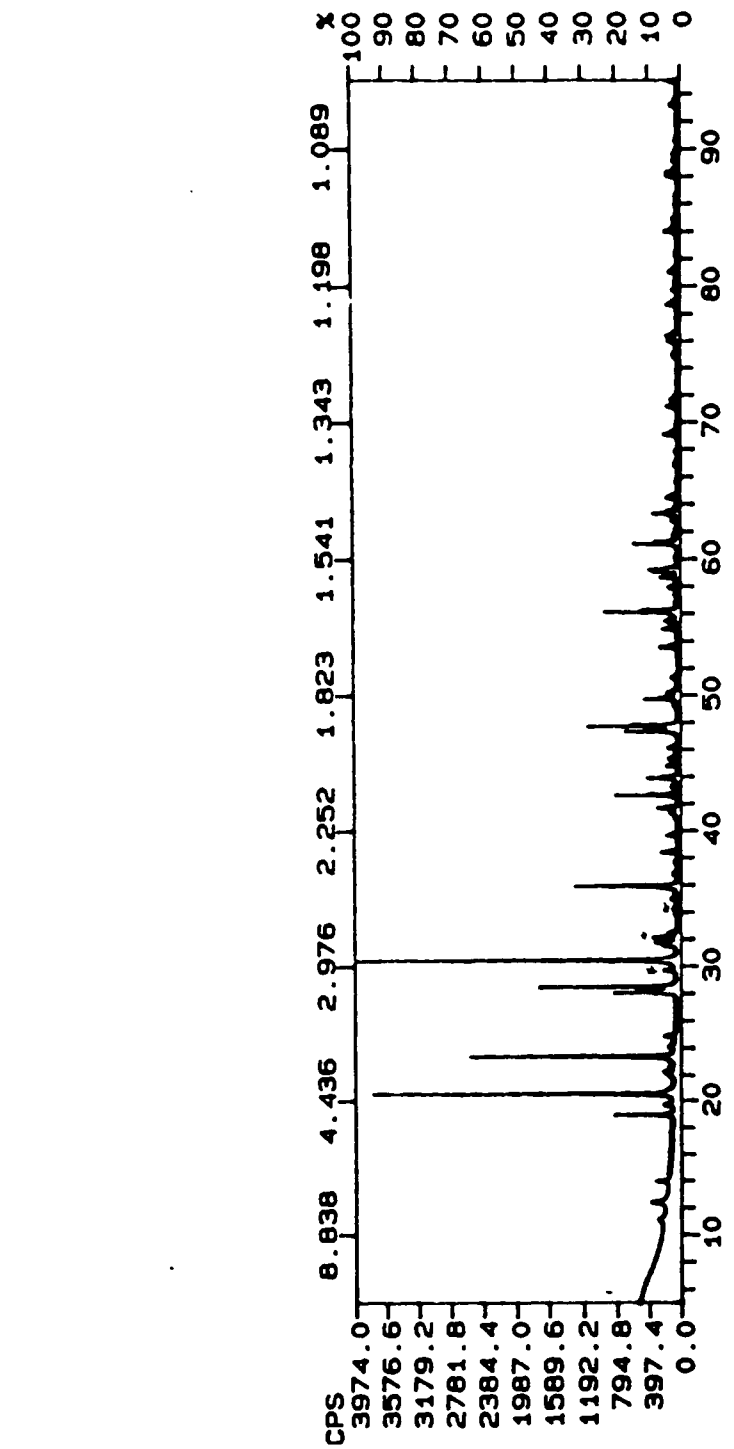

Figure 4.2 Room temperature x-ray diffraction pattern of BS173

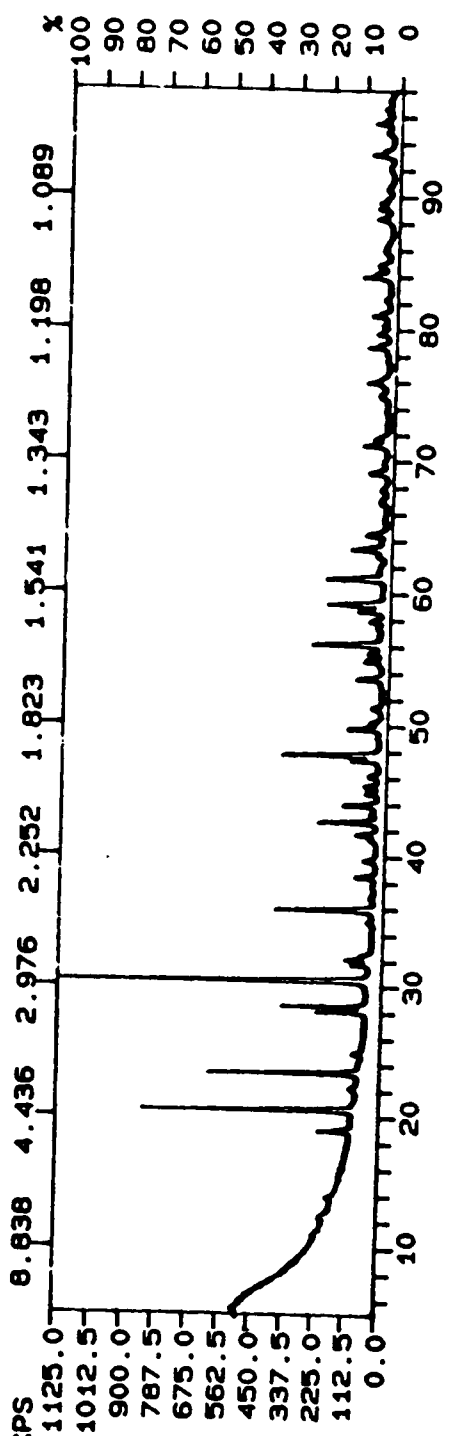

Figure 4.3 Room temperature x-ray diffraction pattern of BS253

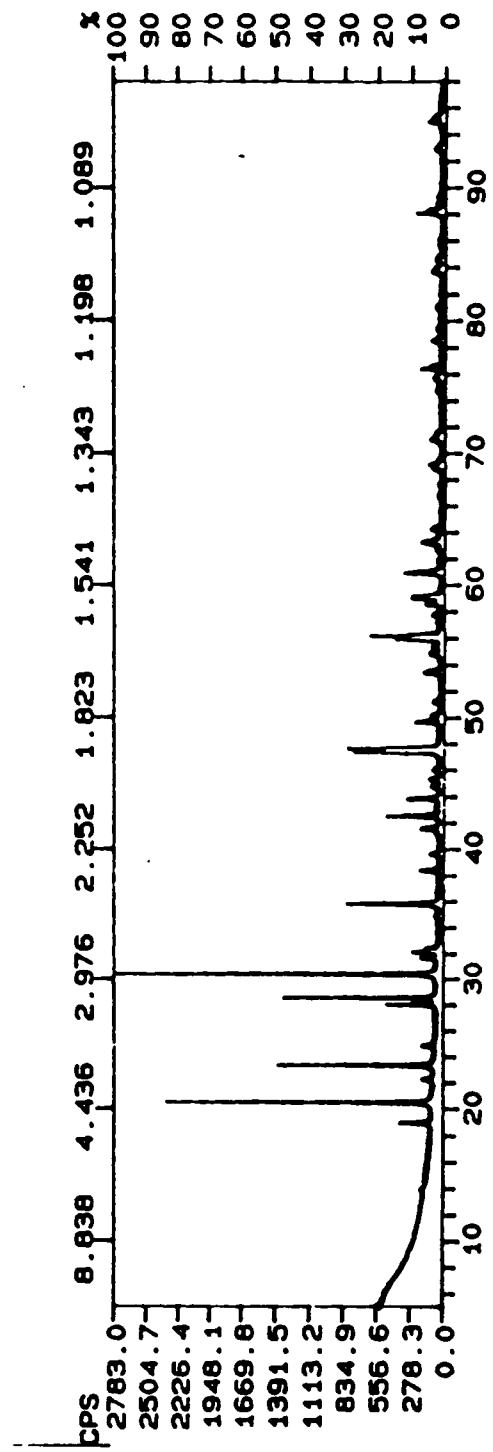

Figure 4.4 Room temperature x-ray diffraction pattern of BS373

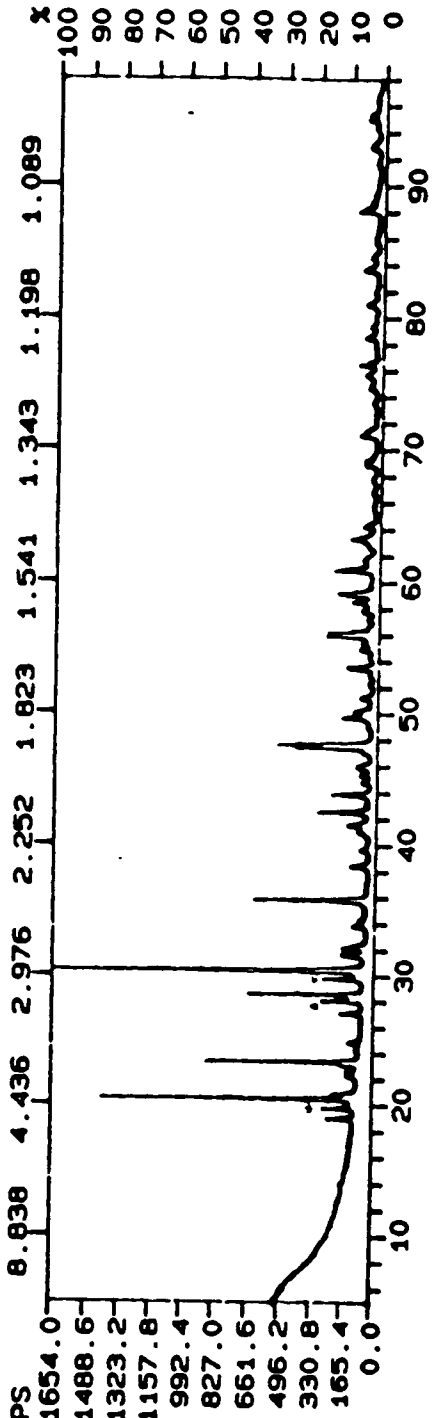

Figure 4.5 Room temperature x-ray diffraction pattern of BS503

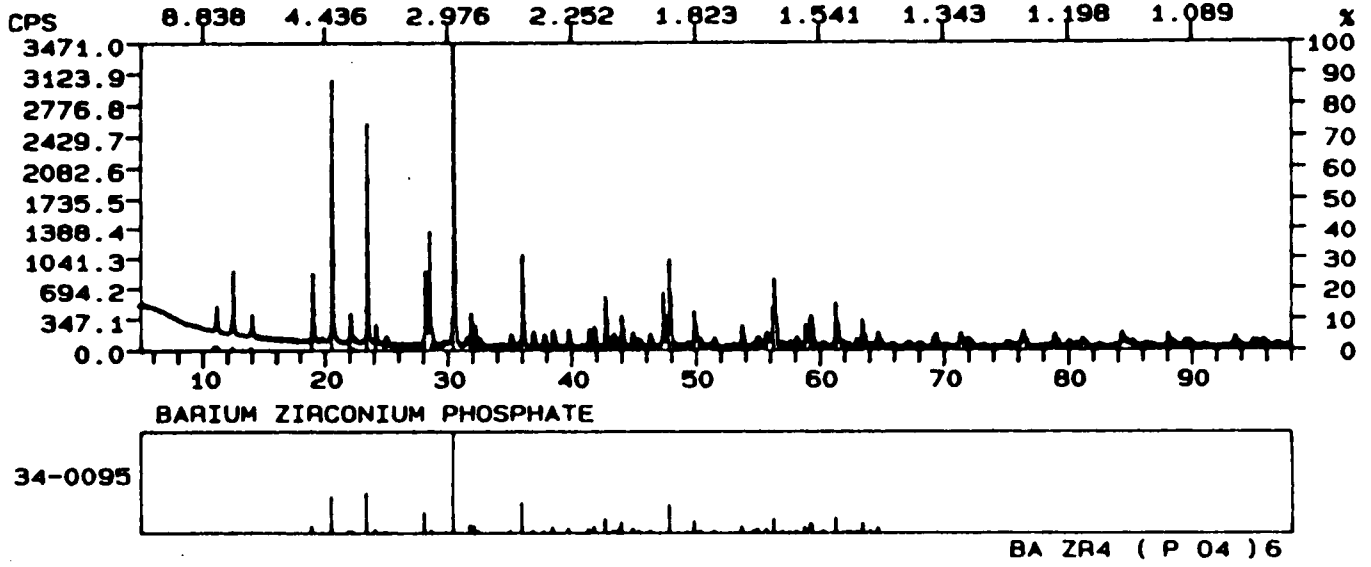

Figure 4.6 Comparison of JCPDS pattern of $BaZr_4P_6O_{24}$ with the room temperature x-ray diffraction pattern of BS03

internal standard. The calibrated peaks were then indexed in the rhombohedral system with the hexagonal setting (space group R-3), and the unit-cell parameters were determined following the procedure described in section 3.3.1. In the case of BS03, BS253, and BS373 all the peaks were indexed suggesting that they were single-phase. However, unindexed peaks were observed in BS173, and BS503 (Table 4.1) and indicated in the x-ray patterns of Figures 4.2, and 4.5. The unindexed peaks of BS173 did not match with any of the available JCPDS patterns. Two unindexed peaks of BS503 matched the JCPDS pattern of $BaZrP_2O_8$ (JCPDS File # 25-85).

The unit-cell parameters along with the number of peaks used for the calculation, unit-cell volume, number of unidexed peaks, and the $\Delta 2\theta$ values are summarized in Table 4.2. $\Delta 2\theta$ represents the average angular deviation of the observed peak positions from the calculated peak positions. The variation of the a parameter, the c parameter, and the volume changes associated with increasing Si content in the BaZPS compositions is shown in Figures 4.7, 4.8, and 4.9, respectively. The a parameter varied between 0.864266 and 0.870415 nm, the c parameter ranged between 2.398754 and 2.402034 nm, and the unit cell volume was between 1.552 and 1.576 nm^3 for the BaZPS compositions with variation in Si content. The a parameter and the unit cell volume increased with increasing Si content till BS173, dropped for BS253, and again increased. However, the c parameter initially increased to BS173, then decreased for BS253, increased for BS373, and again decreased for BS503 with increasing Si content in the BaZPS

Table 4.1 Unindexed peaks of BS173 and BS503

BS173		BS503	
Unidexed 2θ peak	Match with the JCPDS pattern of	Unidexed 2θ peak	Match with the JCPDS pattern of
29.697	None	19.737	$BaZrP_2O_8$
31.771	None	27.051	None
34.202	None	29.744	$BaZrP_2O_8$

Table 4.2 Unit cell parameter results for BaZPS compositions

Composition with # peaks used	a (x 10^{-10} m)	c (x 10^{-10} m)	Unit cell volume (x 10^{-30} m^3)	# peaks unindexed	Δ2θ
BS03 - 66	8.64266(21)*	23.98754(112)*	1552	0	0.000
BS173 - 68	8.66645(23)	24.00839(113)	1562	3	0.002
BS253 - 52	8.66398(46)	23.99634(209)	1560	0	-0.015
BS373 - 48	8.69730(31)	24.03785(129)	1575	0	0.001
BS503 - 48	8.70415(47)	24.02034(220)	1576	3	-0.001

*Data within the brackets indicate the standard deviations of the last few digits

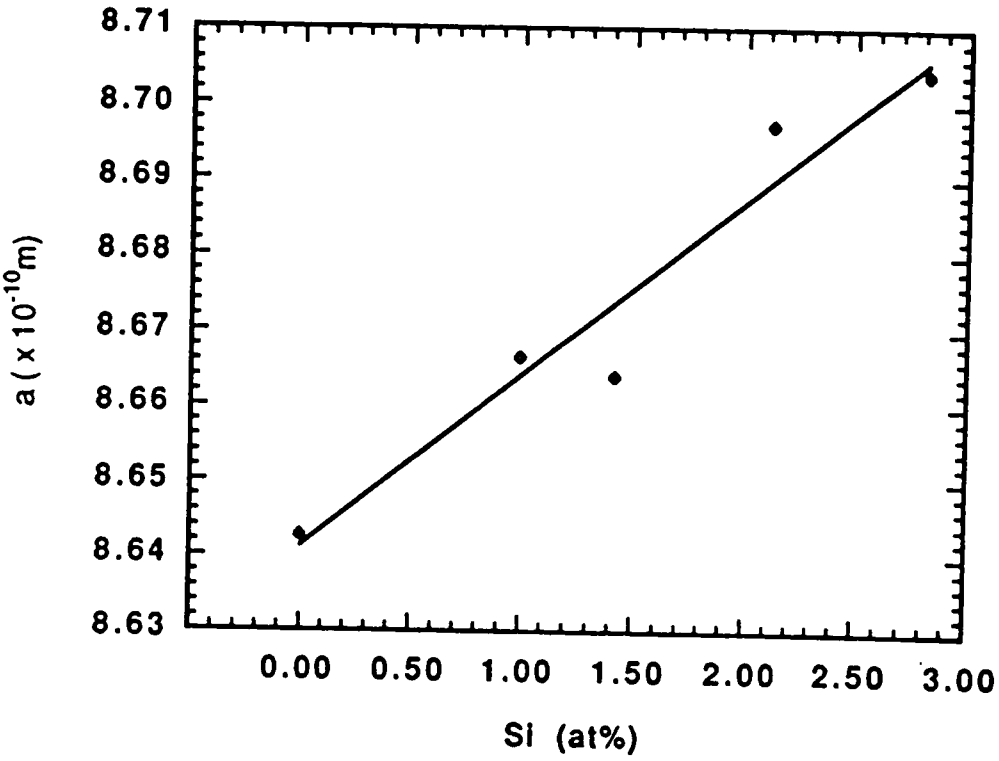

Figure 4.7 Variation of cell parameter "a" with increasing silicon content

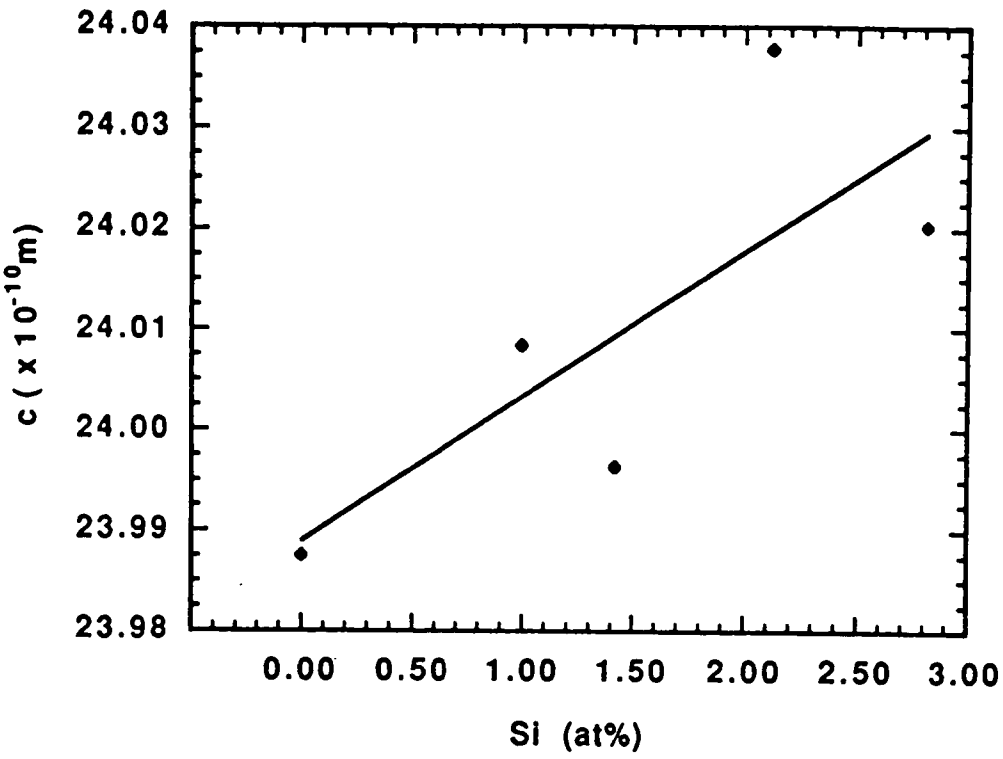

Figure 4.8 Variation of cell parameter "c" with increasing silicon content

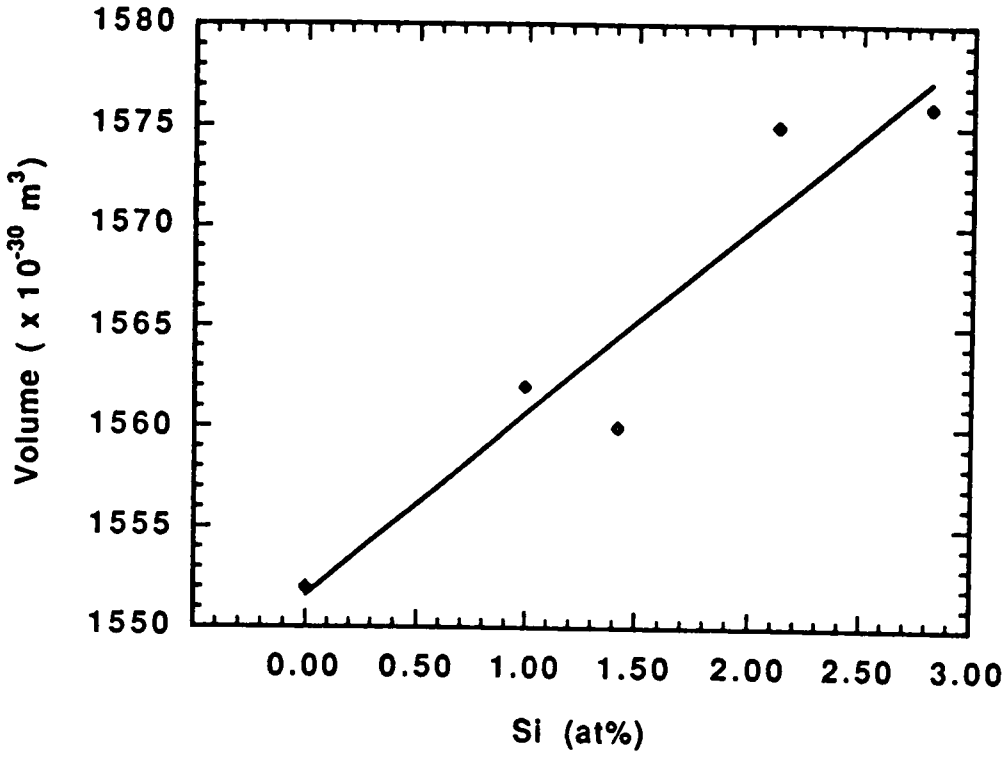

Figure 4.9 Variation of unit-cell volume with increasing silicon content

compositions.

4.3 Density

The densities of the BaZPS compositions were measured using geometrical and specific gravity methods (Table 4.3). The theoretical densities of the BaZPS compositions were determined using the computed lattice parameter values obtained from the room temperature XRD patterns (Table 4.3). The theoretical densities increased with increasing Si content for the BaZPS compositions The experimental densities ranged from 77.5% to 98.5% of theoretical. It was observed that the experimental densities decreased with increasing Si content, with BS373 being the exception (Figure 4.10). The experimental densities also increased with increasing sintering time (Table 4.4) and could be ascribed to the densification and elimination of pores that occurs with longer sintering.

4.4 Microstructure

The secondary electron images of the polished cross sections of the various specimens are shown in Figures 4.11-4.15. The amount of porosity, and secondary phase particles were determined for all the sintered compositions using a point counting method, and the results reported are an average obtained from 7 micrographs and is shown in Table 4.5. The grain sizes of each of the five compositions were determined from the optical micrographs of the etched specimens and the results reported are an average obtained from 5 micrographs

Table 4.3 Variation of density with composition

Composition	Theoretical density (gm/cm^{3})	Experimental density (gm/cm^{3})	% of theoretical density
BS03	3.44	3.24	94.18
BS173	3.49	3.21	91.97
BS253	3.53	3.20	90.90
BS373	3.55	3.50	98.59
BS503	3.60	3.04	84.44

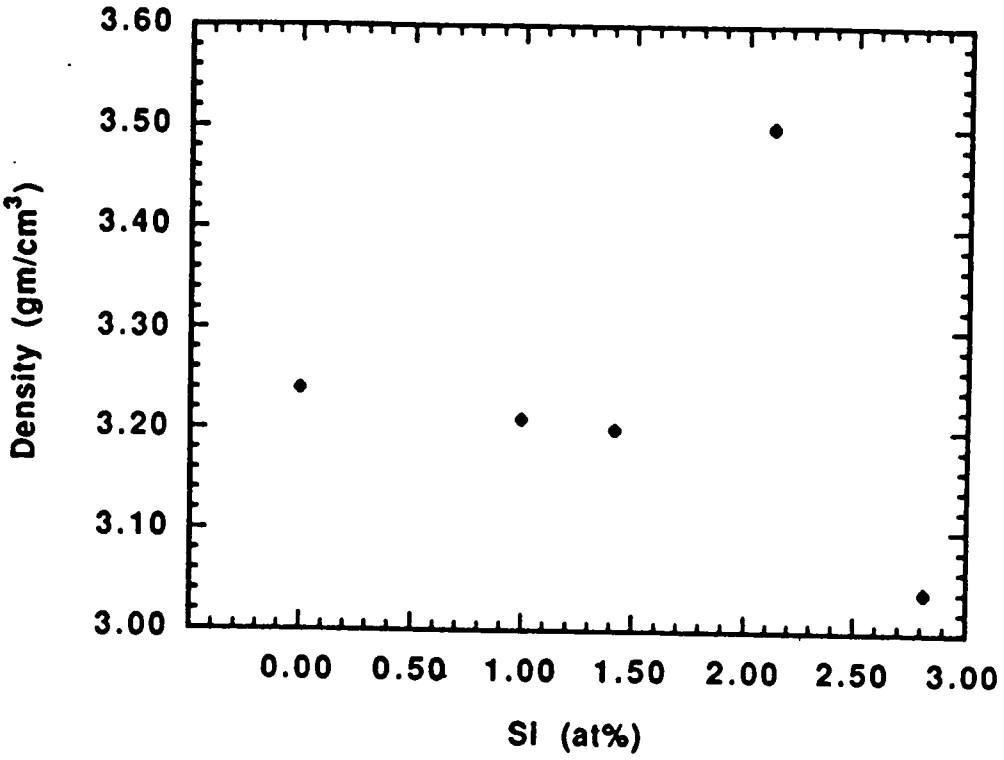

Figure 4.10 Variation of density with increasing silicon content

Table 4.4 Effect of sintering time on the density of BaZPS compositions

Composition Sintering time (min)--->	Theoretical density (gm/cm^3)	Experimental density, gm/cm^3 (% of theoretical density)		
		30	300	3000
BS0	3.44	2.98 (86.63)	3.10 (90.11)	3.24 (94.18)
BS17	3.49	2.90 (83.09)	3.01 (86.38)	3.21 (91.97)
BS50	3.60	2.79 (77.5)	2.92 (81.11)	3.04 (84.44)

(a)

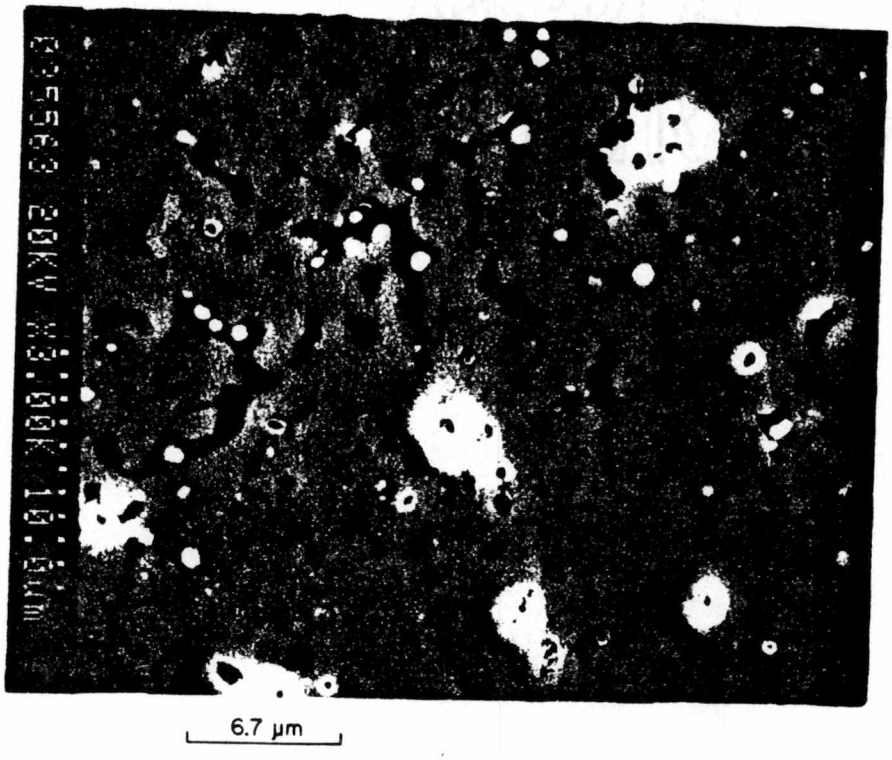

(b)

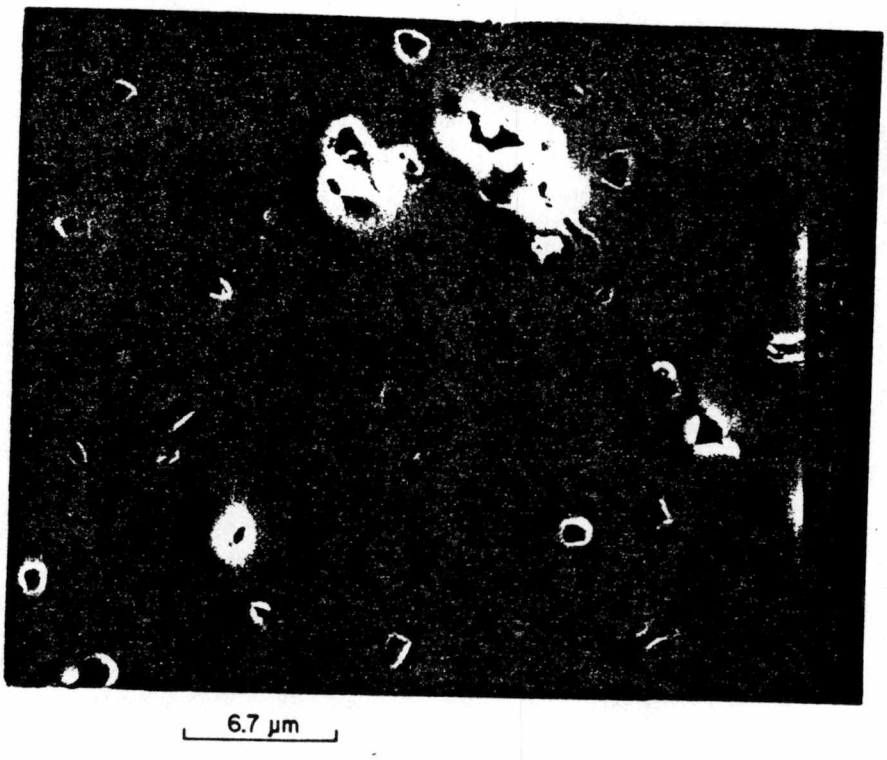

Figure 4.11 Secondary electron images of polished cross-sections of BS0 (a) BS01 (b) BS02 (c) BS03

(c)

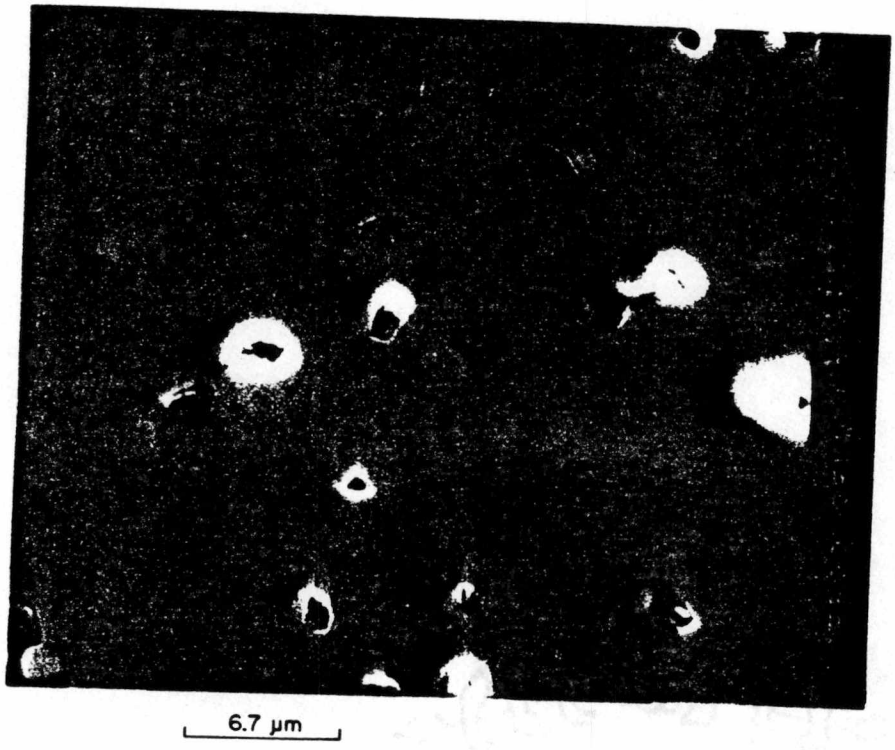

Figure 4.11 (continued) (c) BS03

(a)

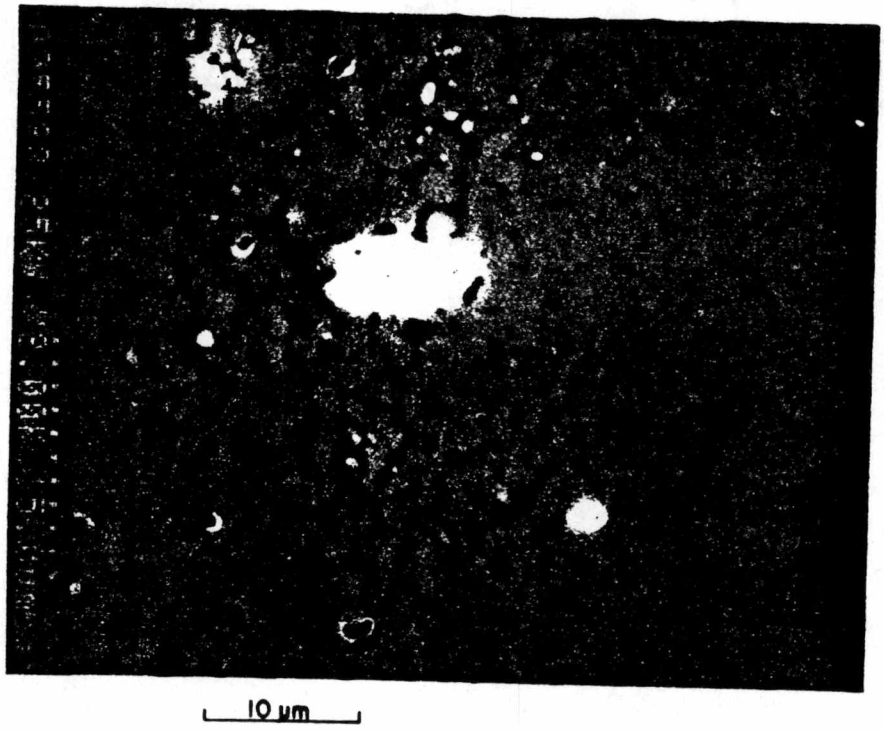

(b)

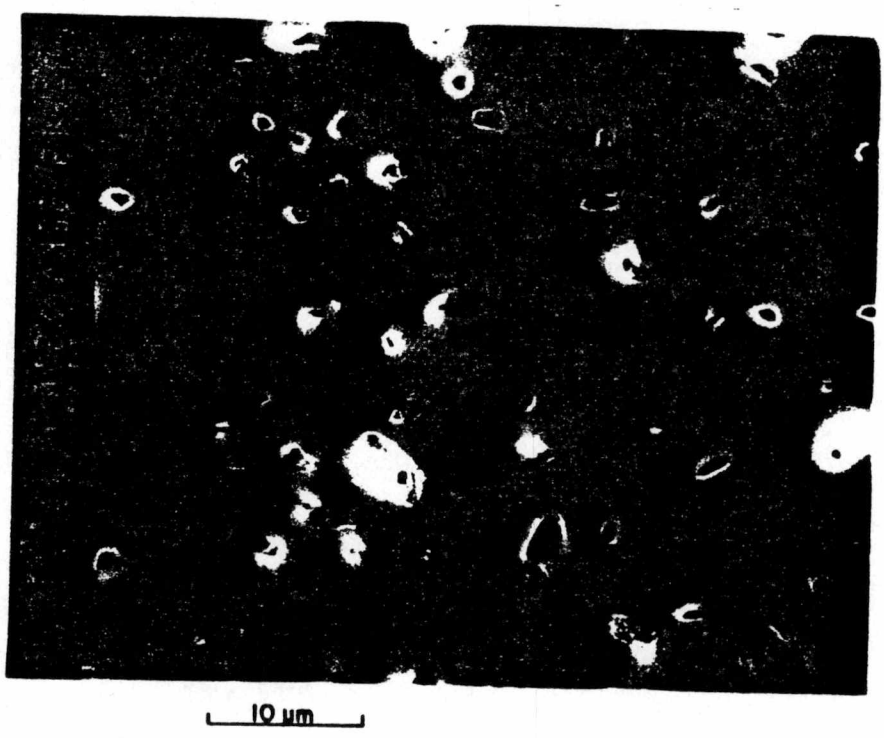

Figure 4.12 Secondary electron images of polished cross-sections of BS17 (a) BS171 (b) BS172 (c) BS173

(c)

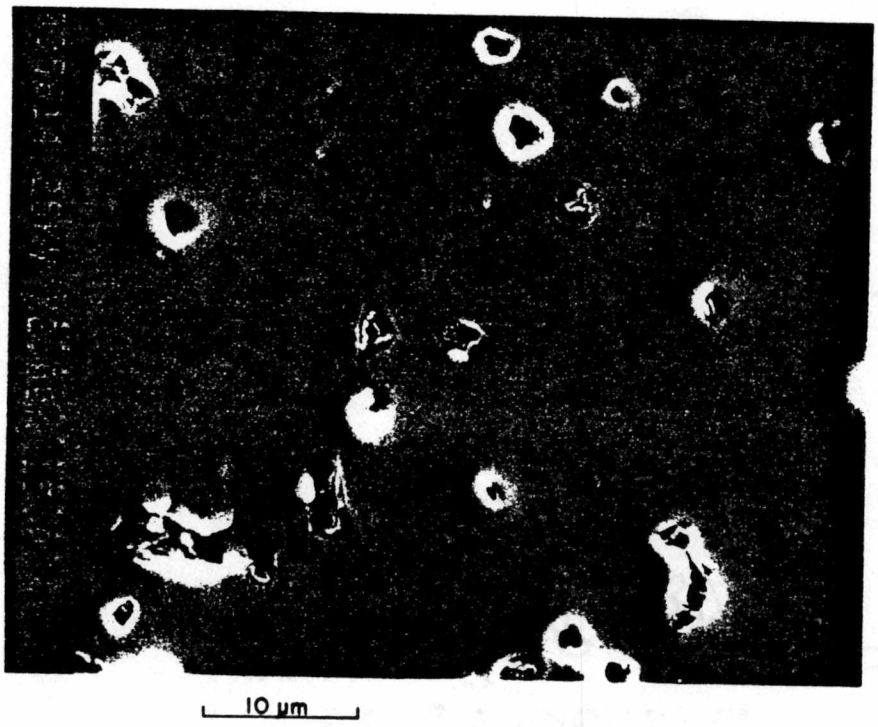

Figure 4.12 (continued) (c) BS173

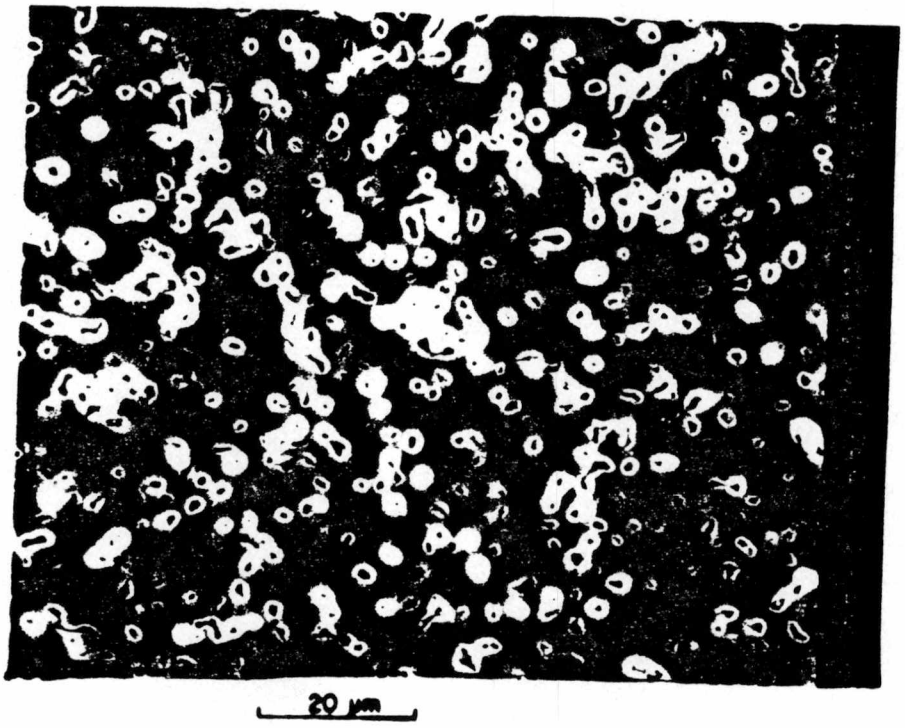

Figure 4.13 Secondary electron image of a polished cross-section of BS253

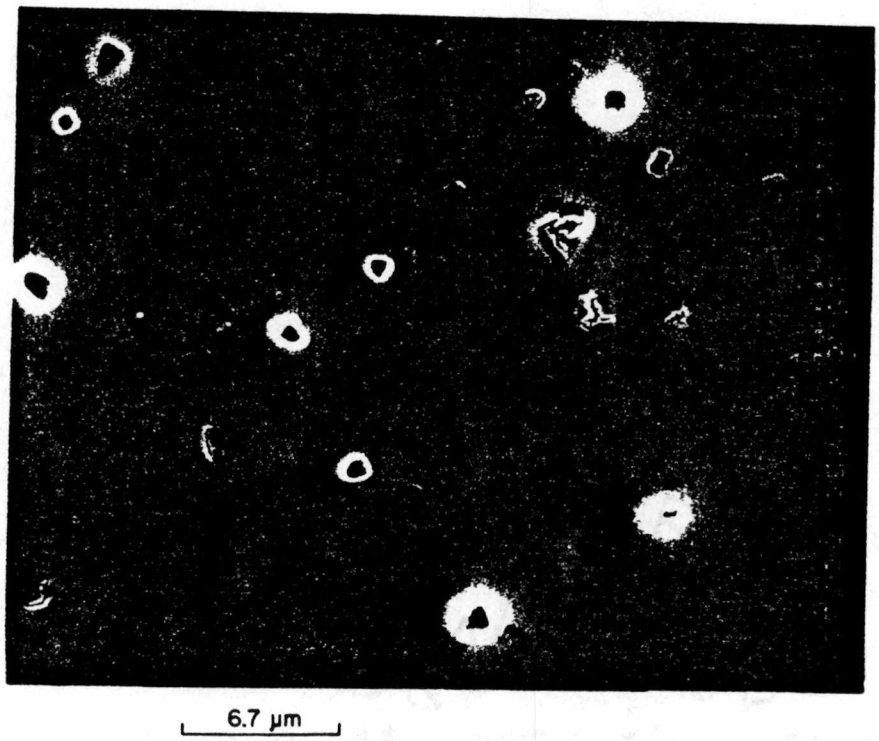

Figure 4.14 Secondary electron image of a polished cross-section of BS373

(a)

(b)

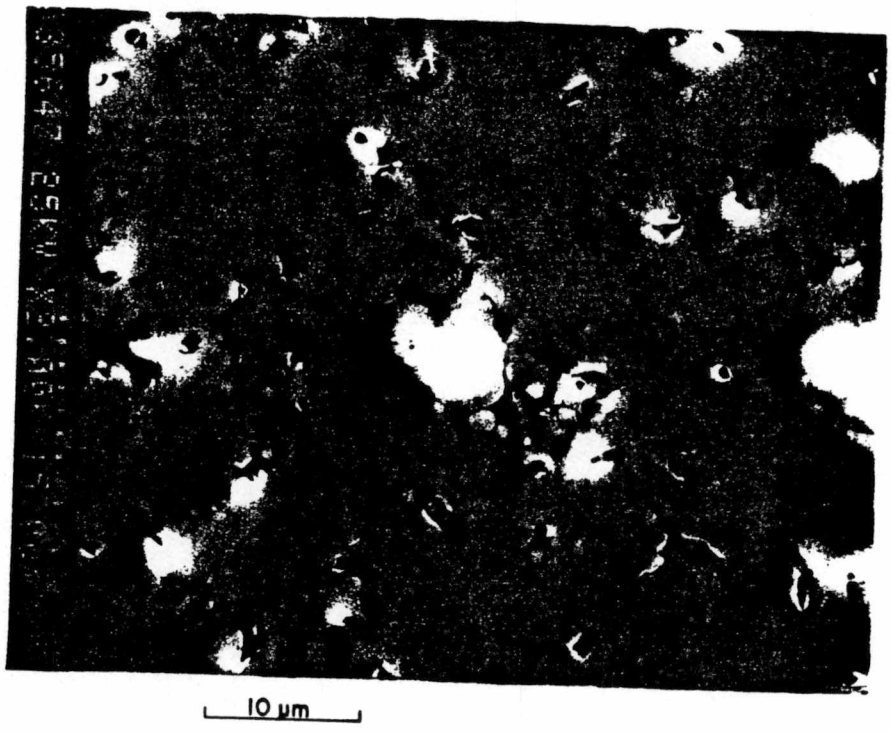

Figure 4.15 Secondary electron images of polished cross-sections of BS50 (a) BS501 (b) BS502 (c) BS503

(c)

Figure 4.15 (continued) (c) BS503

Table 4.5 Amount of porosity and secondary phase particles in BaZPS compositions

Composition	% porosity*	% second-phase particles*
BS01	14.4	2.4
BS02	9.9	2.1
BS03	5.1	1.3
BS171	19.8	1.5
BS172	14.2	1.0
BS173	7.8	0.5
BS253	9.8	0.0
BS373	2.1	0.0
BS501	25.2	4.7
BS502	23.0	2.9
BS503	15.8	2.0

* accurate within ±10%

and are shown in Table 4.6.

The SEM micrographs of the BS0 compositions (Figures 4.11a, b, and c) indicate that the secondary phase particles were mostly associated with porosity. It was also observed that the majority of the microcracks found in the samples were associated with both porosity and secondary phase particles. In addition, the micrographs indicate that the amount of microcracking increased with increasing sintering time. This could be attributed to the grain size increase that takes place in sintering for longer time periods. As expected, the amount of porosity decreased with longer sintering time and the secondary phase particles were less than 2.5%.

The SEM micrographs revealed that the BS17 compositions did not microcrack (Figures 4.12a, b, and c). The amount of porosity decreased from 19.8% to 7.8% as the sintering time was increased from 30 minutes to 3000 minutes. Few secondary phase particles were observed (<1.5%) in comparison with the BS0 compositions.

BS253 (Figure 4.13), and BS373 (Figure 4.14) also did not exhibit any microcracking, and were virtually free of secondary phase particles. Further, BS373 had porosity less than 2.1%. However, some amount of microcracking was observed in the BS50 samples (Figures 4.15a, b, and c), which had relatively more secondary phase particles than did the BS0 samples. As in the BS0 samples, the secondary phase particles in BS50 samples were found in the pores.

Secondary electron images of the fracture surfaces of the various

Table 4.6 Grain size measurements of the BaZPS compositions

Composition Sintering time(min)--->	Grain size* (μm)		
	30	300	3000
BS0	1.83	2.70	5.08
BS17	1.64	2.42	4.16
BS25			2.89
BS37			3.28
BS50	1.36	1.91	2.67

* accurate within ±10%

specimens are shown in Figures 4.16-4.20, with the fracture surface of the BS0 samples (Figures 4.16a, b, and c) indicating that the mode of fracture was predominantly transgranular, thus confirming that the grains were strongly interconnected. However, increasing grain size results in more intergranular fracture (Figures 4.16b, and c), suggesting that the grains are not as well bonded in comparison to BS01. Back scattered image of BS02 (Figure 4.21) shows some secondary phase particles in the pores.

In the case of the BS17 compositions, the mode of fracture was mostly transgranular (Figures 4.17a, b, and c). Little intergranular fracture was observed even for large-grain sized sample (BS173). BS253 (Figure 4.18), and BS373 (Figure 4.19) failed only by transgranular mode suggesting that the grains in these samples are bonded strongly, and possibly may translate into higher strength and hardness values. BS50 samples (Figures 4.20a, b, and c) have fracture surfaces which reveal a very porous material and the mode of fracture was a combination of intergranular and transgranular indicating that the grains were poorly interconnected. In BS503 a particularly large amount of intergranular fracture was observed. The pores of all the compositions were highly faceted.

Electron diffraction and EDS studies were performed on the polished surfaces of BS03, and BS503. EDS results of BS03 and BS503 phase matched well with their corresponding simulated spectrums, thus confirming the stoichiometry of the synthesized compositions. The model and experimental spectra of BS503 are shown in Figure 4.22.

(a)

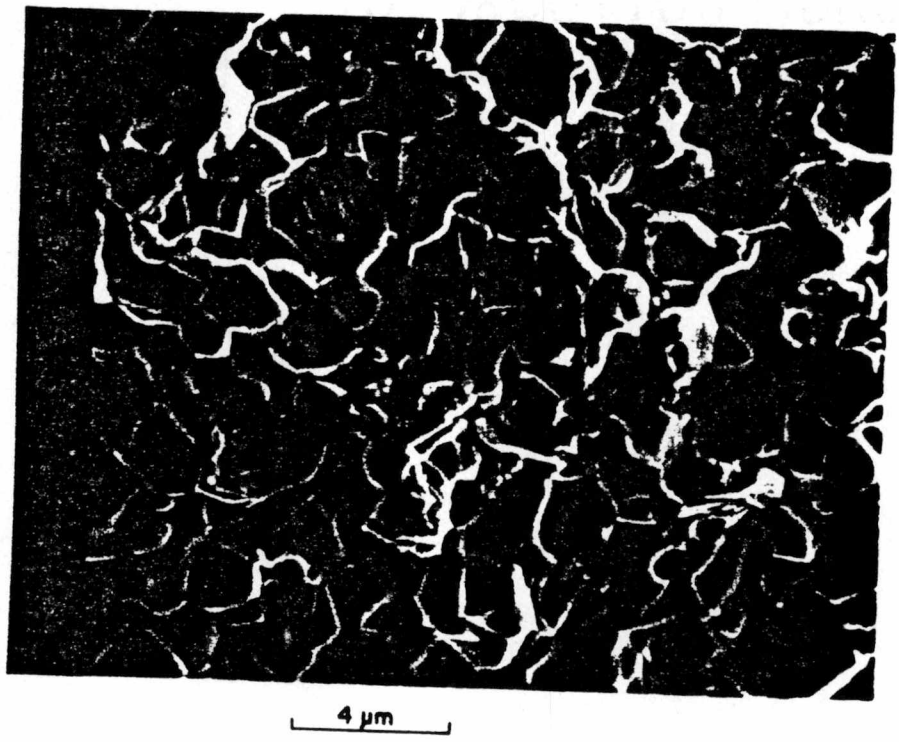

(b)

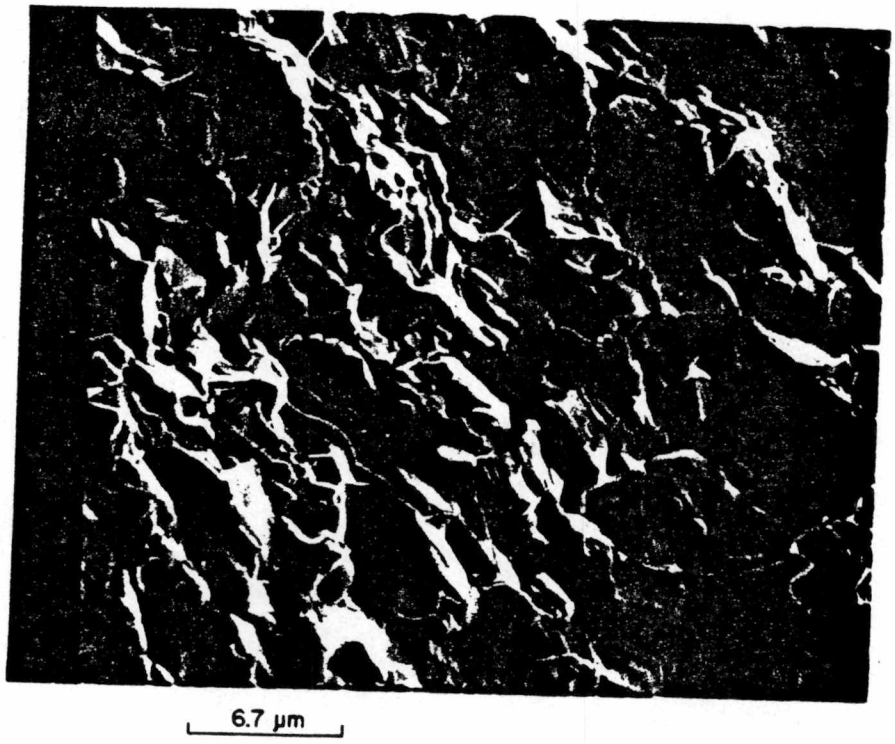

Figure 4.16 Secondary electron images of fracture surfaces of BS0 (a) BS01 (b) BS02 (c) BS03

(c)

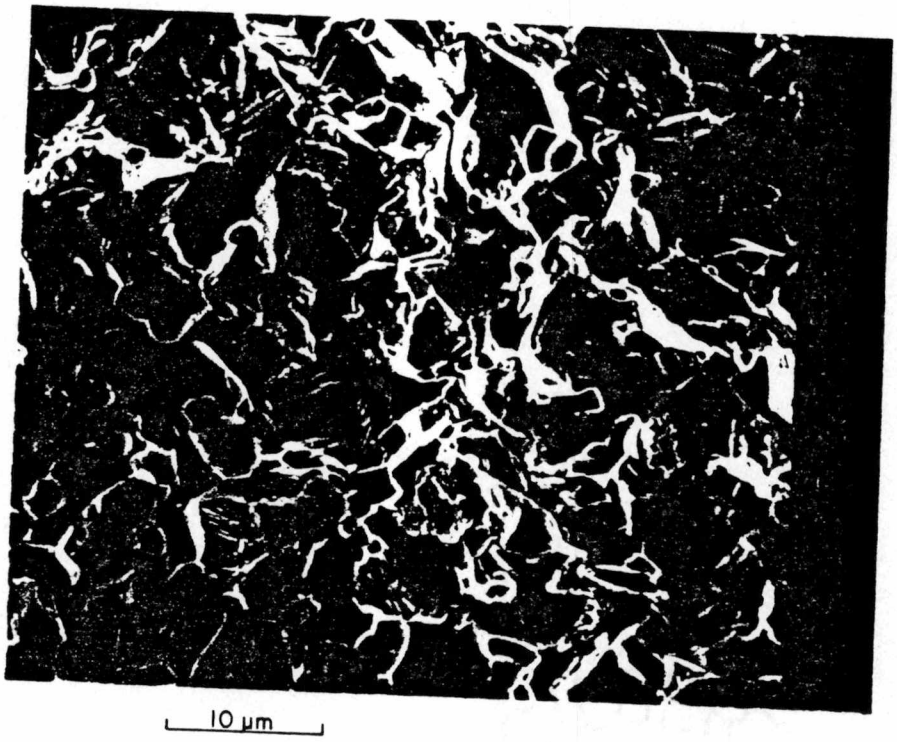

Figure 4.16 (continued) (c) BS03

(a)

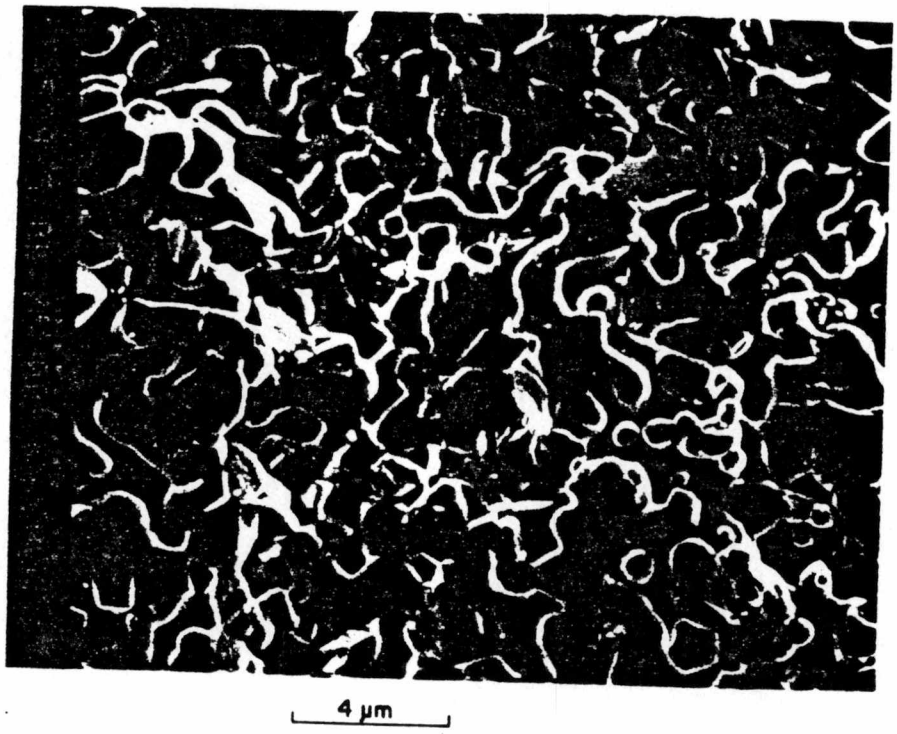

(b)

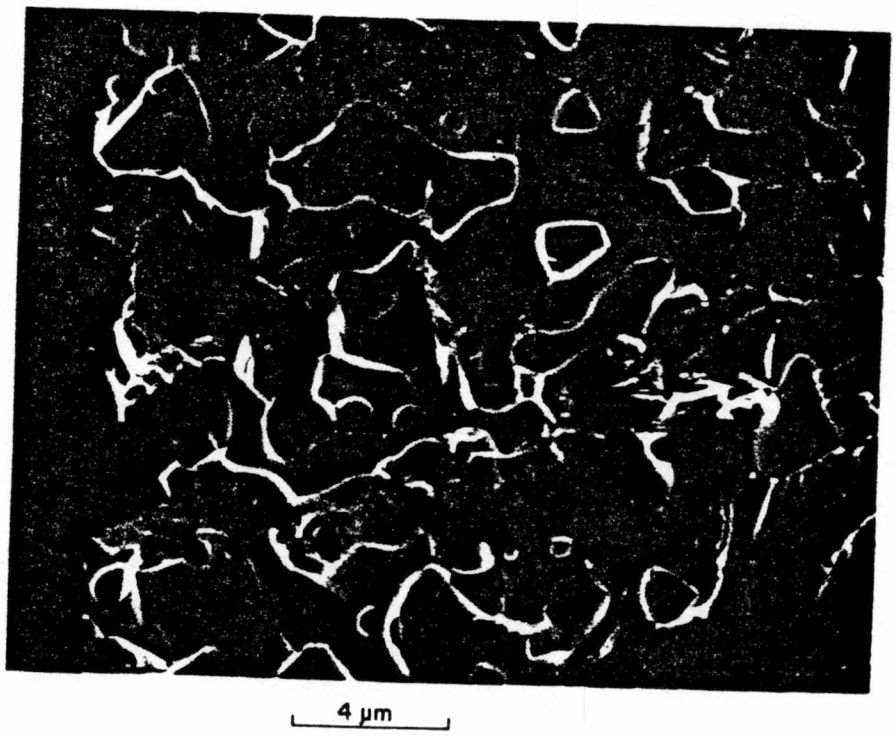

Figure 4.17 Secondary electron images of fracture surfaces of BS17 (a) BS171 (b) BS172 (c) BS173

(c)

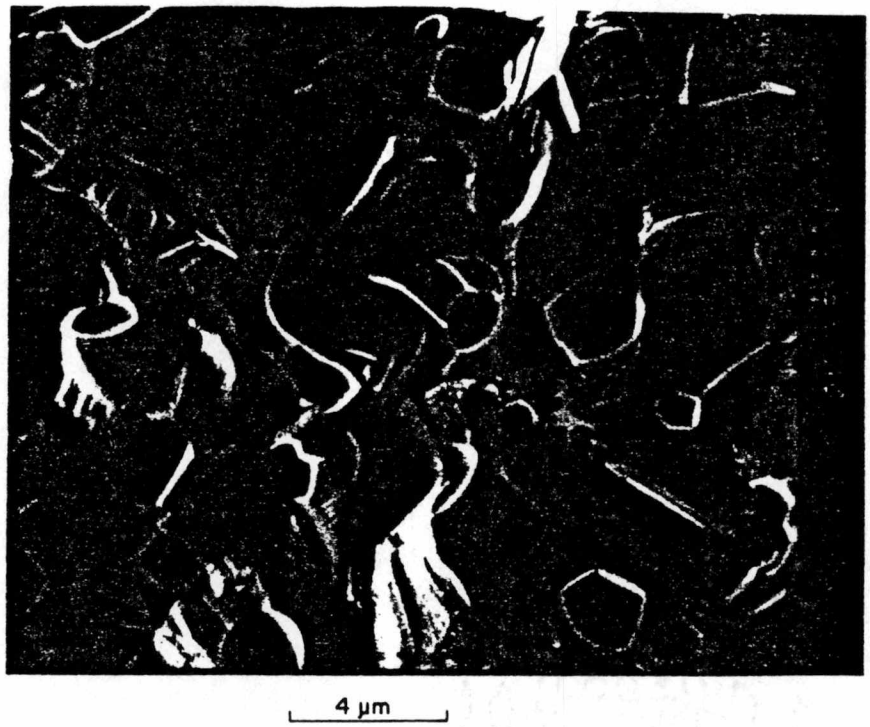

Figure 4.17 (continued) (c) BS173

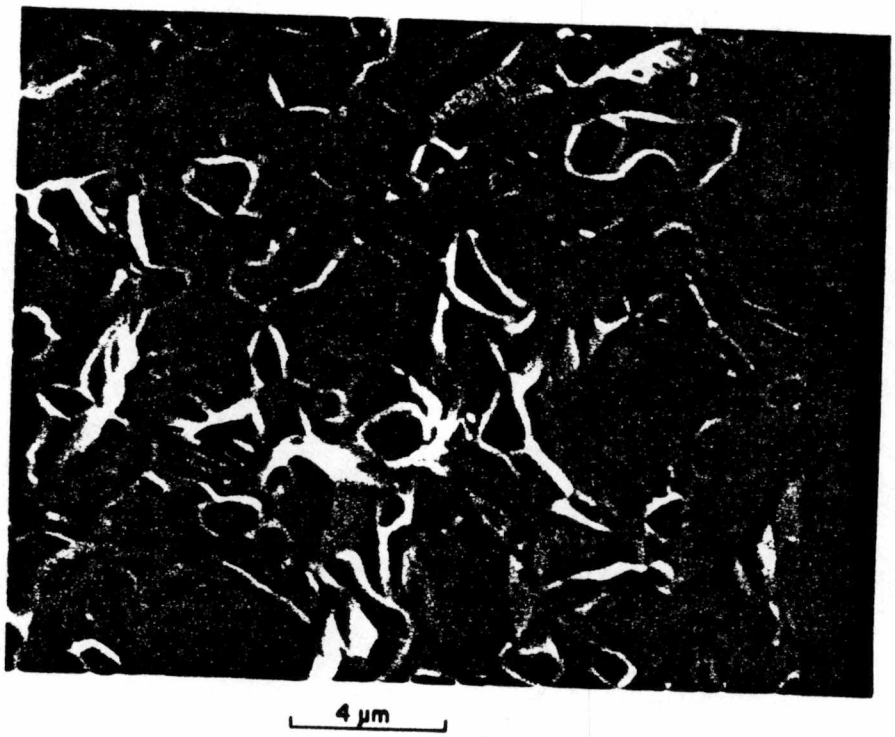

Figure 4.18 Secondary electron image of a fracture surface of BS253

Figure 4.19 Secondary electron image of a fracture surface of BS373

(a)

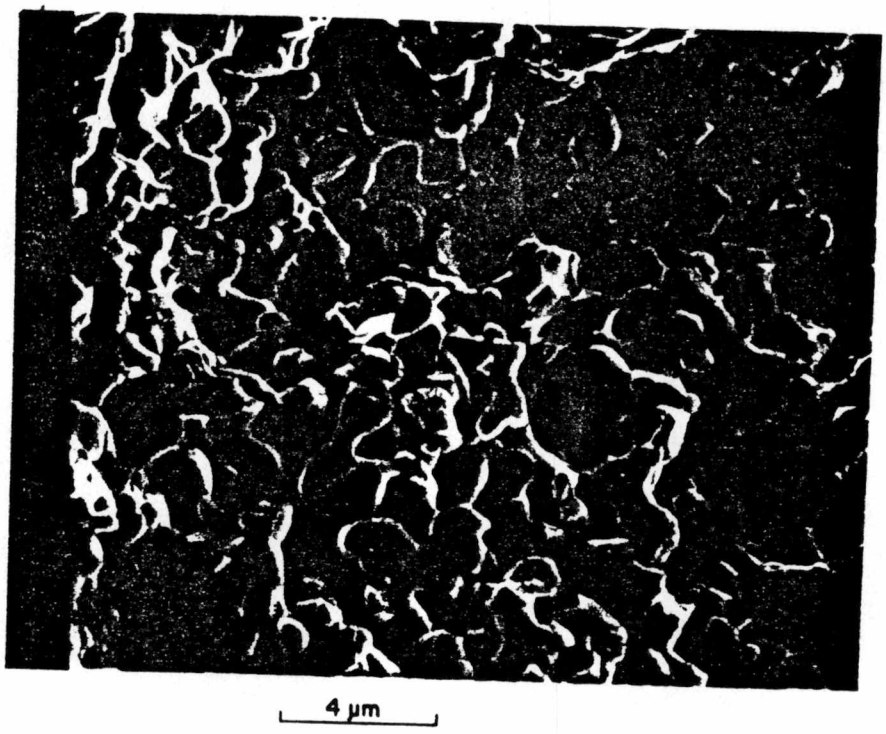

(b)

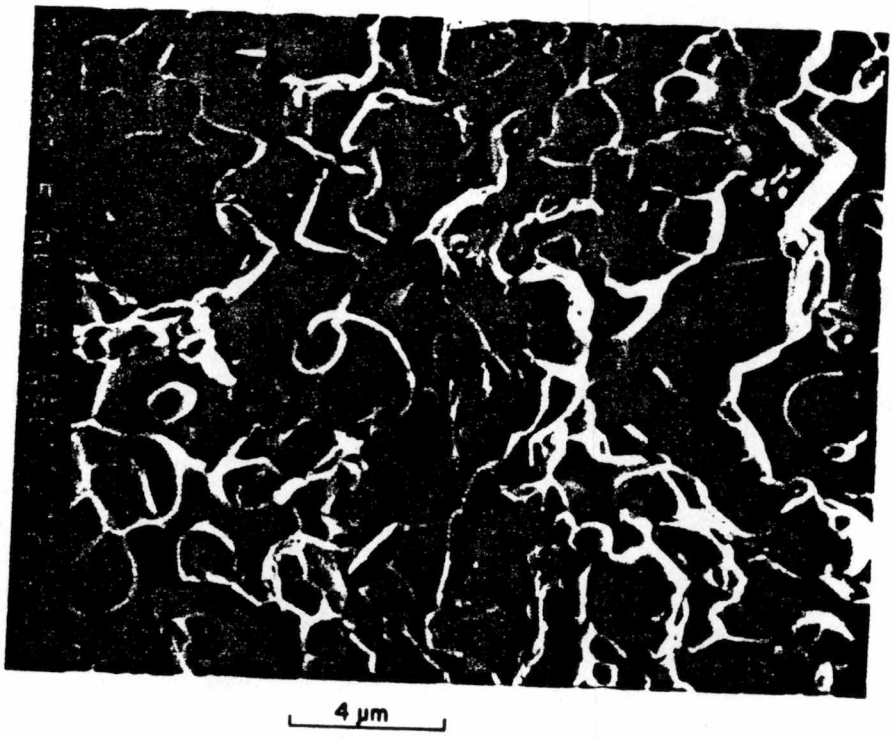

Figure 4.20 Secondary electron images of fracture surfaces of BS50 (a) BS501 (b) BS502 (c) BS503

(c)

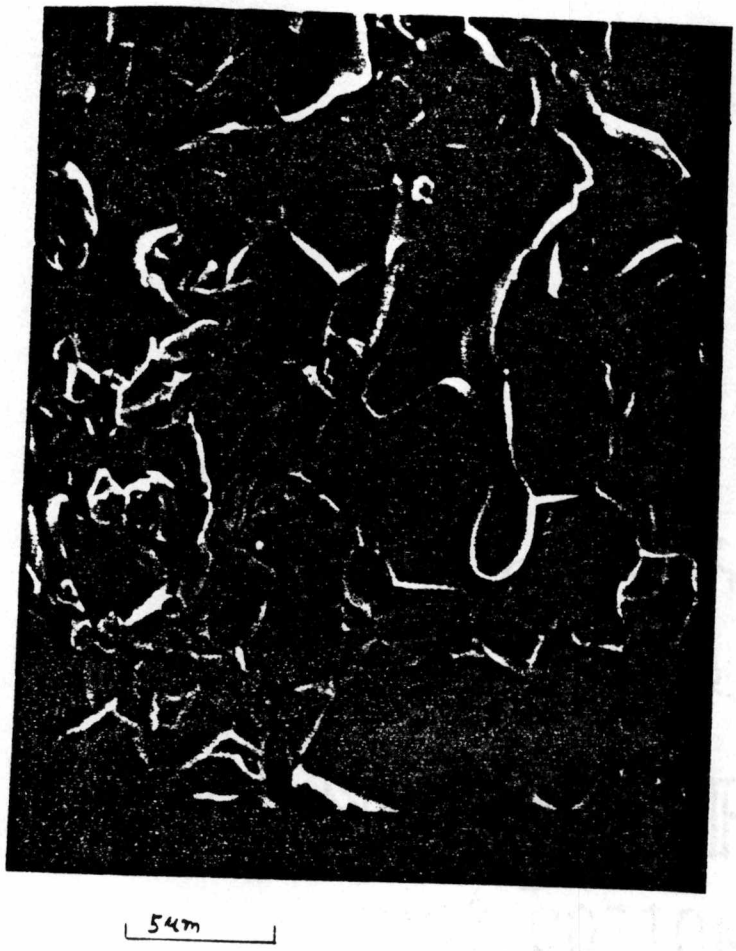

Figure 4.20 (continued) (c) BS503

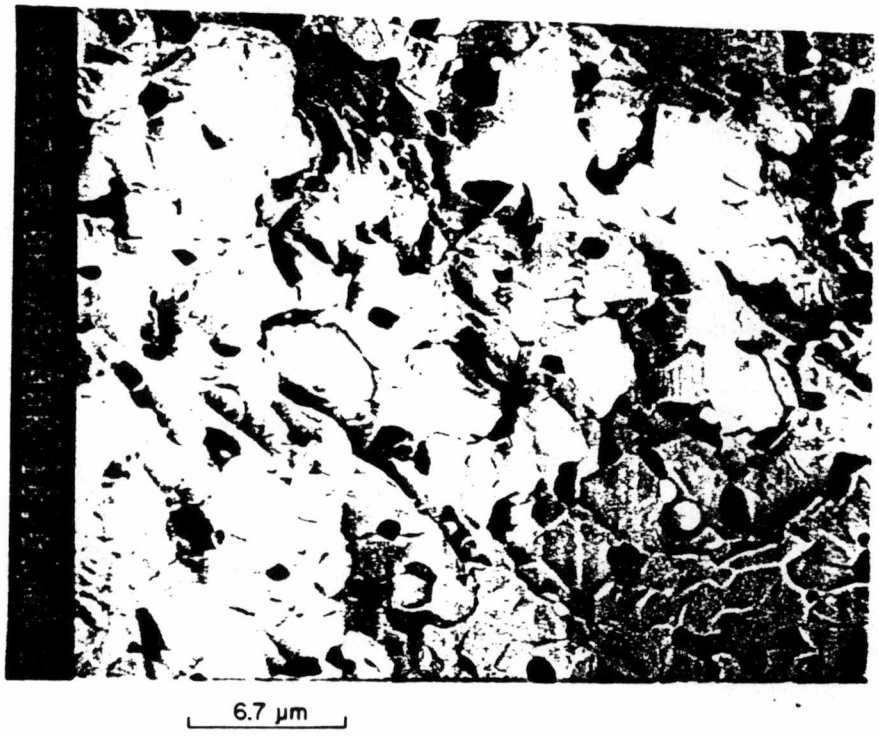

Figure 4.21 Back scattered image of a fracture surface of BS02

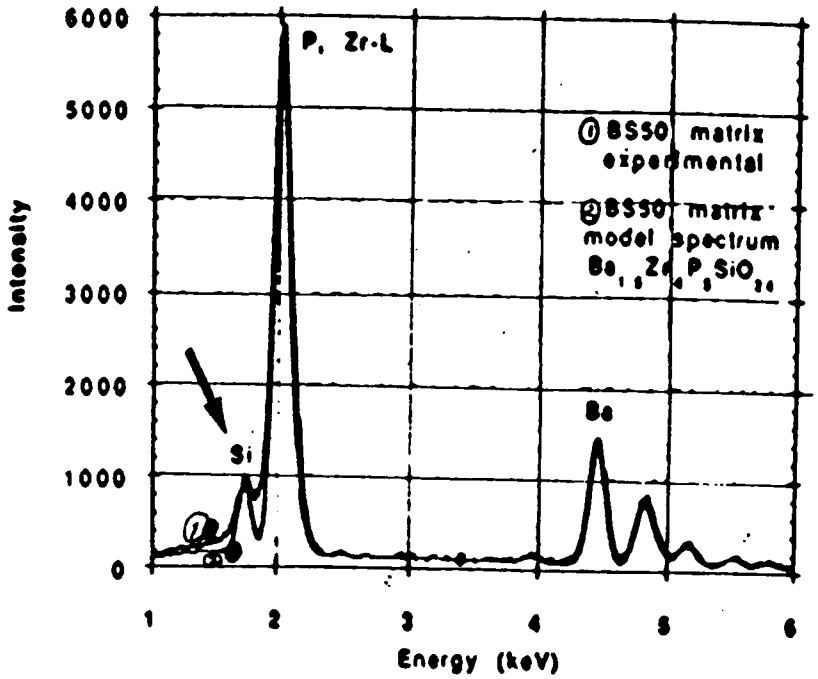

Figure 4.22 Comparison of model and experimental EDS spectra of BS503

The EDS data from the secondary phase particles of BS03 indicated that it contained Zr and P. Electron diffraction data indicated that this phase was cubic and the d-spacings measured here matched closely with those given for either ZrP_2O_7 (JCPDS #36-189) or ZrP_3O_{12} (JCPDS #28-1496). However, when these compositions were modeled for EDS and compared with the experimental spectrum, there was no match, and the experimental spectra contained much more Zr. In the case of BS173, the secondary phase particles had the same composition as that of the secondary phase particles in BS03. BS503 contained three different secondary phase particles: one had a composition similar to the secondary phase particles observed in BS03 and BS173, the second being $BaZrP_2O_8$, and the third was a Zr-P-Si phase.

4.5 Bulk linear thermal expansion

The bulk linear thermal expansions were determined from the dilatometric curves obtained using the procedure described in Section 3.2.4. The results are presented in Figures 4.23-4.33 and tabulated in Table 4.7. The bulk linear thermal expansion decreased, and changed from positive (BS03) to negative (BS503), with increasing Si content.

4.6 High temperature X-ray diffraction

High temperature XRD was carried out on BS173 between 27°C and 900°C and the technique is described in detail in section 3.3.5. The variation of unit cell

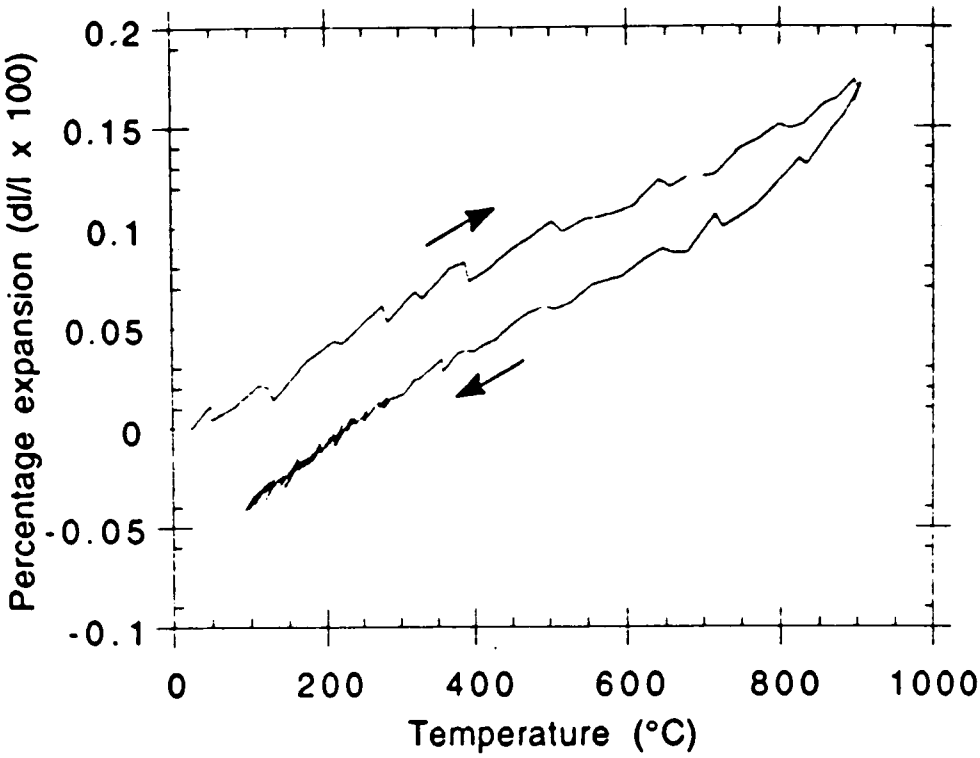

Figure 4.23 Thermal expansion curve for BS01

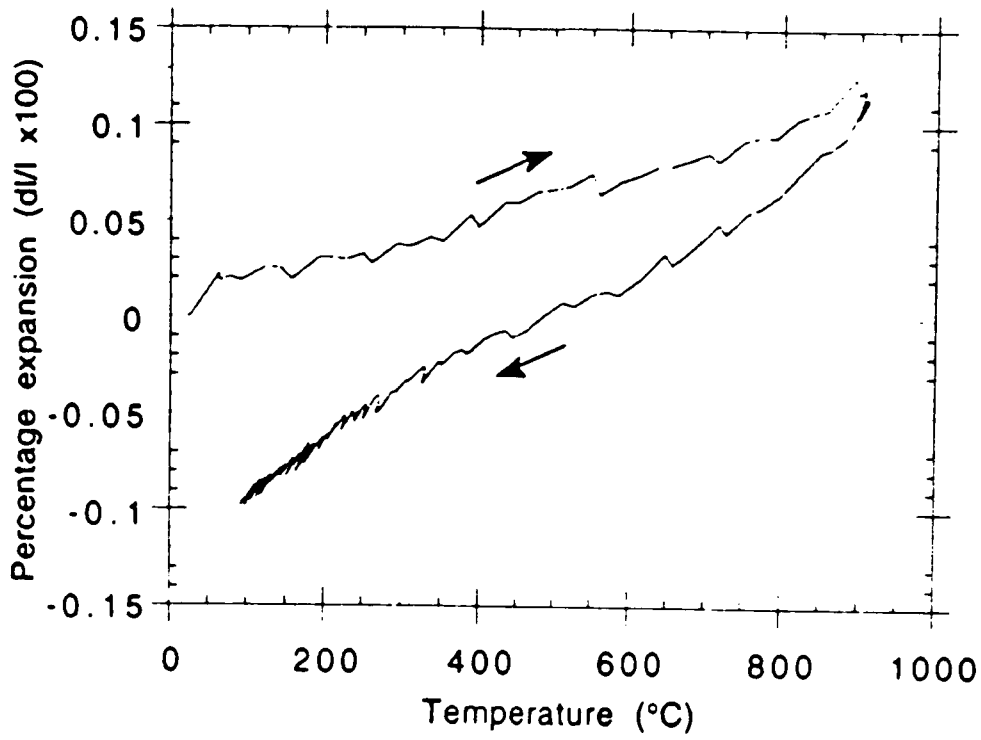

Figure 4.24 Thermal expansion curve for BS02

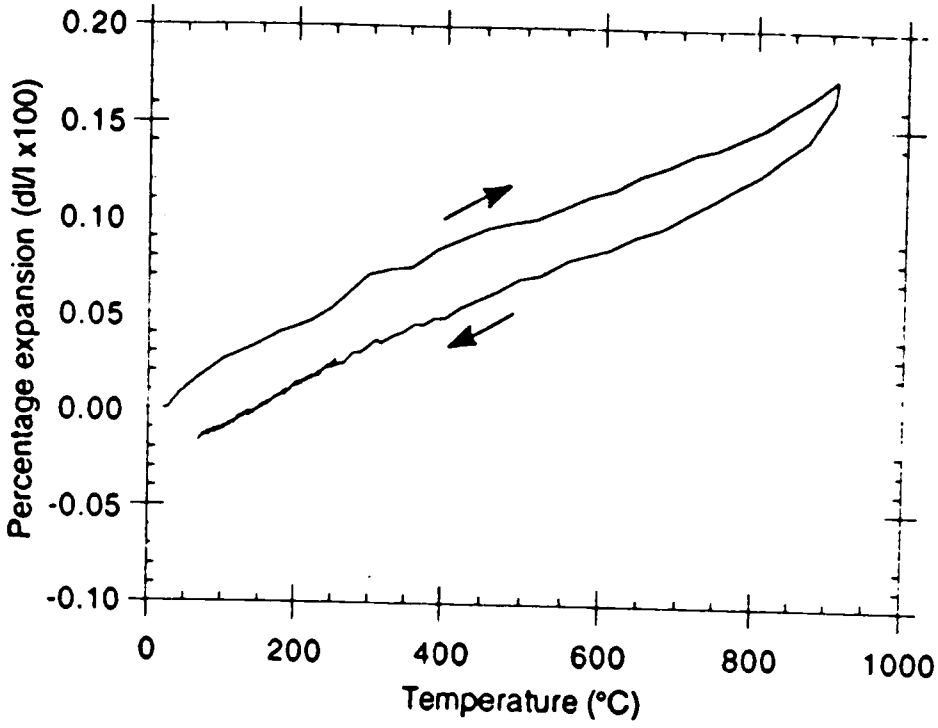

Figure 4.25 Thermal expansion curve for BS03

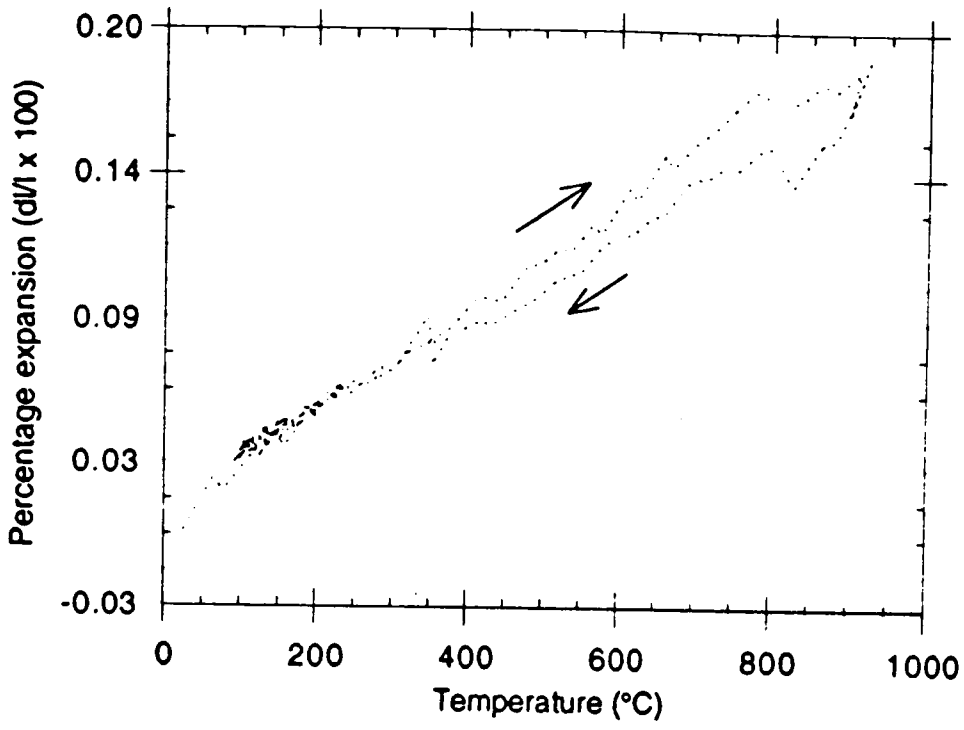

Figure 4.26 Thermal expansion curve for BS171

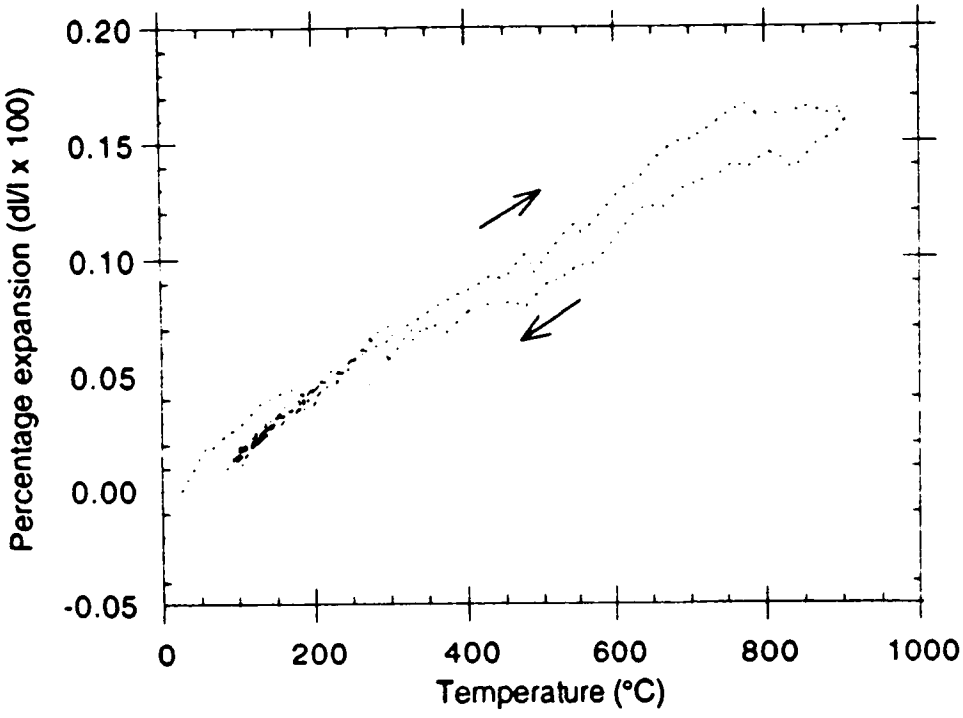

Figure 4.27 Thermal expansion curve for BS172

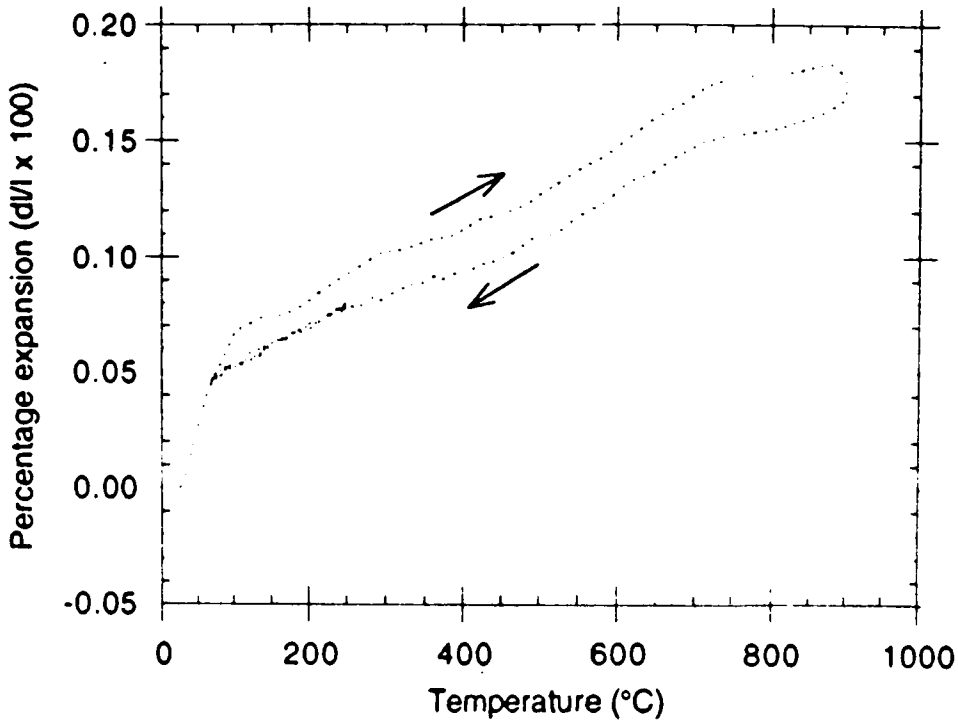

Figure 4.28 Thermal expansion curve for BS173

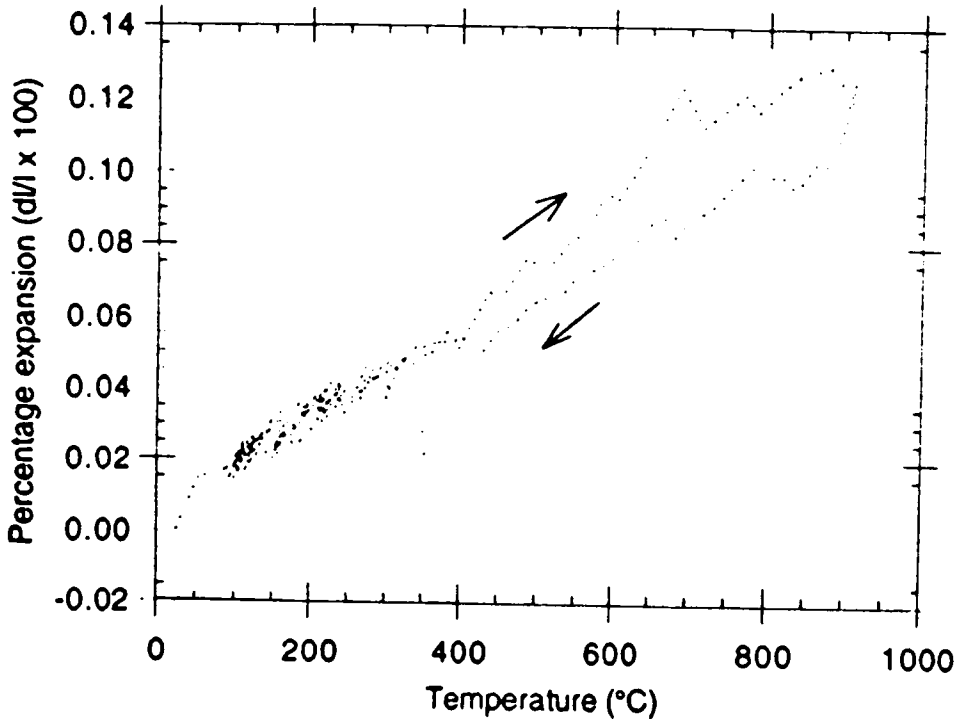

Figure 4.29 Thermal expansion curve for BS253

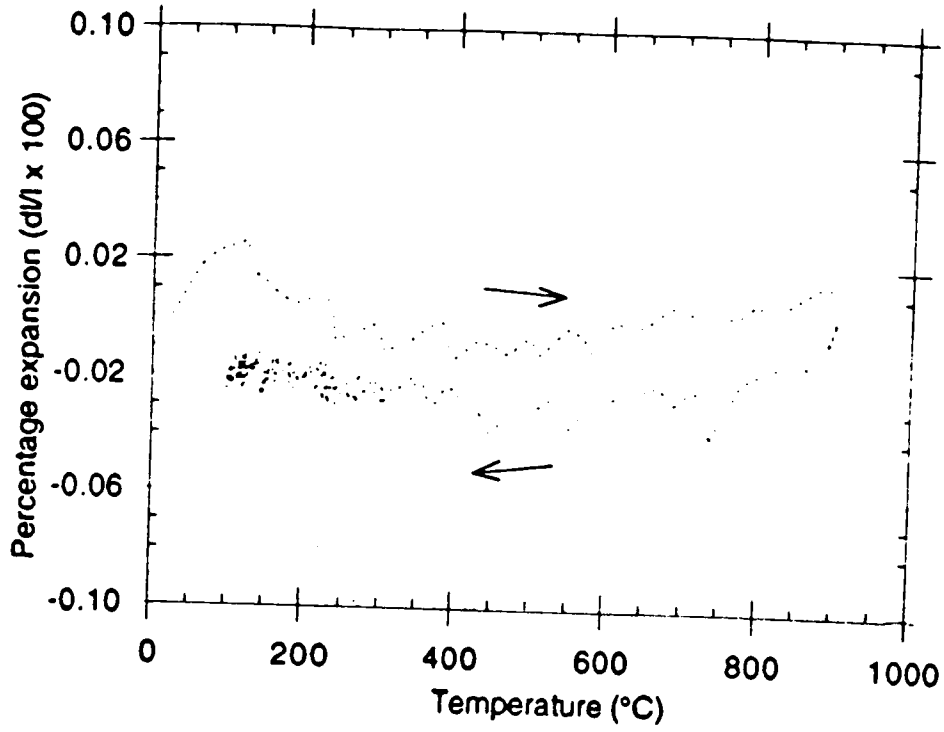

Figure 4.30 Thermal expansion curve for BS373

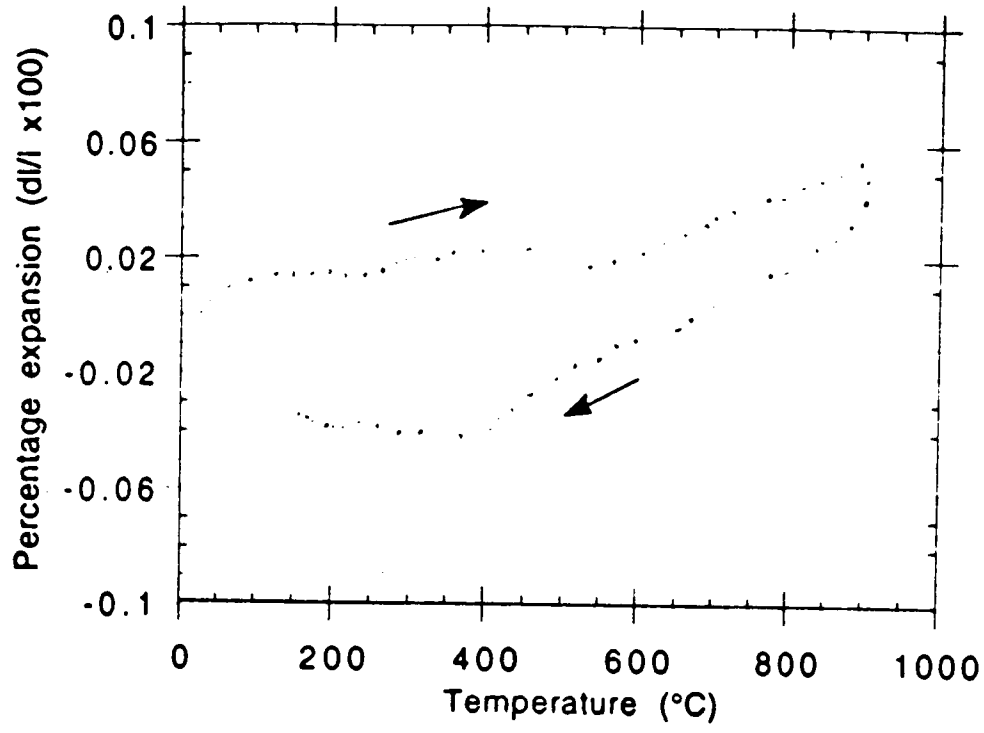

Figure 4.31 Thermal expansion curve for BS501

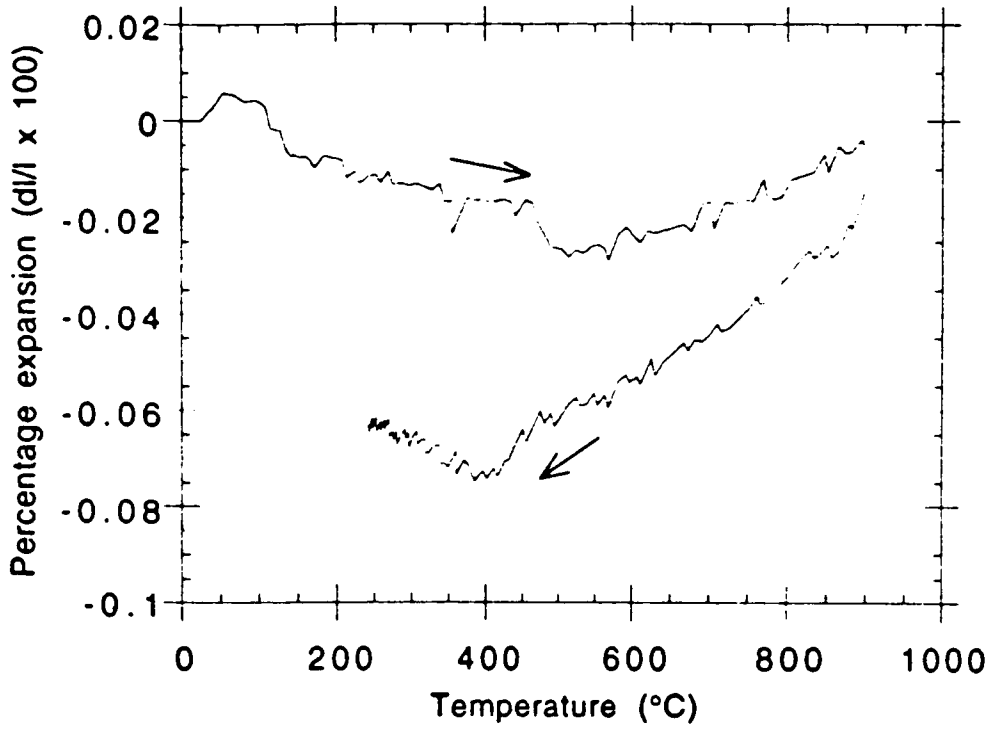

Figure 4.32 Thermal expansion curve for BS502

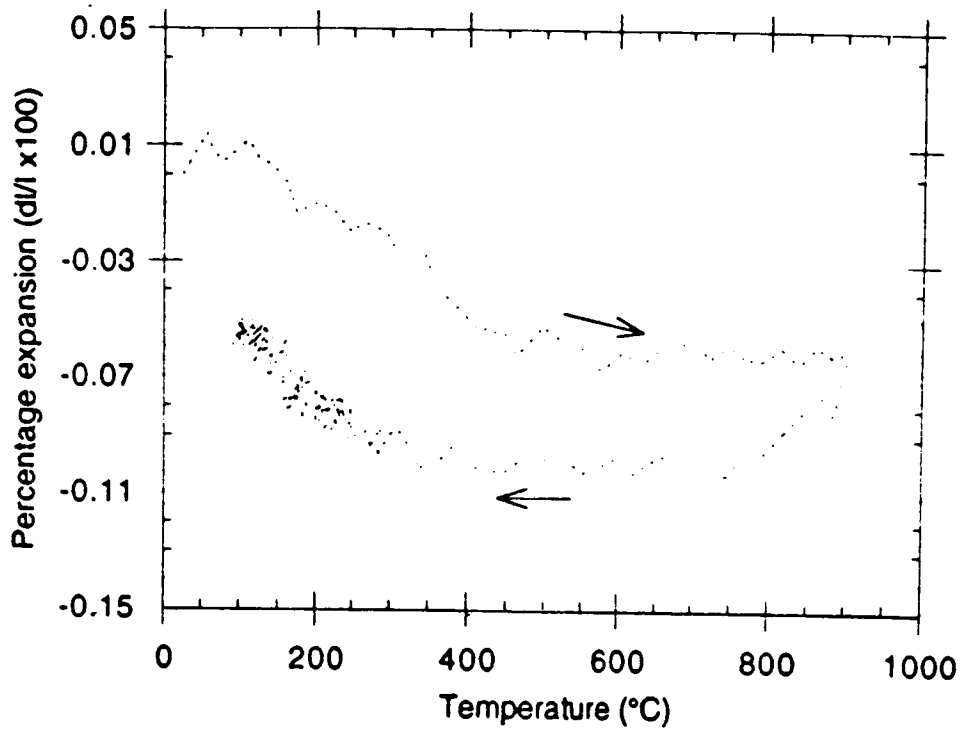

Figure 4.33 Thermal expansion curve for BS503

Table 4.7 Bulk linear thermal expansion coefficient of BaZPS compositions

Composition	Coefficient of bulk linear thermal expansion* x 10^{-6} °C^{-1}		
	α_1	α_2	$\alpha_{ave}= (\alpha_1+\alpha_2) / 2$
BS01	1.95	2.58	2.26
BS02	1.35	2.65	2.00
BS03	2.00	2.28	2.14
BS171	2.08	1.86	1.97
BS172	1.82	1.78	1.80
BS173	2.00	1.58	1.79
BS253	1.42	1.28	1.36
BS373	0.14	0.46	0.30
BS501	0.50	1.00	0.75
BS502	-0.17	0.72	0.27
BS503	-0.62	-0.08	-0.35

* accurate within ±10%

parameters a and c, and volume with temperature is plotted in Figures 4.34-4.36 and summarized in Table 4.8. It was observed that the volume increased from 27°C to 400°C, then decreased between 600°C, and 800°C, again increased until 850°C, and then decreased at 900°C. The axial thermal expansion results are also shown in Table 4.8.

4.7 Young's modulus

The Young's modulus was determined by the impulse excitation technique described in section 3.2.6 and the results are summarized in Table 4.9. The Young's modulus decreased with increasing grain size for compositions BS0 and BS50. However, for the BS17 composition, the Young's modulus increased with increasing grain size. It was also observed that increasing Si content caused the Young's modulus to increase from BS03 to BS173, decrease for BS253, again increase for BS373, and drop sharply for BS503.

4.8 Flexural Strength

4.8.1 Room temperature flexural strength

Room temperature flexural strengths were measured using the procedure described in section 3.3.7. The flexural strength varied between 50 MPa to 112.75 MPa. The results are summarized in Table 4.10 and the trend with composition is shown in Figure 4.37. The flexural strength increased with increasing Si content

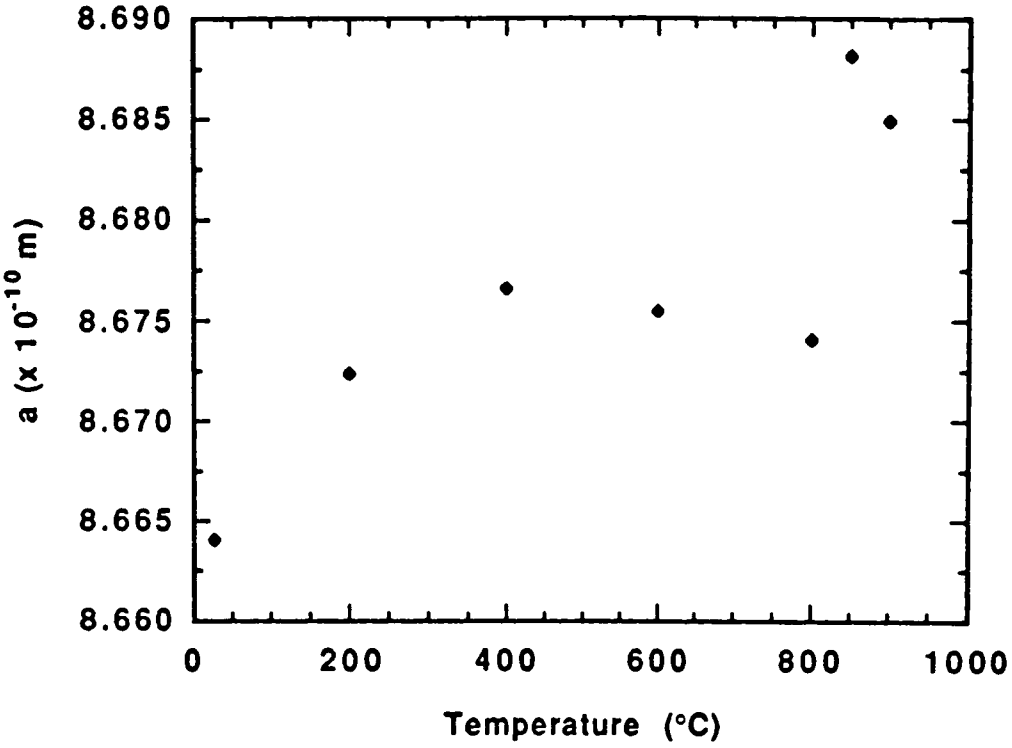

Figure 4.34 Variation of cell parameter "a" with temperature for BS173

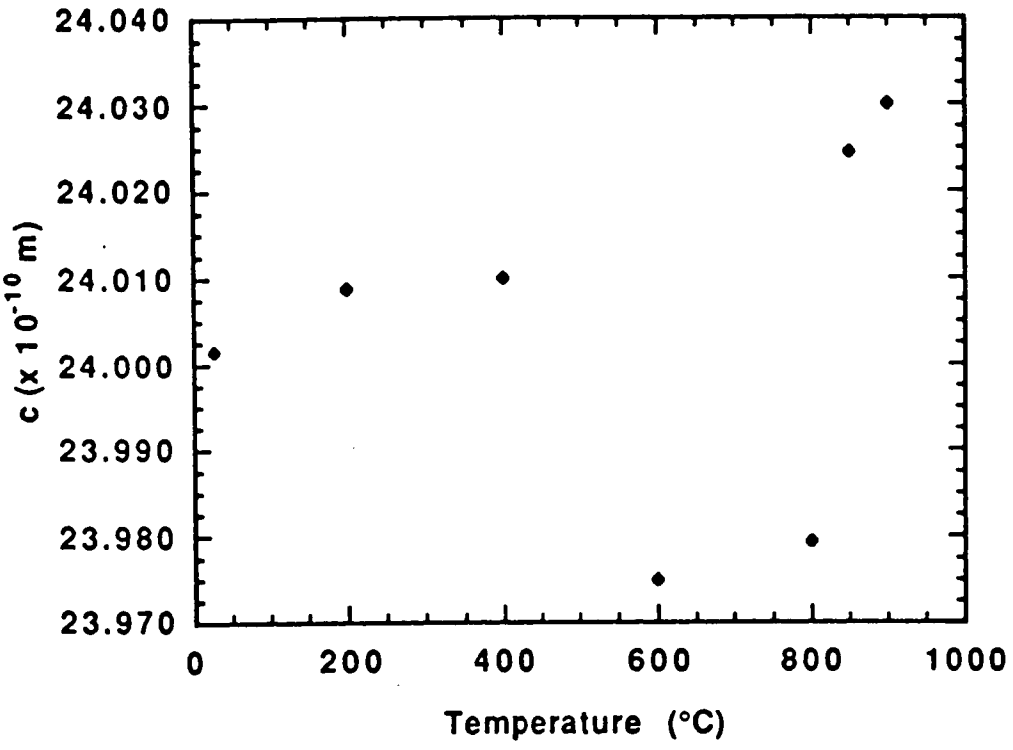

Figure 4.35 Variation of cell parameter "c" with temperature for BS173

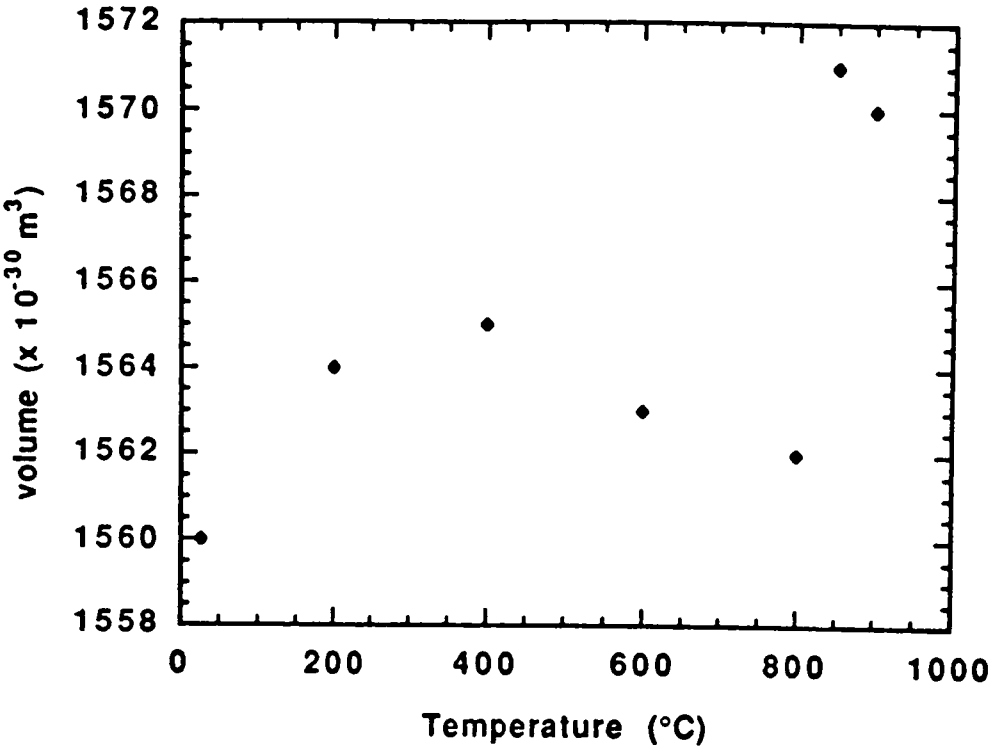

Figure 4.36 Variation of unit-cell volume with temperature for BS173

Table 4.8 High temperature x-ray diffraction results for BS173

Temperature (°C)	a ($x10^{-10}$ m)	c ($x10^{-10}$ m)	Volume ($x10^{-30}$ m^3)	#peaks used	$\Delta 2\theta$
27	8.66407(75)*	24.00157(244)*	1560	24	-0.006
200	8.67236(85)	24.00879(275)	1564	25	-0.006
400	8.67659(95)	24.01002(284)	1565	25	-0.002
600	8.67549(165)	23.97498(804)	1563	10	0.026
800	8.67407(263)	23.97939(684)	1562	11	0.039
850	8.68818(107)	24.02442(354)	1571	24	-0.003
900	8.68495(68)	24.03002(204)	1570	23	-0.001

*data within the brackets indicate the standard deviation of the last few digits

$\alpha_a = (a_{900} - a_{27})/ (a_{27} \times (T_{900} - T_{27})) = 2.76 \times 10^{-6}\ °C^{-1}$ (27-900 °C)

$\alpha_c = (c_{900} - c_{27})/ (c_{27} \times (T_{900} - T_{27})) = 1.35 \times 10^{-6}\ °C^{-1}$ (27-900 °C)

$\frac{\alpha_v}{3} = (2\alpha_a + \alpha_c)/3 = 2.055 \times 10^{-6}\ °C^{-1}$ (27-900 °C)

Table 4.9 Young's modulus results for BaZPS compositions

Composition	Young's modulus (GPa)
BS01	45.1 ± 0.1
BS02	41.9 ± 1.4
BS03	34.4 ± 0.3
BS171	41.5 ± 0.3
BS172	49.7 ± 0.1
BS173	51.7 ± 0.7
BS253	44.7 ± 0.5
BS373	60.0 ± 0.1
BS501	25.8 ± 0.5
BS502	24.8 ± 0.5
BS503	20.6 ± 0.8

Table 4.10 Room temperature flexural strength results for BaZPS compositions

Composition	Flexural strength (MPa)
BS01	79.14 ± 5.36
BS02	61.85 ± 1.10
BS03	55.36 ± 13.69
BS171	78.09 ± 2.30
BS172	84.99 ± 11.29
BS173	84.67 ± 12.26
BS253	98.40 ± 5.70
BS373	112.75 ± 10.47
BS501	54.00 ± 4.04
BS502	36.03 ± 5.48
BS503	49.66 ± 7.63

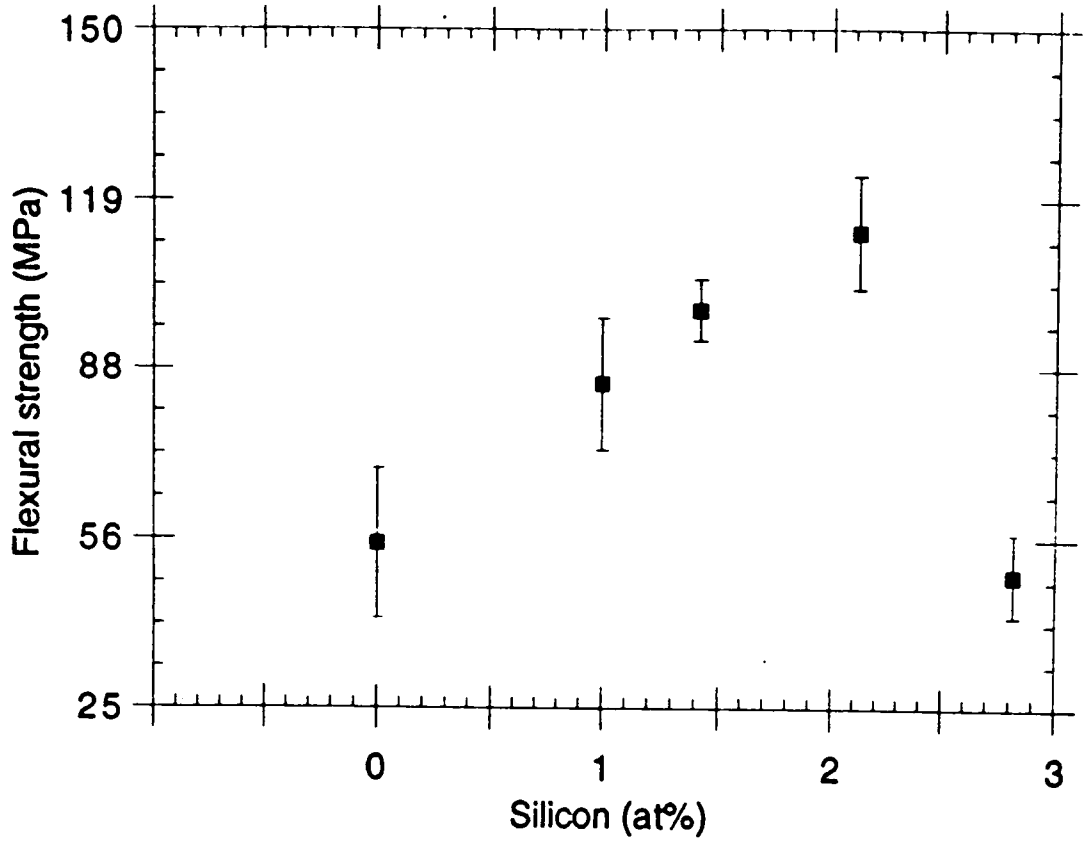

Figure 4.37 Variation of room temperature flexural strength with increasing silicon content

until BS373, and then decreased sharply for BS503. The flexural strength decreased with increasing grain size for BS0, and remained almost constant for BS17 and BS50.

4.8.2 High temperature flexural strength

The high temperature flexural strengths were measured following the procedure described in section 3.3.8 and the results are tabulated in Table 4.11 and presented in Figures 4.38-40. The flexural strength of BS17 compositions ranged from 67 MPa to 96.6 MPa between 25 and 1000°C. In the case of BS03, BS171, BS172, and BS173, the flexural strength increased from room temperature to 200°C, then decreased at 600°C, and again increased at 1000°C.

For the BS0 compositions (BS01, and BS02), the flexural strength increased with increasing temperature between 25 and 1000°C. In the BS50 compositions, the flexural strength did not vary much between 25 and 1000°C. The above trend was also observed in BS253 and BS373.

4.9 Hardness

Microhardness measurements were conducted at room temperature as described in section 3.2.9 and the results are summarized in Table 4.12. The hardness increased with increasing Si content until BS373, and then dropped sharply for BS503. Among the BaZPS compositions, BS373 showed the highest hardness value (7.61 GPa). At lower loads, the indentation dimensions varied

Table 4.11 High temperature flexural strength results for BaZPS compositions

Composition	Flexural strength (MPa)			
	25 °C	200 °C	600°C	1000°C
BS01	79.14 ± 5.36	81.46 ± 10.64	92.53 ± 9.09	95.28 ± 11.01
BS02	61.85 ± 1.10	74.38 ± 5.94	80.29 ± 4.71	122.78 ± 14.06
BS03	55.36 ± 4.9	66.05 ± 2.41	41.43 ± 14.39	83.02 ± 34.78
BS171	78.09 ± 2.3	76.61 ± 16.21	67.47 ± 25.27	93.79 ± 5.52
BS172	84.99 ± 11.29	94.09 ± 15.36	79.71 ± 16.70	96.63 ± 9.30
BS173	84.67 ± 12.26	84.21 ± 2.39	79.32 ± 9.62	95.22 ± 1.55
BS253	98.40 ± 5.70	84.35 ± 14.90	89.82 ± 17.10	83.34 ± 13.92
BS373	112.75 ± 10.47	101.97 ± 19.84	92.67 ± 7.05	117.65 ± 18.66
BS501	54.00 ± 4.04	48.46 ± 4.29	56.82 ± 6.37	55.83 ± 5.80
BS502	36.03 ± 5.48	43.38 ± 1.46	56.59 ± 1.39	56.58 ± 1.39
BS503	49.66 ± 7.63	45.13 ± 1.89	50.94 ± 3.50	50.94 ± 3.50

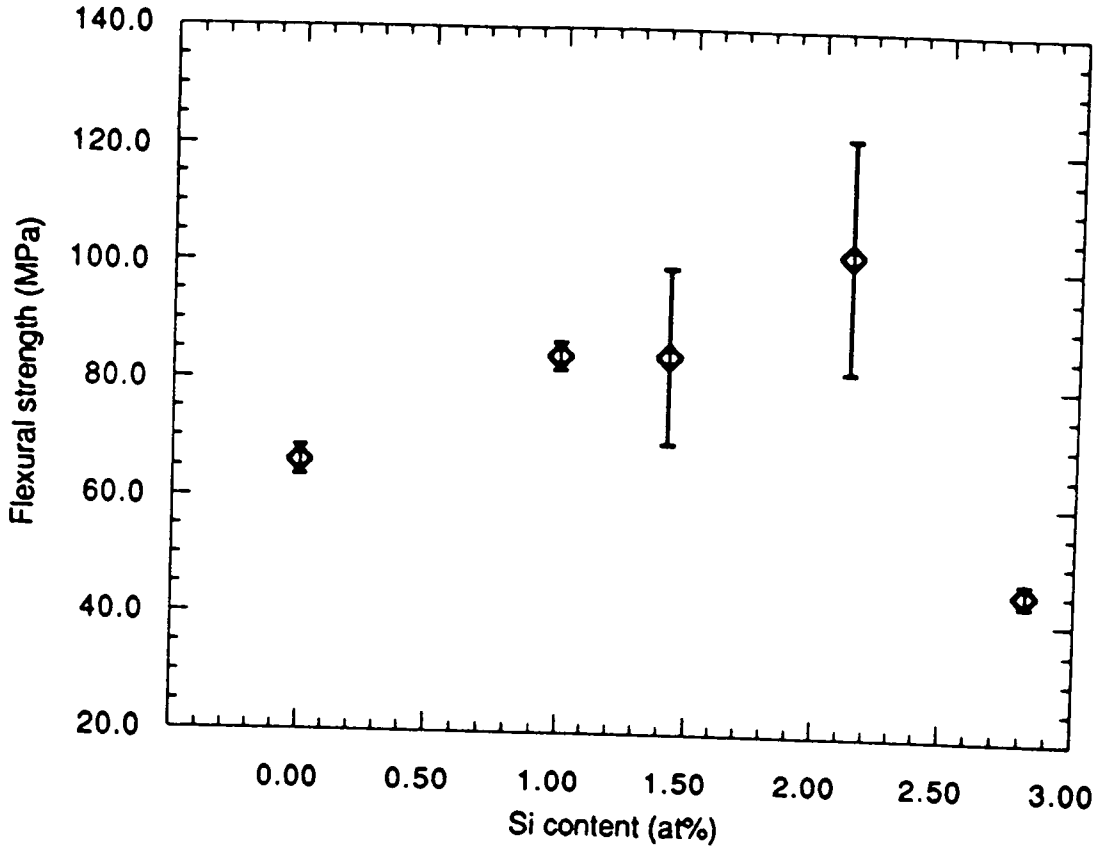

Figure 4.38 Variation of flexural strength at 200°C with increasing silicon content

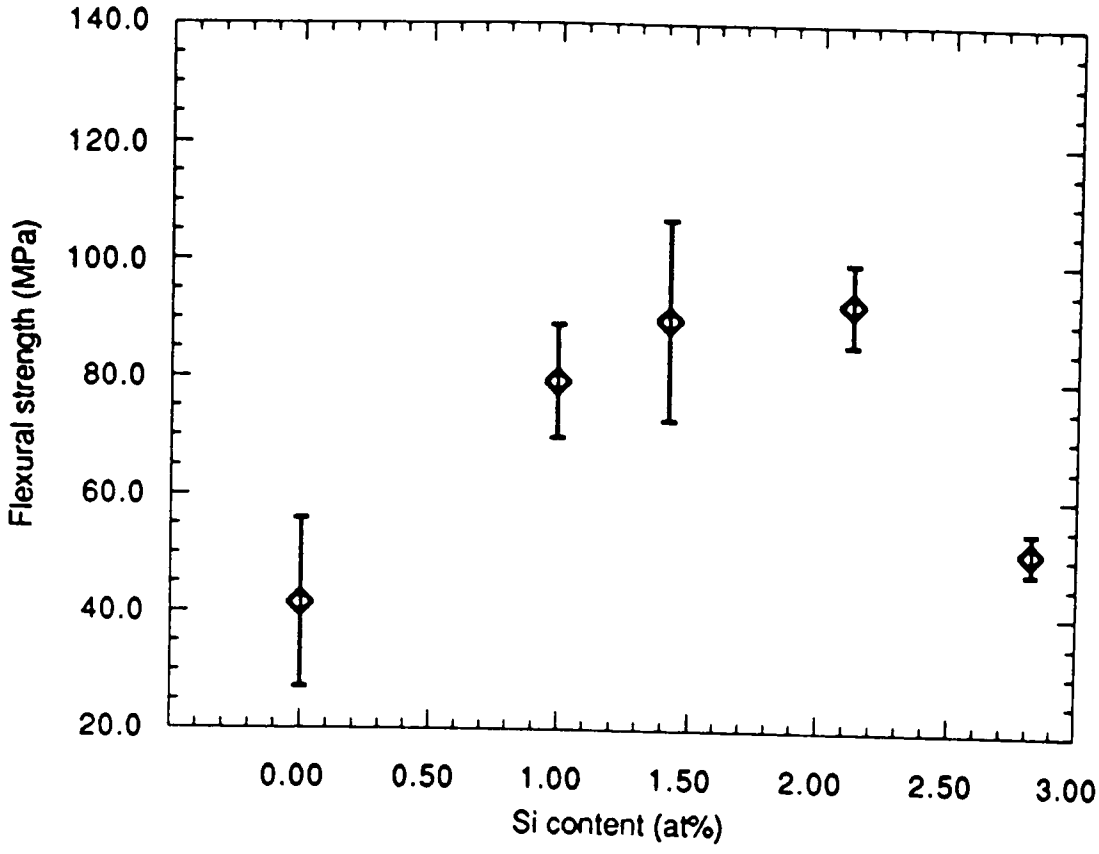

Figure 4.39 Variation of flexural strength at 600°C with increasing silicon content

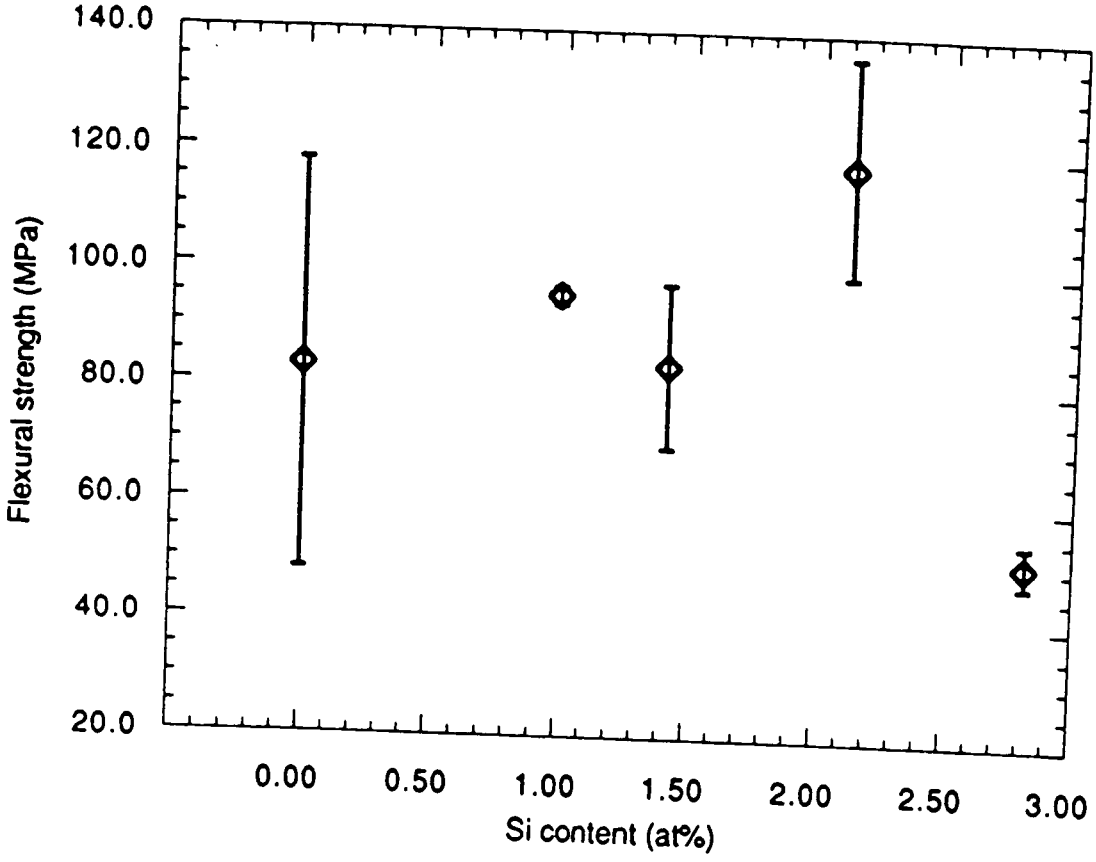

Figure 4.40 Variation of flexural strength at 1000°C with increasing silicon content

Table 4.12 Hardness results for BaZPS compositions

Composition Load (gms)--->	Hardness (GPa)			
	50	100	200	300
BS01	4.08±0.09	3.10±0.06	2.75±0.05	2.71±0.03
BS02	4.25±0.14	3.49±0.04	3.03±0.04	3.05±0.05
BS03	4.42±0.10	4.12±0.04	3.45±0.08	3.29±0.10
BS171	3.60±0.18	3.39±0.07	2.99±0.04	2.95±0.06
BS172	5.38±0.17	4.08±0.03	3.56±0.11	3.16±0.08
BS173	4.65±0.16	4.30±0.18	4.11±0.10	3.66±0.12
BS253	5.30±0.09	4.65±0.13	4.12±0.06	3.73±0.04
BS373	7.61±0.26	5.55±0.15	5.03±0.10	5.19±0.06
BS501	1.22±0.03	1.23±0.03	1.12±0.01	1.12±0.01
BS502	1.56±0.08	1.34±0.04	1.29±0.05	1.29±0.03
BS503	3.18±0.19	2.72±0.04	2.46±0.04	2.41±0.06

between 30 to 75 μm, and between 89 to 190 μm for higher loads. Also, the hardness values decreased with increase in indentation loads for all the BaZPS compositions. Further, for BS0, BS17 and BS50, the hardness values increased with increasing grain size.

4.10 Phase transition in BS17

A DSC study was carried out for BS172 following the procedure described in section 3.3.10. A broad endothermic peak was observed between 560°C and 780°C suggesting that there was a reaction taking place between those temperatures, and is shown in Figure 4.41. In addition, a sharp endothermic peak was observed between 480°C and 530°C and when the DSC was ramped at 20°C/min, the above peak was not observed suggesting that the reaction between 480°C and 530°C is kinetically controlled.

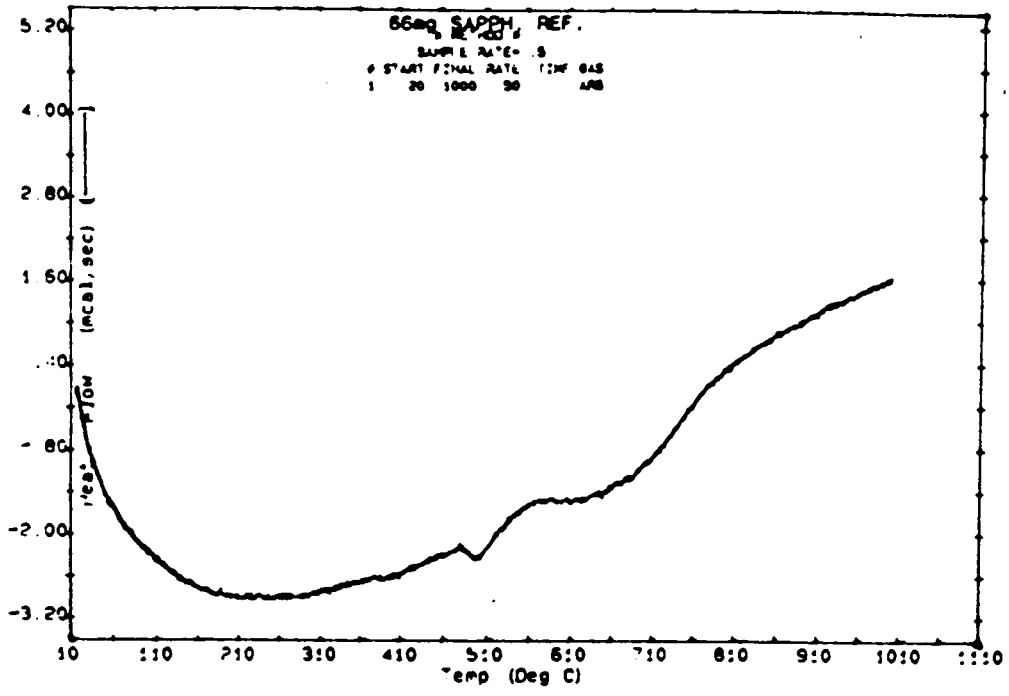

Figure 4.41 DSC curve of BS172

Chapter 5

Discussion

In this chapter, the results are interpreted and discussed, and wherever possible, the results of the present work are compared with those in the literature. As indicated in the Introduction, the present study is the first of its kind to comprehensively look at the thermal and mechanical properties of BaZPS ceramics as a function of composition and grain size. The axial thermal expansion of BS173, the hardness values of the BaZPS compositions, and the critical grain sizes of BS0, BS17, and BS50 have been determined for the first time.

The unit-cell parameters of the BS03 composition matched well with the National Bureau of Standards (1984) results. The bulk linear thermal expansion decreased and changed from positive to negative (BS503) with increasing Silicon content and is consistent with the results of Limaye (1988). The flexural strength of the BaZPS compositions increased at higher temperatures and may be attributed to the healing of microcracks at those temperatures. The critical grain size results indicate that the higher the thermal expansion anisotropy, the lower is the critical grain size transition. For example, BS17 had the lowest thermal expansion anisotropy, and showed the maximum critical grain size transition.

5.1 Variation of cell parameters with composition

The variation in unit cell parameters with composition at room temperature is compared with previous studies in Table 5.1. The BS03 results agreed with the National Bureau of Standards (1984), but differed from that of Huang (1990). Huang (1990) did not describe his synthesis procedure and possibly may have adopted a different method which could account for the discrepancy in the results. The above explanation is also valid for the variation in the results of the present study and Huang (1990) for BS253, BS373, and BS503. The cell parameters of BS173 have been determined for the first time in the present work.

5.2 Effect of composition on the bulk linear thermal expansion

The bulk linear thermal expansion decreased with increasing silicon content for the BaZPS compositions, and the values were positive for BS03, BS173, BS253 and BS373, and negative for BS503. The results are compared with those of Limaye (1988) in Table 5.2 and match well for BS503 and BS373, but are much higher in the case of BS03, BS173, and BS253. Thermal expansion of these materials being very low, such differences in the results may not be significant.

5.3 Axial thermal expansion results of BS173

High temperature x-ray results of BS173 are presented in Table 4.8. The degree of anisotropy, $|\alpha_a - \alpha_c|$, of BS173 is 1.41 x 10^{-6} $°C^{-1}$ (27 - 900°C) and compared with that of the other BaZPS ceramics in the literature in Table 5.3.

Table 5.1 Comparison of the unit-cell parameter results with previous studies

Composition	a ($\times 10^{-10}$ m)	c ($\times 10^{-10}$ m)	Volume ($\times 10^{-30}$ m^3)
BS03	8.64266(21) [1] 8.6468(5) [2] 8.6524(4) [3]	23.98754(112) [1] 23.984(2) [2] 23.9459(11) [3]	1552 [1] 1552.97 [2] 1552.51 [3]
BS173	8.66645(23) [1]	24.00839(113) [1]	1562 [1]
BS253	8.66398(46) [1] 8.6839(2) [3]	23.99634(209) [1] 24.0084(5) [3]	1560 [1] 1567.92 [3]
BS373	8.69730(31) [1] 8.7006(3) [3]	24.03785(129) [1] 24.0322(8) [3]	1575 [1] 1575.72 [3]
BS503	8.70415(47) [1] 8.7045(3) [3]	24.02034(220) [1] 24.0437(8) [3]	1576 [1] 1577.68 [3]

data within the brackets indicate the standard deviation of the last few digits

[1] present work
[2] NBS Monograph 25 (1984)
[3] Huang, C. Y. (1990)

Table 5.2 Comparison of the bulk linear thermal expansion results with Limaye

Composition	Bulk linear thermal expansion (x 10^{-6} $°C^{-1}$)	
	Present study	Limaye (1988)
BS03	2.14	1.90
BS173	1.80	1.20
BS253	1.36	0.80
BS373	0.30	0.40
BS503	-0.35	-0.35

Table 5.3 Thermal expansion anisotropy for BaZPS compositions

Composition	Degree of anisotropy $\lvert\alpha_a - \alpha_c\rvert \times 10^{-6}\ °C^{-1}$
BaZPS with x=0.0(BS0)	4.77 [1]
BaZPS with x=0.125(BS12)	3.79 [1]
BaZPS with x=0.175(BS17)	1.41 [2]
BaZPS with x=0.250(BS25)	1.80 [1]
BaZPS with x=0.375(BS37)	5.19 [1]
BaZPS with x=0.500(BS50)	6.14 [1]

[1] Huang (1990)
[2] present work

The cell parameters a and c initially increased from 27°C to 400°C, then decreased at 600°C and 800°C (however, the c parameter increased again at 800°C), and again increased at 850°C and 900°C (however, the a parameter decreased). It was also observed that several peaks (14-16) deviated to a large extent from that of the calculated values at 600°C and 800°C. However, below and above these temperatures the differences were observed to be very low. Also, the unit cell volume decreased at 600°C and 800°C. From the above results it was conjectured that a phase transition might be occurring between 400°C and 800°C.

DSC results revealed a broad endothermic peak between 560°C and 780°C (Figure 4.41) suggesting that there was a phase transition taking place between those temperatures and could possibly be responsible for large deviations of several observed x-ray peaks from that of the calculated values at 600°C and 800°C. The phase in BS173 between 600°C and 800°C is yet to be ascertained. However, below 600°C and above 800°C, the phase is rhombohedral.

Ohasi and Matsuhiro (1989) reported an order-disorder phase transition at 900°C in BS0 and noted that the material did not expand nor contract above that temperature. Also, several x-ray diffraction peaks disappeared above 900°C. It appears that all the BaZPS compositions may show phase transitions and should be examined to determine their behavior.

5.4 Flexural strength variation with composition and temperature

The room and high temperature flexural strength results are presented in Table 4.11 and indicate that the flexural strength of the BS0 and BS50 compositions increased with increasing temperature. Bush and Hummel (1958) reported that the flexural strength of magnesium titanate increased with increasing temperature from 25°C to 1000°C. They attributed the strength increase to the healing of microcracks during heating, and reported extensive healing of microcracks between 600°C to 1000°C. This could explain the strength increase in the BS0 and BS50 compositions as well. In the case of the BS17 compositions, the strength increased from room temperature to 200°C, then decreased at 600°C, and again increased at 1000°C. The initial strength increase could be ascribed to the healing of microcracks during heating. The sudden drop in the strength of the BS17 compositions at 600°C may be attributed to the phase that exists between 560°C and 780°C. The high temperature x-ray results of BS173 at 850°C indicate the formation of a phase different from that at 600°C and 800°C, which may be a higher strength phase. Hence, the strength increase at 1000°C may be ascribed to the new phase and also to the extensive healing of microcracks at temperatures between 800°C and 1000°C.

5.5 Critical grain size of BS0, BS17 and BS50

Several investigators (Kuszyk and Bradt 1973, Cleveland and Bradt 1978) have reported that in a single phase polycrystalline material there exists a critical

grain size below which microcracking does not occur. It has also been observed that the greater the thermal expansion anisotropy, the smaller is the critical grain size transition. Below the critical grain size, the flexural strength and Young's modulus increased with increasing grain size. Beyond the critical grain size the flexural strength, Young's modulus and thermal expansion coefficient decreased sharply. For example, Kuszyk and Bradt (1973) observed a sharp, critical grain size transition from a high strength, fine-grained, microcrack-free body to a weak, large-grained, severely microcracked structure in $MgTi_2O_5$. It would be worthwhile to mention that most of the studies in the above area deal with the effect of grain size, independent of porosity. Some studies have studied the effect of porosity on the mechanical properties independently, and have concluded that the mechanical properties like Young's modulus and flexural strength increase with decreasing porosity. However, the combined effect of grain size and porosity effect is not well understood. Hence in the discussion below, the effect of grain size on the thermal and mechancial properties is dealt ignoring the effect of porosity, and the critical grain size thus derived for BS0, BS17 and BS50 compositions are not very conclusive. In the case of the BS0 compositions, there was not much variation in the bulk linear thermal expansion with grain size (Table 4.7). Young's modulus results summarized in Table 4.9 indicate a sudden drop between BS02 and BS03 composition. However, the difference between the Young's modulus values of BS01 and BS02 was not significant. Also, the flexural strength results in Table 4.11 suggest decreasing strength with increasing grain size, with the drop

in strength between BS02 and BS03 significant at higher temperatures. All the above results seem to indicate that the critical grain size of the BS0 composition should lie between 2.70μm and 5.08μm.

There was not much variation in the bulk linear thermal expansion with increasing grain size in the BS17 compositions (Table 4.7). Also, the Young's modulus results in Table 4.9 and the flexural strength results in Table 4.11 indicate an increase with increasing grain size for BS17. Hence, the critical grain size of the BS17 composition must be greater than 4.16 μm.

The difference in the Young's modulus between BS501 and BS502 was not significant, but the decrease in the modulus between BS502 and BS503 is substantial (Table 4.9). In addition, the thermal expansion was positive for BS501 and BS502, but negative in the case of BS503 (Table 4.7). Hence, the critical grain size of the BS50 composition probably lies between 1.91 μm and 2.67 μm.

The degree of thermal expansion anisotropy decreases in the following order: BS50, BS0, and BS17 (Table 5.3). In the present study, the critical grain size transition decreased in the following order: BS17, BS0, and BS50. The results are thus consistent with those of previous studies on analogous materials (Yamai and Ota 1993), which have established that the critical grain size is inversely proportional to the square of the thermal expansion anisotropy.

Chapter 6

Conclusions and Suggestions for Future Work

6.1 Conclusions

Five BaZPS compositions with x=0.000, 0.175, 0.250, 0.375 and 0.500 were synthesized using a solid-state reaction method. The solid-state reaction method was found to be a simple and inexpensive method to produce BaZPS ceramics with good homogeneity.

The room temperature x-ray diffraction patterns revealed that all the compositions were essentially single-phase and the cell parameters were determined. The microstructural characterization results indicated that the BS253 and BS373 compositions were free of any secondary phase particles. Secondary phase particles, however, were present in BS0, BS17 and BS50 compositions and the amount decreased in the following order: BS50, BS0 and BS17. The amount of secondary phase particles was less than 4.7% and longer sintering times appeared to lower the secondary phase content.

The densities of the BaZPS compositions ranged from 77.5% to 98.59% of theoretical. The densities were greater than 90% of the theoretical in all the compositions sintered for 3000 minutes, except for BS503, and was highest in BS373 (98.59%).

The bulk linear thermal expansions of the BaZPS ceramics were determined

to be less than 2.26 x 10^{-6} $°C^{-1}$. The bulk linear thermal expansion decreased with increasing silicon content in the BaZPS compositions and varied between 2.26 and -0.35 x 10^{-6} $°C^{-1}$. Interpolation of the bulk linear thermal expansion variation with the composition suggests that a BaZPS phase with x=0.430 is likely to exhibit near-zero bulk linear thermal expansion. The high temperature x-ray results of BS173 indicated that this phase possessed very low thermal expansion anisotropy. Also, the variation of thermal expansion anisotropy with composition based on the results of Huang (1990) and this study seem to indicate that the composition x=0.21 may show the least thermal expansion anisotropy.

The room temperature Young's modulus was a minimum in the case of the BS50 compositions (<25.8 GPa), and maximum for BS373 (60.0 GPa). The flexural strength of the BaZPS compositions were measured from room temperature to 1000°C. BS373 had the highest flexural strength value at all the temperatures except 1000°C. The flexural strength increased with increasing temperature for BS0 compositions and could be ascribed to the healing of microcracks during heating. BS17 compositions exhibited low flexural strength at 600°C (<79.71 MPa), which could be caused by a different phase forming at that temperature. The room temperature hardness measurements were performed using a Knoop indenter, with BS373 having the highest hardness value (>5.19 GPa).

With longer sintering times, the grain size increased along with decreasing porosity. The combined effect of porosity and grain size on the mechanical and

thermal properties are not well understood. However, an attempt was made to determine the critical grain size ignoring the effect of porosity. Hence, the critical grain size reported is not conclusive. The critical grain sizes of BS0, BS17 and BS50 compositions were determined from the observed variations of Young's modulus, flexural strength and bulk linear thermal expansion. The critical grain size of BS17 was found to be greater than 4.16 μm, for BS0 to be between 2.70 μm and 5.08 μm, and for BS50 to be between 1.91 μm and 2.67 μm.

Among the BaZPS ceramics investigated, BS373 possessed the highest strength and hardness, and almost zero thermal expansion (0.30×10^{-6} $°C^{-1}$). These properties suggest that the material may be attractive for high temperature applications. BS17 compositions and BS253 exhibit very low thermal expansion anisotropy, low thermal expansion, good strength and hardness, and therefore should have good thermal shock resistance. The BS503 composition showed a negative thermal expansion and hence, could be a promising candidate for anti-expansion applications.

6.2 Suggestions for Future Work

Process optimization studies should be carried out by studying the effect of various sintering temperatures on the microstructure. Such a study could provide insight into how the microstructure could be tailored to obtain the desired microstructure for a given application.

In the present study, an effort was made to understand the effect of

sintering time on the thermal and mechanical properties of the BS0, BS17 and BS50 compositions. The same systematic approach should be done on the BS25 and BS37 compositions as well. Thermal cycling effects on the mechanical and thermal properties, as well as the thermal shock behavior under cyclic quenching, should be examined

It is suggested that the BaZPS with x=0.43 will exhibit near-zero thermal expansion, and the composition with x=0.21 will show the least thermal expansion anisotropy. These should be synthesized and examined for verification.

The author observed a unit cell contraction at 600°C and 800°C, and also very low flexural strength for BaZPS with x=0.175 at 600°C. DSC results revealed a broad endothermic peak between 560°C and 780°C and indicated the existence of a phase transition occurring between those temperatures. A study should be undertaken to provide a better understanding of the phase transition taking place. Ohasi and Matsuhiro (1989) reported an order-disorder phase transition at 900°C in BaZPS with x=0.0. The author believes that all the BaZPS compositions may show phase transformations and should be examined.

Very few chemical stability studies have been reported on NZP materials in the literature and an effort devoted to such a study would be worthwhile.

LIST OF REFERENCES

LIST OF REFERENCES

Adams, T. E. (1980) Dynamic Fatigue of Alumina Refractories at Room Temperature, M.S. Thesis, The Pennsylvania State University, University Park, Pennsylvania

Agrawal, D. K. and R. Roy (1985) "Composite route to "zero" expansion ceramics," J. Mater. Sci. **20**, 4617-4623

Agrawal, D. K. and V. S. Stubican (1985) "Synthesis and Sintering of $Ca_{0.5}Zr_2P_3O_{12}$- A Low Thermal Expansion Material," Mat. Res. Bull. **20**, 99-106

Agrawal, D. K., K. R. Kanak, and H. A. McKinstry (1986) "Synthesis and Thermal Expansion of $NaGe_2P_3O_{12}$," Mat. Res. Bull. **21**, 1295-1298

Agrawal, D. K. and R. Roy (1986) "Synthesis and thermal expansion of $Na_{3-x}Ca_{x/2}M_2P_3O_{12}$ (M=Fe, Cr)," J. Mat. Sci.Letters **5**, 138-140

Agrawal, D. K. and J. H. Adair (1990) "Low Temperature Sol-Gel Synthesis of $NaZr_2P_3O_{12}$," J. Am. Ceram. Soc. **73**, 2153-2155

Agrawal, D. K. (1992) Personal Communication to D. P. Stinton, Workshop on Low-Expansion Ceramics, Knoxville, Tennessee

Alamo, J. and R. Roy (1984) "Ultralow-Expansion Ceramics in the System Na_2O-ZrO_2-P_2O_5-SiO_2," J. Am. Ceram. Soc. **67**, C78-C80

Alamo, J. and R. Roy (1986) "Crystal Chemistry of the $NaZr_2(PO_4)_3$, NZP or CTP, Structure Family," J. Mater.Sci. **21**, 444-450

Balagopal, S. (1989) Synthesis and Mechanical Properties of Calcium Strontium Zirconium Phosphate Ceramics, M.S.Thesis, The Pennsylvania State University, University Park, Pennsylvania

Baudry, A., P. Boyer, and J. P. Boilot (1985) "Study of Phase Transitions in Nasicon-Type Compounds by ^{181}Ta Nuclear Quadrupole Spectroscopy," Transport-Structure Relations in Fast Ion and Mixed Conductors, F.W. Poulsen et al. Eds., Proc. Sixth Riso Intern. Symp. Metall. Mat. Sci., 431-437

Boas, W. and Honeycombe, R. W. K. (1946) "The Plastic Deformation of Non-

Cubic Metals by Heating and Cooling," Proc. R. Soc. London, A. **186**, 57-71

Boilot, J. P., J. P. Salanie, G. Desplanches, and D. Le Potier (1979) "Phase Transformation in $Na_{1+x}Zr_2Si_xP_{3-x}O_{12}$ Compounds," Mat. Res. Bull. **14**, 1469-1477

Boilot, J. P., Ph. Colomban, and G. Collin (1986) "NASICON: Amorphous to Crystalline Compounds," Solid State Ionics **18 & 19**, 974-980

Boilot, J.P., G. Collin, and Ph. Colomban (1988) "Relation Structure - Fast Ion Conduction in the Nasicon Solid Solution," J. Solid State Chem. **73**, 160-171

Buessem, W. R., N. R. Thielke, and R. V. Sarakauskas (1952) "Thermal Expansion Hysterisis of Aluminium Titanate," Ceramic Age **60**, 38-40

Buessem, W. R. (1961) "Internal Ruptures and Recombinations in Anisotropic Ceramic Materials," Mechanical Properties of Engineering Ceramics, W. W. Kreigel and H. Palmour III Eds., Interscience Publ., Inc., New York, 127-148

Buessem, W. R. and F. F. Lange (1966) "Residual Stresses in Anisotropic Ceramics," Interceram **15**, 229-231

Bush, E. A. and F. A. Hummel (1958) "High-Temperature Mechanical Properties of Ceramic Materials: I, Magnesium Dititanate," J. Am. Ceram. Soc. **41**, 189-195

Bush, E. A. and F. A. Hummel (1959) "High-Temperature Mechanical Properties of Ceramic Materials: II, Beta-Eucryptite," J. Am. Ceram. Soc. **42**, 388-391

Byrappa, K., G. S. Gopalakrishna, and A. B. Kulkarni (1986) "Synthesis and Characterization of $NaNi_2ZrP_3O_{12}$ Crystals," J. Mat. Sci. Letters **5**, 519-521

Clarke, F. J. P. (1964) "Residual Strain and the Fracture Stress-Grain Size Relationship in Brittle Solids," Acta Metallurgica **12**, 139-143

Clearfield, A., P. Jirustithipong, R. N. Cotman, and S.P. Pack (1980) "Synthesis of Sodium Dizirconium Triphosphate from α-Zirconium Phosphate," Mat. Res.Bull. **15**, 1603-1610

Clearfield, A., P. Jerus, and R. N. Cotman (1981) "Hydrothermal and Solid State Synthesis of Sodium Zirconium Silicophosphates," Solid State Ionics **5**, 301-304

Clearfield, A., B. D. Roberts, and M. A. Subramanian (1984) "Preparation of $(NH_4)Zr_2(PO_4)_3$ and $HZr_2(PO_4)_3$," Mat.Res. Bull. **19**, 219-226

Cleveland, J. J. and R. C. Bradt (1978) "Grain Size/Micro-cracking Relations for Pseudobrookite Oxides," J. Am. Ceram. Soc. **61**, 478-481

Crouch, A. G. and K. H. Joliffe (1970) "The Effect of Stress Rate on the Strength of Alumina and Mullite Refractories," Proc. Brit. Cer. Soc. **15**, 37-46

Cuadrado, M. C. and J. Alamo (1988) "Cr-Doped Zirconium Phosphate Pigments," Br. Ceram. Trans. J. **87**, 141-144

Delmas, C., R. Olazcuaga, G. Le Flem, P. Hagenmuller, F. Cherkaoui, and R. Brochu (1981) "Crystal Chemistry of the $Na_{1+x}Zr_{2-x}L_x(PO_4)_3$ (L=Cr, In, Yb) Solid Solutions," Mat. Res. Bull. **16**, 285-290

Dongare, M. K., P. Singh, and P. M. Suryavanshi (1992) "Hydrothermal Synthesis and Characterization of Crystalline Sodium Zirconium Phosphates," Mat. Res. Bull. **27**, 637-645

Effremov, V. A. and V. B. Kalinin (1978) "Determination of the Crystal Structure of $Na_3Sc_2(PO_4)_3$," Sov. Phys. Crystallogr. **23**, 393-396

Evans, A. G. (1978) "Microfracture from Thermal Expansion Anisotropy-I. Single Phase Systems," Acta Metallurgica **26**, 1845-1853

Goodenough, J. B., H. Y-P. Hong, and J. A. Kafalas (1976) "Fast Na^+-Ion Transport in Skeleton Structures," Mat. Res. Bull. **11**, 203-220

Gordon, R. S., G. R. Miller, B. J. McEntire, E. D. Bech, and J. R. Rasmussen (1981) "Fabrication and Characterization of Nasicon Electrolytes," Solid State Ionics **3/4**, 243-248

Gupta, T. K. (1976) "Crack Healing and Strengthening of Thermally Shocked Alumina," J. Am. Ceram. Soc. **58**, 5-6

Hagman, L. O. and P. Kierkegaard (1968) "The Crystal Structure of $NaMe_2^{IV}(PO_4)_3$; Me^{IV}=Ge, Ti, Zr," Acta Chemica Scandianvica **22**, 1822-1832

Hazen, R. M., L. W. Finger, D. K. Agrawal, H. A. McKinstry, and A. J. Perrotta (1987) "High-Temperature Crystal Chemistry of Sodium Zirconium Phosphate (NZP)," J. Mater.Res. **2**, 329-337

Hirschfeld, D. A., S. M. Van Aken, T. K. Li, Y. P. Yang, and J. J. Brown (1991) "Development of Ultra-Low-Expansion Ceramics: Synthesis, Thermal Expansion, and Thermal Conductivity of $(Ca_{1-x},Mg_x)Zr_4(PO_4)_6$," Proceedings of the Annual Automotive Technology Development Contractor's Coordination Meeting, P-243, SAE, Inc., Warrendale, Pennsylvania, 239-244

Howe, J. P. (1952) "Properties of Graphite," J. Am. Ceram. Soc. **35**, 275-282

Hong, H. Y-P. (1976) "Crystal Structures and Crystal Chemistry in the System $Na_{1+x}Zr_2Si_xP_{3-x}O_{12}$," Mat. Res. Bull. **11**, 173-182

Hong, H. Y-P. (1979) "Crystal Structure and Ionic Conductivity of a New Superionic Conductor, $Na_3Sc_2P_3O_{12}$,"Fast Ion Transport in Solids, Vashista, Mundy, and Shenoy Eds., Elsevier North Holland, Inc., New York, 431-433

Hong, H. Y-P., J. A. Kafalas, and M. Bayard (1987) "High Na^+-Ion conductivity in $Na_5YSi_4O_{12}$," Mat. Res. Bull. **13**, 757-761

Huang, C. Y. (1990) Thermal Expansion Behavior of Sodium Zirconium Phosphate Structure Type Materials, Ph. D. Thesis, The Pennsylvania State University, University Park, Pennsylvania

Hubbard, C. R. and R. R. Sokol (1990) ORNL Calibration and least squares software package, High Temperature Materials Laboratory, Oak Ridge, Tennessee

Inglis, C. E. (1913) "Stresses in a Plate Due to the Presence of Cracks and Sharp Corners," Trans. Inst. Naval Arch. **55**, 219

Kafalas, J. A. and R. J. Cava (1979) "Effect of Pressure and Composition on Fast Na^+-Ion Transport in the System $Na_{1+x}Zr_2Si_xP_{3-x}O_{12}$," Fast Ion Transport in Solids, Vashishta, Mundy, and Shenoy, Eds., Elsevier North Holland, Inc., New York, 419-422

Kirchner, H. P. and R. M. Gruver (1970) "Strength-Anisotropy-Grain Size Relations in Ceramic Oxides," J. Am. Ceram. Soc. **53**, 232-236

Komarneni, S., G. E. Lenain, and R. Roy (1986) "Thermal Expansion of $NH_4Zr_2(PO_4)_3$," J. Mat. Sci. Letters **5**, 1-3

Komarneni, S. (1988) "Hydrothermal Preparation of the Low-Expansion NZP Family of Materials," Int. J. High Tech. Ceram. **4**, 31-39

Krstic, V. D. (1984) "Fracture of Brittle Solids in the Presence of Thermoelastic Stresses," J. Am. Ceram. Soc. **67**, 589-593

Kuszyk, J. A. and R. C. Bradt (1973) "Influence of Grain Size on Effects of Thermal Expansion Anisotropy in $MgTi_2O_5$," J. Am. Ceram. Soc. **5**, 420-423

La Ginestra, A., C. Ferragina, and P. Patrono (1979) "Ag-Zirconium Phosphate System: Characterization off the Phases Obtained at Different Temperatures," Mat. Res. Bull. **14**, 1099-1109

Lange, F. F. (1970) "Interaction of a Crack Front with Second-phase Dispersion," Phil. Mag. **22**, 983-992

Lenain, G. E., H. A. McKinstry, S. Y. Limaye, and A. Woodward (1984) "Low Thermal Expansion of Alkali-Zirconium Phosphates," Mat. Res. Bull. **19**, 1451-1456

Lenain, G. E., H. A. McKinstry, S. Y. Limaye (1985) "Low Thermal Expansion of Alkali Zirconium Phosphates Using a Microcomputer Automated Diffractometer," Advances in X-Ray Analysis, Barrett, Predecki, and Leyden Eds., Plenum Publ. Co., **28**, 345-352

Likhachev, V. A. (1961) "Microstructural Strains Due to Thermal Anisotropy," Soviet Phys.-Solid State **3**, 1330-1336

Limaye, S. Y., D. K. Agrawal, and H. A. McKinstry (1987) "Synthesis and Thermal Expansion of $MZr_4P_6O_{24}$ (M=Mg, Ca, Sr, Ba)," J. Am. Ceram. Soc. **70**, C232-C236

Limaye, S. Y. (1988) Unpublished work

Limaye, S. Y. (1989) "New Low Thermal Expansion Materials for High Use Temperatures," Materials and Processing Report **4**, 1-2

Limaye, S. Y., D. K. Agrawal, R. Roy, and Y. Mehrotra (1991) "Synthesis, Sintering and Thermal Expansion of $Ca_{1-x}Sr_xZr_4P_6O_{24}$-an ultra-low thermal expansion ceramic system," J. Mater. Sci. **26**, 93-98

Manning, W. R., O. Hunter, Jr. (1973) "Anomalous Elastic Behavior of Polycrystalline Nb_2O_5," J. Am. Cer. Soc. **56**, 602-603

Masse, R. (1970) "Etude des monophosphates du type $MITi_2(PO_4)_3$ pour MI=Li, Ag, K, Rb et Tl," Bull. Soc. fr. Mineral. Cristallogr. **93**, 500-503

Masse, R. (1972) "Monophosphates $M^{III}BaTi(PO_4)3M^{III}$=Cr et FeMonophosphates du type langbeinite," Bull. Soc. fr. Mineral. Cristallogr. **95**, 405-411

MIL-STD-1942A (1990) "Flexure Strength of High Performance Ceramics at Ambient Temperature," U.S. Army Materials Technology Laboratory, Watertown, Massachussets

Miller, G. R., B. J. McEntire, T. D. Hadnagy, J. R. Rasmussen, R. S. Gordon, and A. V. Virkar (1979) "Processing and Properties of Sodium β"-Alumina and Nasicon Ceramic Electrolytes," Fast Ion Transport in Solids, P.Vashishta, J. N. Mundy, and G. K. Shenoy Eds., Elsevier North Holland, Inc., New York, 83-86

Nagai, M., S. Fujitsu, and T. Kanazawa (1980) "Ionic Conductivity in the System $NaZr_2(PO_4)_3$-$Na_3Y_2(PO_4)_3$," J. Am. Ceram. Soc. **63**, 476-477

NBS Monograph 25 (1984) Standard X-Ray Diffraction Powder Patterns, Sec. 20, M. C. Morris et al. Eds., National Bureau of Standards, U. S. Dept. of Commerce

Ohashi, T. and K. Matsuhiro (1989) "Synthesis and Low Thermal Expansion Behavior of $NaZr_2(PO_4)_3$-Type Structure Zirconium Phosphates," 91st Ann. Mtg. Am. Ceram. Soc., Indianapolis, Indiana

Ohya, Y., Z. Nakagawa, and K. Hamano (1987) "Grain-Boundary Microcracking Due to Thermal Expansion Anisotropy in Aluminium Titanate Ceramics," J. Am. Ceram. Soc. **70**, C184-C186

Okonenko, S. A., S. Yu. Stefanovich, V. B. Kalinin, and Yu. N. Venevtsev (1978) "New Ferroelectric $Na_3Sc_2(PO_4)_3$," Sov. Phys. Solid State **20**, 1647-1648

Oota, T. and I. Yamai (1986) "Thermal Expansion Behavior of $NaZr_2(PO_4)_3$-Type Compounds," J. Am. Ceram. Soc. **69**, 1-6

Padgett, G. C. and J. F. Clemens (1970) "High Temperature σ-ε Behavior of Commercial Ceramics," Proc. Brit. Cer. Soc. **15**, 61-68

Perret, R., A. Thrierr-Sorel, J.-P. Peter, and R. Masse (1975) "Les sulfates triples $M^IM^{II}M^{III}(SO_4)_3$. I. Les sulfates rhomboedriques $NaM^{II}M^{III}(SO_4)_3$ (M^{II}=Mg, Mn, Co, Ni, Zn; M^{III}=Al, Ga, In, Cr, Fe)," Bull. Soc. fr. Mineral. Cristallogr. **98**, 103-106

Petit, D., Ph. Colomban, G. Collin, and J. P. Boilot (1986) "Fast Ion Transport in $LiZr_2(PO_4)_3$: Structure and Conductivity," Mat. Res. Bull. **21**, 365-371

Ramasesha, S. K. and K. T. Jacob (1988) "X-Ray and IR Characterization of Nasicon Solid Solution, $Na_{1+x}Zr_2Si_xP_{3-x}O_{12}$," Materials Letters **7**, 61-64

Rice, R. W. and R. C. Pohanka (1979) "Grain-Size Dependence of Spontaneous Cracking in Ceramics," J. Am. Ceram. Soc. **62**, 559-563

Rice, R. W., S. W. Freiman, and P. F. Becher (1981) "Grain-Size Dependence of Fracture Energy in Ceramics: I, Experiment," J. Am. Ceram. Soc. **64**, 345-350

Rodrigo, J. L., P. Carrasco, and J. Alamo (1989) "Thermal Expansions of $NaTi_2(PO_4)_3$ Studied by Rietveld Method from X-ray Diffraction Data," Mat. Res. Bull. **24**, 611-618

Rodrigo, J. L. and J. Alamo (1991) "Phase Transition in $NaSn_2(PO_4)_3$ and Thermal Expansion of $NaM_2^{IV}(PO_4)_3$; M^{IV}=Ti, Sn, Tr," Mat. Res. Bull. **26**, 475-480

Roy, R., E. R. Vance, and J. Alamo (1982) "[NZP], A New Radiophase for Ceramic Nuclear Waste Forms," Mat. Res. Bull. **17**, 585-589

Roy, R., D. K. Agrawal, J. Alamo, and R. A. Roy (1984) "[CTP]: A New Structural Family of Near-Zero Expansion Ceramics," Mat. Res. Bull. **19**, 471-477

Roy, R., D. K. Agrawal, and H. A. McKinstry (1989) "Very Low Thermal Expansion Coefficient Materials," Annu. Rev. Mater. Sci. **19**, 59-81

Rudolf, P. R., M. A. Subramaniam, A. Clearfield, and J. D. Jorgensen (1985) "The Crystal Structures of a Nonstoichiometric Nasicon," Mat. Res. Bull. **20**, 643-651

Scintag (1989) "Diffraction Management System 2000, Ver 1.0.," Scintag Inc., USA

Sizova, R. G., A. A. Vornokov, N. G. Shumyatskaya, V. V. Ilyukhin, and N. V.Belov (1973) "Crystal Structure of $Na_4Zr_2(SiO_4)_3$," Soviet Physics-Doklady **17**, 618-620

Sljukic, M., B. Matkovic, B. Prodic, and S. Scavnicar (1967) "Preparation and Crystallographic Data of Phosphates with Common Formula $M^IM_2^{IV}(PO_4)_3$ (M^I=Li, Na, K, Rb, Cs; M^{IV}=Zr, Hf)," Croatica Chemica Acta **39**, 145-148

Sljukic, M., B. Matkovic, B. Prodic, and D. Anderson (1969) "The Crystal Structure of $KZr_2(PO_4)_3$," Z. Krist. **130**, 148-161

Sosman, R. B. (1927) Properties of Silica, Am. Chem. Soc. Monograph Series, No. 37, Chem. Catalog Co., Inc., New York

Spinner, S. and H. E. Tefft (1961) " A Method for Determining Mechanical Resonance Frequencies and for Calculating Elastic Moduli from these Frequencies," Proc. ASTM **61**, 1221-1238

Subramaniam, M. A., B. D. Roberts, and A. Clearfield (1984) "On the Proton Conductor $(H_3O)Zr_2(PO_4)_3$," Mat. Res. Bull. **19**, 1471-1478

Takahashi, T., K. Kuwabara, and M. Shibata (1980) "Solid-State Ionics Conductivities of Na^+ Ion Conductors Based on Nasicon," Solid State Ionics **1**, 163-175

Tarte, P., A. Rulmont, and C. Merckaert-Ansay (1986) "Vibrational Spectrum of Nasicon-Like, Rhombohedral Orthophosphates $M^IM_2^{IV}(PO_4)_3$," Spectrochimica Acta **42A**, 1009-1016

Taylor, B. E., A. D. English, and T. Berzins (1977) "New Solid Ionic Conductors," Mat. Res. Bull. **12**, 171-182

Tran Qui, D. and S. Hamdoune (1988) "Structure of the Ortho-rhombic Phase of $Li_{1+x}Ti_{2-x}In_xP_3O_{12}$, x=1.08," Acta Cryst. **C44**, 1360-1362

Tvergaard, V. and J. W. Hutchinson (1988) "Microcracking in Ceramics Induced by Thermal Expansion of Elastic Anisotropy," J. Am. Ceram. Soc. **71**, 157-166

von Alpen, M. F.Bell, and W. Wichelhaus (1979) "Phase Transition in Nasicon $(Na_3Zr_2Si_2PO_{12})$," Mat. Res. Bull. 14, 1317-1322

Wolfenden, A., M. R. Harmouche, G. V. Blessing, Y. T. Chen, P. Terranova, V. Dayal, V. K. Kinra, J. W. Lemmens, R. R. Phillips, J. S. Smith, P. Mahmoodi, and R. J. Wann (1989) "Dynamic Young's Modulus Measurements in Metallic Materials: Results of an Interlaboratory Testing Program," JTEVA **17**, 2-13

Wright, R. E. (1972) "Acoustic Emission of Aluminium Titanate," J. Am. Ceram. Soc. **55**, 54

Yamai, I. and T. Ota (1987) "Low-Thermal-Expansion Polycrystalline Zirconyl Phosphate Ceramic: Solid-Solution and Microcracking-Related Properties," J. Am. Ceram. Soc. **70**, 585-590

Yamai, I. and T. Ota (1993) "Grain Size-Microcracking Relation for $NaZr_2(PO_4)_3$ Family Ceramics," J. Am. Ceram. Soc. **76**, 487-491

Yang, L. J., S. Komarneni, and R. Roy (1984) "Gel Adsorption Processing for Waste Solidification in 'NZP' Ceramics," Scientific Basis for Nuclear Waste Management Vol. 7, G. L. McVay Ed., 567-574

VITA

Shanmugham Subramaniam was born in Chinnalapatti, Tamil Nadu, India on December 4, 1970. He attended P. S. Senior Secondary School in Madras, India and graduated with Distinction in March, 1987. The following August he entered Anna University in Madras, India and in April, 1991 received the degree of Bachelor of Engineering in Mechanical Engineering. He won several academic accolades during this period including the "Anna University Gold Medal" for being the first rank student in Mechanical Engineering. In August, 1991 he joined The University of Tennessee, Knoxville and in August, 1993 received a Master of Science degree in Metallurgical Engineering.

He is presently employed as a research associate with the Department of Materials Science and Engineering, University of Tennessee, Knoxville and is also pursuing a Ph. D. degree in Metallurgical Engineering.